Title
A METHOD FOR RECYCLING RADIOACTIVE NOBLE GASES FOR FUNCTIONAL PULMONARY IMAGING

Author
Forouzan-Rad, Massoud.

Publication Date
1976-05-01

LBL-4759
c 1

A METHOD FOR RECYCLING RADIOACTIVE NOBLE GASES FOR FUNCTIONAL PULMONARY IMAGING

DONNER LABORATORY

Massoud Forouzan-Rad
(Ph. D. thesis)

May 1976

Prepared for the U. S. Energy Research and Development Administration under Contract W-7405-ENG-48

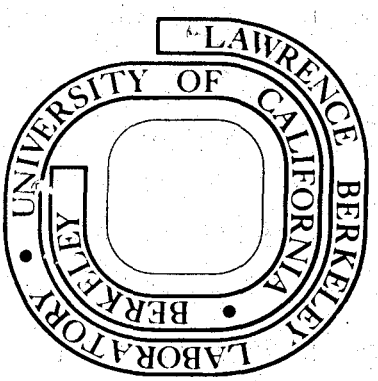

LBL-4759
c.1

DISCLAIMER

ACKNOWLEDGMENTS

I wish to express my deep appreciation to Professor Selig N. Kaplan and Doctor James McRae for their helpful guidance and constructive criticism in the conduct of this research; to Professor Michael L. Goris for his invaluable contribution; and to Professor Harvey J. Amster for reviewing the dissertation.

I gratefully thank the staff of the Donner Laboratory, especially Mr. Edward Dowling for his assistance in the mechanical construction of the apparatus.

My thanks is further extended to Ms. Mary Wildensten for editing, to Mr. Robert Stevens for completing the figures, and to Ms. Cathy Dickinson for typing.

This dissertation would not have been possible without the continued encouragement of my brother, Saiid, and financial support of my parents to whom I express my sincere gratitude.

This work was done under the auspices of the U.S. Energy Research and Development Administration.

TABLE OF CONTENTS

A METHOD FOR RECYCLING RADIOACTIVE NOBLE GASES FOR FUNCTIONAL PULMONARY IMAGING

Massoud Forouzan-Rad

Doctor of Philosophy Nuclear Engineering

ABSTRACT

A theoretical treatment of the dynamic adsorption and desorption processes in the adsorption column is developed. The results of this analysis are compared with the space-time measurements of ^{133}Xe activity distribution in a charcoal column, when trace amounts of this gas in exponentially decreasing concentrations are fed into the column.

Based on these investigations, a recycling apparatus is designed for use with xenon isotopes, especially ^{127}Xe, in studies of pulmonary function. The apparatus takes advantage of the high adsorbability of activated coconut charcoal for xenon a low temperature (-78°C) in order to trap the radioactive xenon gas that is exhaled during each ventilation-perfusion study. The trapped xenon is then recovered by passing low-pressure steam through the charcoal column. It is found that steam removes xenon from the surface of the charcoal more effectively than does heating and evacuation of the charcoal bed. As a result, an average xenon recovery of 96% has been achieved. Improved design parameters are discussed.

A mathematical model is described that introduces a new relationship between the disappearance rate constant and the functional air exchange for any region in the lung by taking the motion of the respiratory cycle into account. The results of this approach were incorporated in computer programs that may be used in data processing systems to provide an analysis of the morphology and dynamics of the lung ventilation and perfusion in a great number of regions in the lung. The recycling apparatus would facilitate the use of ^{127}Xe, which has more favorable physical characteristics than has the more commonly used ^{133}Xe. Use of this model and the apparatus would improve the quantitation of ventilation and perfusion defects because of the high resolution and detection efficiency obtained with ^{127}Xe.

INTRODUCTION

The first investigations involving radionuclides for the study of regional distribution of ventilation were undertaken by Knipping et al. in 1953 at the University Clinic of Cologne [1]. After preliminary experiments with volatile ^{131}I labeled alkyl iodides, these investigators developed a technique in which patients inhaled ^{133}Xe. The accumulation of radioactivity in various regions of the lung was measured with external counters [2,3]. This procedure enabled the detection of regional differences in ventilation caused by local disease. Regional blood flow was first measured with ^{15}O at Hammersmith Hospital in London [4]. When ^{15}O is inhaled in the form of carbon dioxide, the rate at which it is removed from a region of the lung during a short breath-holding period is a measure of local blood flow [5,6]. However, the use of ^{15}O is impractical because its very short half-life, two minutes, would require that the clinical laboratory be adjacent to a source-producing cyclotron. Several later investigations, beginning with Ball et al. [7] at the Royal Victoria Hospital in Montreal, demonstrated that ^{133}Xe may be used for studies of regional ventilation as well as regional lung volume and regional perfusion [8,9].

In addition to these gases, radionuclides in a nongaseous state have been used for determining regional pulmonary perfusion [10-23]. The first agent used was macroaggregated human serum albumin labeled with either ^{131}I or ^{51}Cr [11-13]. The short-lived radionuclides ^{113m}In

[14] and ^{99m}Tc were used subsequently, either incorporated in inorganic salts such as iron hydroxide, or bound to microspheres made of human serum albumin [15-23]. This method is widely used for detecting regional disturbances of pulmonary arterial blood flow, as in the diagnosis of pulmonary embolism.

Early radionuclide studies of regional pulmonary perfusion and ventilation provided useful physiological information and the potential clinical usefulness of this approach was quickly appreciated. However, the radioactivity detectors used for these studies consisted of several individual scintillation probes positioned over the chest, which provided only limited anatomical detail within the lungs. Development of the gamma camera by H.O. Anger [14] has recently renewed interest in the use of radioactive gases for determination of regional ventilation in patients [25,26]. These cameras offer better spatial reoslution than multiprobe systems and, when fitted with a diverging collimator, can view both lungs. They have an additional advantage in that they provide serial images during the uptake and clearance phases of xenon in the lungs.

Images of the distribution of gamma radiation may also be displayed in a digital matrix after accumulation in a multichannel analyzer, or in a digital computer, or after storage on a magnetic tape or disc [27-34]. A number of systems are now commercially available to provide this sort of data collection and processing [35-39]. In addition, small computers have been interfaced successfully with the Anger scintillation camera, so that the flexibility of a computer is immediately available for data processing.

One area where data processing systems may be usefully applied is in the evaluation of pulmonary function. By using the gamma camera coupled to a suitable data handling system, numerical indication of either ventilation or perfusion can be obtained. Of considerable interest is the ability of some of these systems to present "functional images" of regional gas exchange, regional blood flow per unit of lung volume, or ventilation-perfusion ratios. In such an image, in which regional rate constants are used, the functional relationships of the lung during the dynamic process are presented by a single display. This display provides in a readily assimilated form an indication of the way in which various parts of the lung are working in comparison to each other.

Several methods have been reported that describe quantitative evaluation of the ventilation and perfusion distribution in the human lung and which use the scintillation camera and a data processing system [40-51]. In all these methods it is assumed that regional ventilation or the fraction of air exchanged is equal to the clearance rate constant during washout of ^{133}Xe from the corresponding site. In this presentation, taking the respiratory cycle into account, a model is described that introduces a new relationship between the disappearance rate constant and the fractional air exchange for any region in the lung. Results of this approach were incorporated in computer programs that may be used in data processing systems to provide simultaneous morphologic and dynamic exploration of lung ventilation and perfusion for hundred regions in the lung.

The qualities of short biological half-life, inert character, and low solubility make noble gases almost ideal for pulmonary function

studies. Xenon-133 is still the most widely used radioactive noble gas, largely because it is the only gas now generally available with suitable physical characteristics. However, this radionuclide is not ideal for use with the scintillation camera because of the low abundance and energy of its gamma rays.

Xenon-127, which has more favorable physical characteristics, has recently become available. The photons of ^{127}Xe are more abundant and in a more appropriate range for providing resolution and efficient detection. Consequently, ^{127}Xe, when used in conjunction with a scintillation camera and computer interface, allows better quantitation of ventilation and perfusion defects. The half-life of ^{127}Xe is 36.4 days, or approximately seven times that of ^{133}Xe. The longer physical life of ^{127}Xe does not increase the radiation dosage, which is governed by the short biological half-life. It is, however, an asset in terms of extended shelf life, and offers the potential for recycling. In addition, this isotope is suitable for measuring cerebral blood flow and flow to other organs.

A major problem in the clinical usage of radioactive inert gases arises from the fact that release of these gases can create problems. Therefore, engineering safeguards must be provided to adequately maintain predetermined emission standards. To reduce the release of radioactive effluent, especially ^{127}Xe, an experimental and theoretical design study of a recycling apparatus was undertaken, and is described in the major portion of the following text.

CHAPTER I.

RADIOACTIVE INERT GASES IN PULMONARY FUNCTION STUDIES

I-1. A Review of Radioactive Inert Gases Used In Pulmonary Function Studies

The radioactive noble gases are used principally in nuclear medicine to assess regions of decreased ventilation and perfusion in the lungs as well as regional blood flow in other areas. These gases provide a method for studying regional lung function which gives information that cannot be obtained in other ways. A partial list of the potentially useful, radioactive inert gases, with their important physical properties, is given in Table I-1.

General availability has made ^{133}Xe the most commonly used radionuclide for ventilation studies. Xenon-133 is a fission product that results from neutron bombardment of ^{235}U. The physical half-life of ^{133}Xe is 5.27 days, and it decays by emission of a beta ray ($E_{\beta max}$ = 347 keV) to the isomeric state of ^{133}Ce. This decay is followed either by emission of an 81-keV photon or an internal conversion electron; the latter is followed by the emission of K characteristic radiation of 31 keV [53]. The decay scheme of ^{133}Xe is shown in Fig. I-1.

Radioactive ^{133}Xe was the first gas used in the investigation of regional lung function [54]. As many as 16 Geiger-Muller tubes were placed over the dorsal thorax, and the external counting rate was

Table I-1. Partial list of radioactive inert gases used for lung function studies.

Isotope	Half-life	Principal gamma emission (keV) (intensity %)		Other modes of decay
^{133}Xe	5.27 day	81	(35%)	$\overline{\beta}(\overline{E}_{\beta}$ = 100 keV)
^{135}Xe	9.13 hr	250	(91%)	$\overline{\beta}(\overline{E}_{\beta}$ = 500 keV)
^{127}Xe	36.40 day	375	(20%)	electron capture
		203	(65%)	
		172	(22%)	
^{81m}Kr	13.00 sec	190	(65%)	$\overline{\beta}(\overline{E}_{\beta}$ = 270 keV)

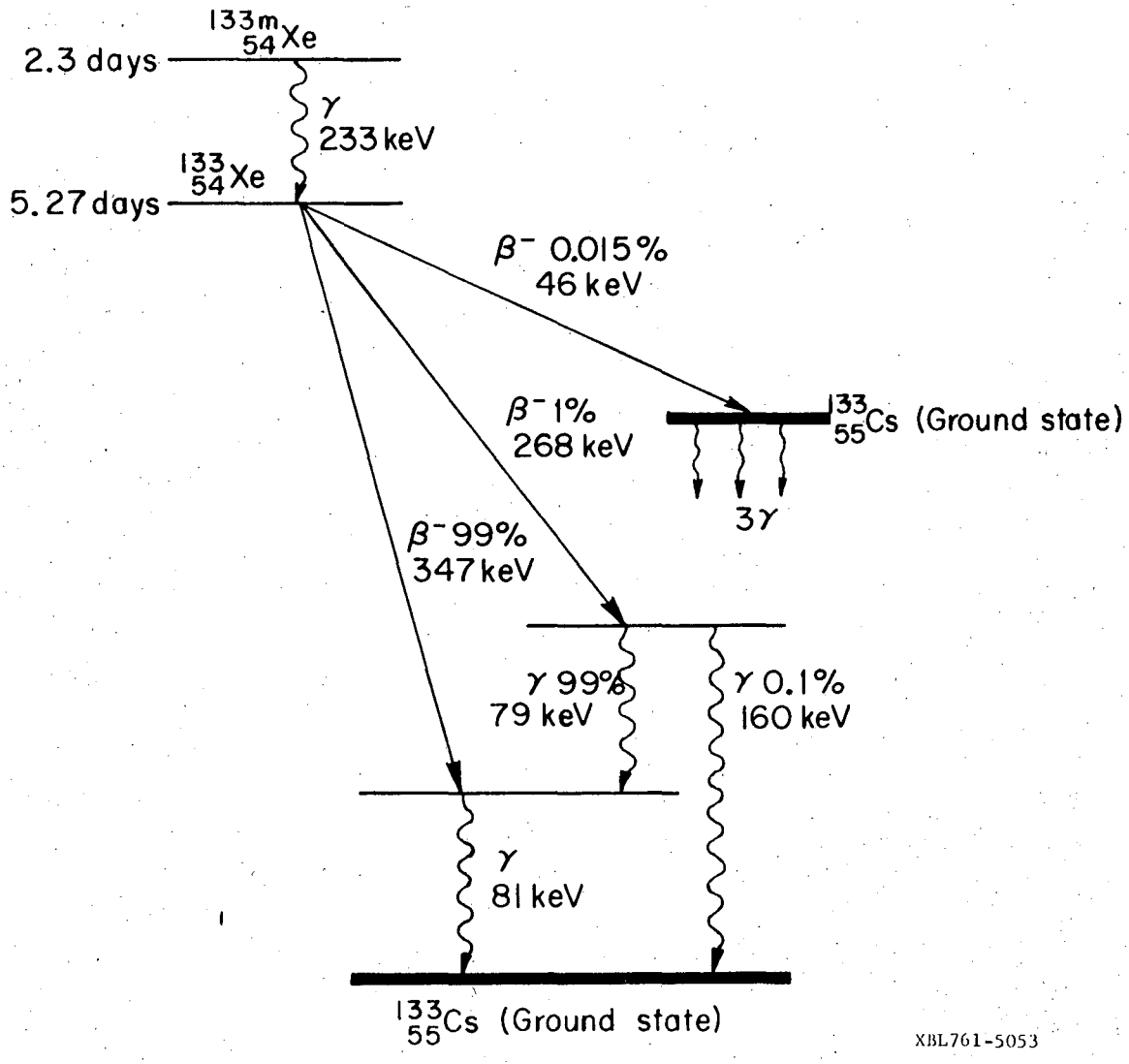

FIGURE I-1. Decay path of $^{133}_{54}Xe$.

recorded over multiple areas of the chest during breathing of air containing ^{133}Xe. The value of these investigations was limited, however, as only the distribution of ventilation was studied. Several later investigations showed that ^{133}Xe could be used for studies of regional ventilation as well as for regional perfusion [7]. In the original method [7] six stationary scintillation counters fitted with cylindrical collimators were positioned over the back of the thorax. Regional ventilation was determined by comparing the counting rate over the lung after a single breath to the equilibrium counting rate when the isotope was uniformly dispersed throughout the lung. An equilibrium count was used as a relative index of the aerated lung volume, and the distribution of ventilation was expressed by static indices based on the distribution during breath holding after a tidal breath and after a maximal inspiration. Since the static index was calculated from the ratio of two external counting rates, it was independent of lung volume seen by the counter, of counter sensitivity, or of chest wall radiation absorption. When most of the ventilated xenon had been washed out of the lung, a known amount of xenon (1 to 3 mCi) was injected rapidly into a peripheral vein and perfusion was determined during breath holding at maximal inspiration. The distribution index for perfusion was calculated similarly to the distribution index for ventilation.

The analysis of wash-out curves is a later method suggested for evaluation of poorly ventilated areas [55]. An assembly of scintillation probes or a gamma-ray camera is placed against the posterior of the subject, who is in either the upright or supine position. The subject is connected to a closed-circuit spirometer containing approximately

1 mCi/liter of radioactive xenon gas. He breathes continuously for a few minutes until xenon becomes uniformly distributed throughout his lung. When equilibrium is reached, the count rate over regions of the chest are followed during the wash-out of ^{133}Xe while the subject breathes room air. The wash-out curves are analyzed into exponential components, whose slopes give some indication of the ventilation rates for the different populations of alveoli in the region being examined.

An alternate approach used for the assessment of regional ventilation was to determine the rate at which ^{133}Xe appeared during rebreathing of xenon in a closed circuit system [8]. This determination is based on the time required to reach 90% of the equilibrium counting rate in the wash-in curve, expressed as a percentage of the calculated time, assuming uniform distribution.

The other xenon isotope used for assessment of regional ventilation and perfusion was ^{135}Xe [26]. It is produced from fission of ^{235}U in the reactor, and has a relatively short physical half-life of 9.13 hr. Its decay scheme is shown in Fig. I-2. Xenon-135 decays by emitting two groups of beta rays to the excited states of ^{135}Cr. Emission of the first group of beta rays (E_{β_1} = 910 keV, 97%) is followed by emission of 250 keV gamma rays. The second group of beta rays (E_{β_2} = 930 keV, 3%) decays by emitting 610-keV gamma rays. Xenon-135 is a particularly useful isotope because it emits essentially monoenergetic, 250-keV gamma rays. In addition, because a photon is emitted in 95% of the decays, ^{135}Xe has a high gamma-to-beta ratio. The use of ^{135}Xe for quantitative and topographical evaluation of ventilation and perfusion distribution in the human lung has been investigated in four normal subjects [26].

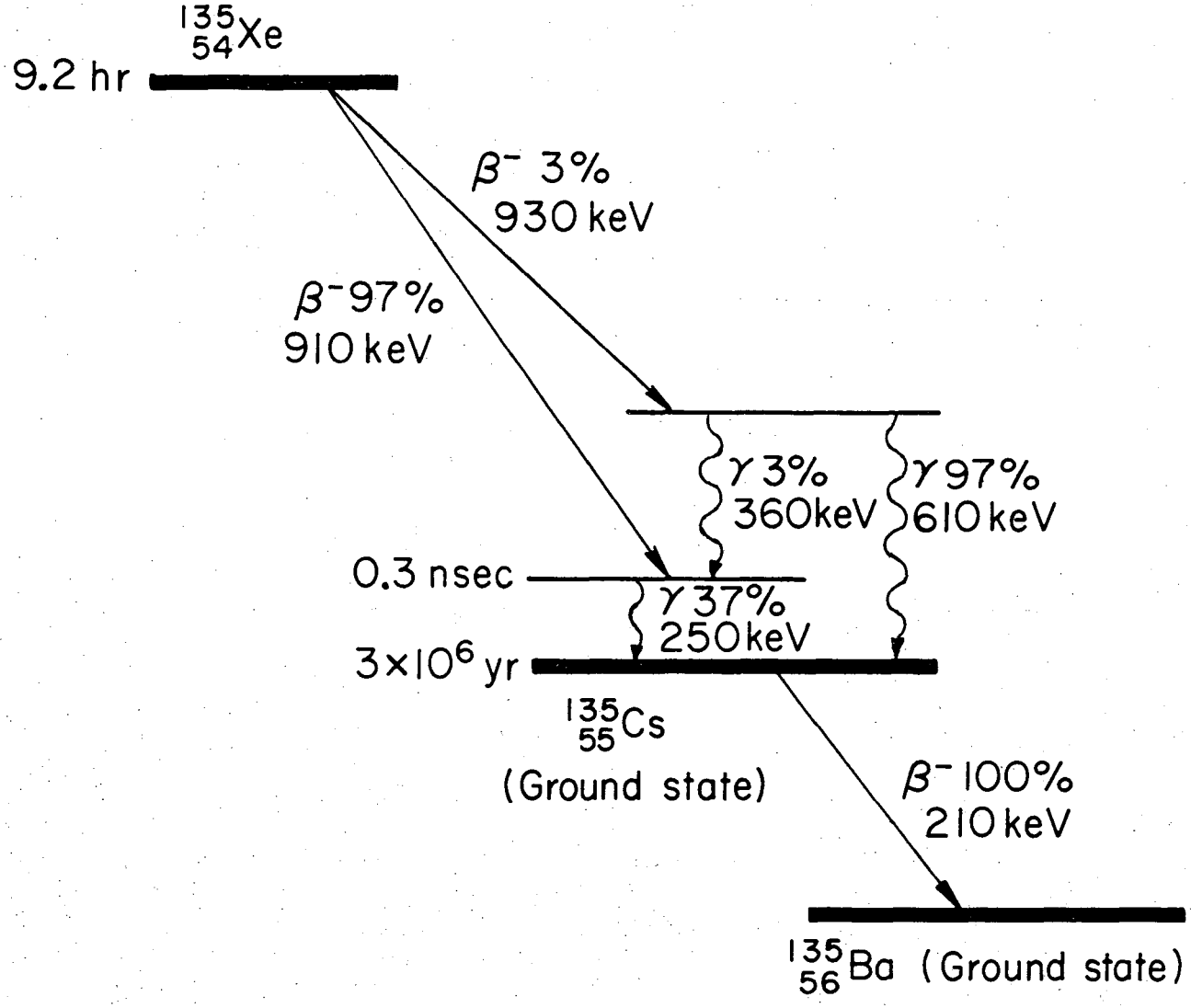

XBL761-5050

FIGURE I-2. Decay path of $^{135}_{54}$Xe.

Recently, the usefulness of a new xenon isotope, ^{127}Xe, has been investigated for lung imaging studies [56]. This xenon isotope has more favorable physical properties than ^{133}Xe and is a more suitable radionuclide for imaging with a gamma camera. Xenon-127 decays by electron capture to the excited states of ^{127}I with a half-life of 36.4 days. The energies and intensities of gamma radiation emitted by these excited states are summarized in Table I-2. Compared to ^{133}Xe, ^{127}Xe has a higher photon yield per millicurie, better photon energy for imaging with the Anger scintillation camera, lower radiation dose to the patient per useful photon detected, and longer shelf life. The longer physical half-life of ^{127}Xe is a substantial practical advantage because the biological half-life of xenon in the lungs is short. Figure I-3 shows the decay scheme of ^{127}Xe.

Krypton is the other noble gas used for lung function studies. Generator-produced ^{81m}Kr has been investigated as a potential isotope for pulmonary perfusion and ventilation studies [57,58]. Krypton-81m (T-1/2 = 13 sec) is milked from its cyclotron-produced parent, ^{81}Rb (T-1/2 = 4.7 hr). It decays by isomeric emission of 190-keV gamma rays (65%) to ^{81}Kr (T-1/2 = 2.1×10^5 yr), which then decays by electron capture to stable ^{81}Br. Although ^{81m}Kr has an ideal gamma-ray energy for imaging with the Anger scintillation camera, its short half-life limits the type of study that can be performed. Other isotopes of the inert krypton, such as ^{85}Kr (T-1/2 = 10.76 yr) that is a weak beta emitter ($E_{\beta max}$ = 0.67 MeV), have been used for assessment of regional blood flow. The unsuitable physical characteristics of these isotopes have discouraged investiagtions of them as tracers for lung function studies.

Table I-2. Photon emissions of $^{127}_{54}Xe$.

Energy (keV)	Intensity (%)
375	20.0
203	65.0
172	22.0
145	4.2
58	1.4

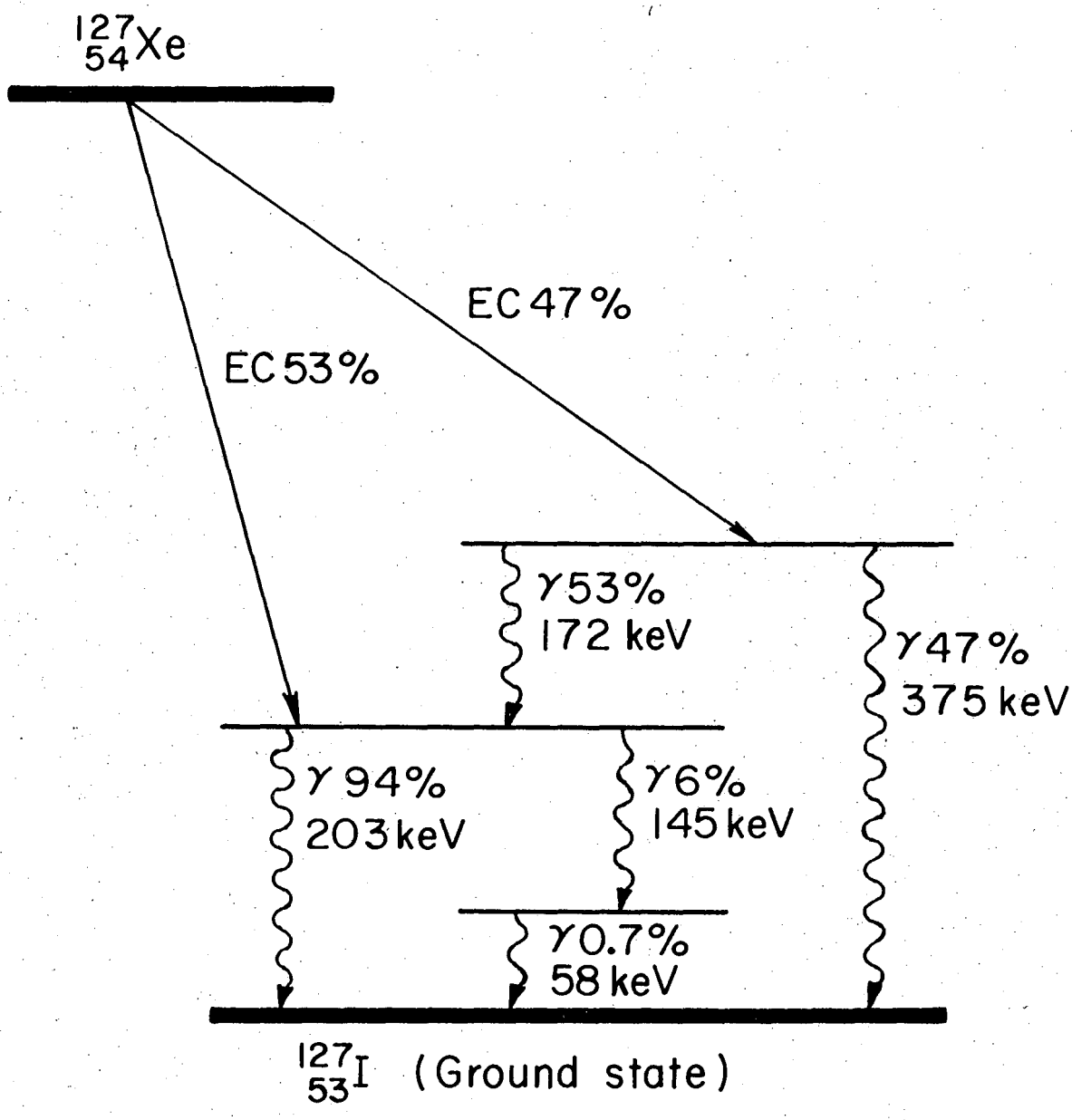

FIGURE I-3. Decay path of $^{127}_{54}$Xe.

I-2. Production and Availability of Xenon Isotopes

The most convenient and inexpensive method of producing radioisotopes is by bombardment of a suitable target with neutrons inside a nuclear reactor. Practically all medically important ratioisotopes are produced in this way; however some target materials must be bombarded with positively charged particles in a cyclotron.

Xenon-133 is now extensively used for the measurement of regional ventilation and blood flow because it is readily available and has reasonably useful physical characteristics. As a radiopharmaceutical, ^{133}Xe mixed with air or dissolved in sterile saline is available from several commercial suppliers. Although the convenience of having it delivered in this form is considerable, the cost is high. As a radiochemical, ^{133}Xe gas is readily and inexpensively obtained from Oak Ridge National Laboratory [59]. It is supplied as a gas either sealed in glass ampules or in metallic cylinders at low pressure and high specific activity. Techniques have therefore been developed by many laboratories for handling curie quantities of this radioisotope and for dispensing individual doses as gas and in saline for administration to the patient [60-68].

Xenon-133 is produced in reactors and obtained through recovery of fission products. At Oak Ridge National Laboratory [69], ^{133}Xe is produced by irradiating aluminum clad fuel cylinders composed of 5 g of 93% ^{235}U alloyed with 31 g of aluminum. When the aluminum is dissolved, the released ^{133}Xe is trapped and purified. The radiochemical purity obtained is greater than 99%; trace quantities of the atmospheric gases, ^{85}Cr, ^{132}Se, and ^{131m}Xe are present. The ^{235}U fission-product

decay chain that leads to ^{133}Xe is given in Fig. I-4. Direct fission yields and physical half-lives are listed below each nuclide. Thermal-neutron fission of ^{235}U yields 6.62% ^{133}Xe.

Xenon-135 is superior to ^{133}Xe because it emits 250-keV photons which, although not strongly absorbed in body tissues, are easily detected in the thin scintillation crystal of the gamma camera. However, ^{135}Xe is not readily available because of its short 9.13-hr half-life. Xenon-135 is produced through fission of ^{235}U in the reactor. The fission-product chain from ^{235}U fission leading to ^{135}Xe is given in Fig. I-5. Thermal-neutron fission of ^{235}U yields 5.9% ^{135}Xe.

Xenon-127 has become recently available. It is being produced in relatively large quantities in the Brookhaven Linear Isotope Producer [52]. Xenon-127 may be obtained by using a reactor or a cyclotron. The possible reactions for cyclotron production of xenon are the following:

$$^{127}_{53}I\ (p,n)\ ^{127}_{54}Xe$$

$$^{127}_{53}I\ (d,2n)\ ^{127}_{54}Xe$$

$$^{127}_{53}I\ (T,3n)\ ^{127}_{54}Xe$$

$$^{133}Cs\ (p,2p5n)\ ^{127}_{54}Xe$$

Iodine may be irradiated in the form of sodium or potassium iodide. When a 15-MeV deuteron beam with a 30 μA current is incident to a NaI powder target, yields of approximately 150 μCi/μA-hr were obtained [70]. Bombardment of the NaI target by a beam of 15-MeV protons has yielded

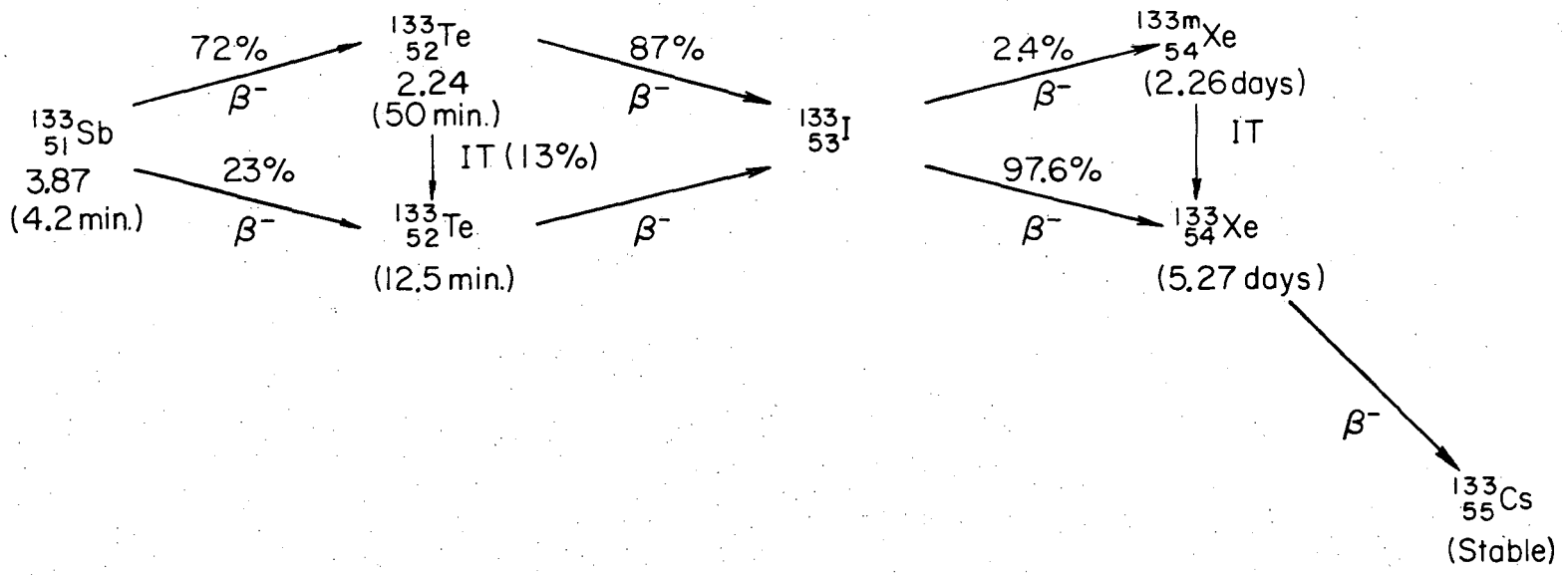

XBL761-5056

FIGURE I-4. Fission product chains from ^{235}U to ^{133}Xe.

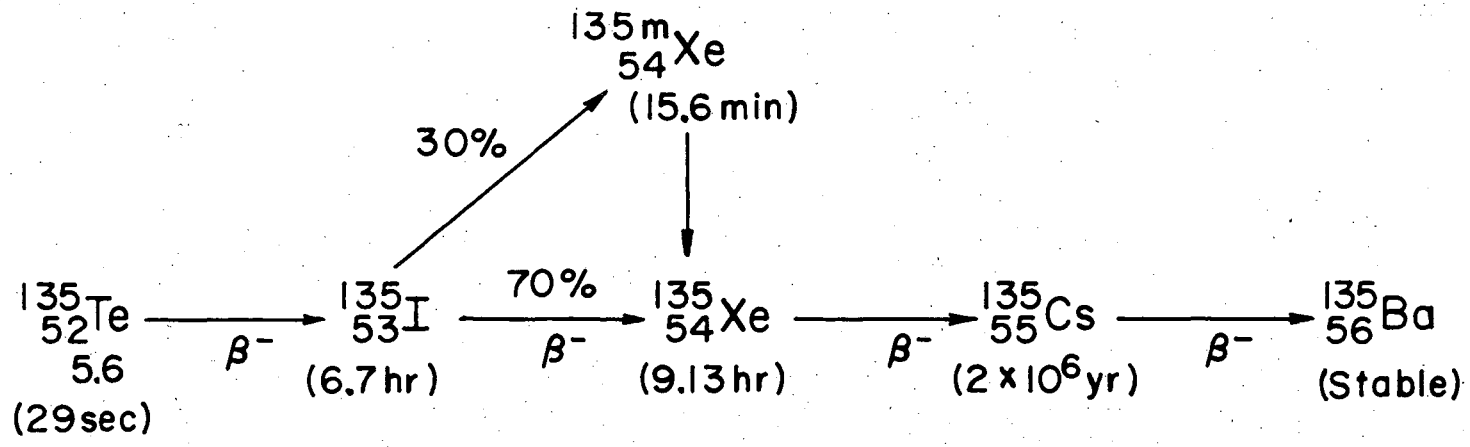

XBL763-5309

FIGURE I-5. Fission product chains from ^{235}U to ^{135}Xe.

60 to 80 μCi/μA-hr [56]. The Brookhaven Linac Isotope Producer, with a time-averaged beam current of ~ 180 μA, yields 15 Ci of ^{127}Xe during 720 hr of photon bombardment (~ 100 to 200 MeV) of a cesium chloride target [52].

I-3. Handling of Xenon-133

Xenon-133 is used clinically for an increasing variety of lung function tests, as well as for circulation studies. Techniques have therefore been developed by many laboratories for handling curie quantities of these radioisotopes and for dispensing individual doses as gas and in saline.

There are some important factors to take into account when manipulating ^{133}Xe. This isotope is highly soluble in oils, greases, rubbers, and a variety of plastics. A specimen of Buna-N-Nitrile placed in xenon solution for 24 hr absorbed 19% of the radioactivity; the quantity absorbed by a similar specimen of Viton was four times less [63]. When a bolus of xenon was injected through Teflon, polyethylene, and polyethane catheters, the uptake was found to be 0.5 to 2.0 percent. Depending upon the duration of contact with the plastic disposable syringes, 5 to 50 percent of the ^{133}Xe was found to be absorbed. Therefore, only glass syringes, which take up less than 1% of the xenon, should be used for dispensing this solution, and the use of lubricants such as paraffin or silicon should be avoided. Another consideration is that the partition ratio between air and water exceeds 10:1 for xenon. For example, in a 15-cm^3 vial containing 10 cm^3 of saline solution,

more than 90% of the ^{133}Xe will be in the gas phase and not available for injection. As a result, it is necessary to avoid the introduction of air bubbles during the preparation and use of such solutions.

I-4. Radiation Dosimetry of Xenon Isotopes

Administration of millicurie amounts of radioactive inert gases such as xenon to patients results in just millirads of tissue radiation exposure. This remarkably low exposure per unit of radioactivity is due to the very rapid and effective elimination of the gases by the lung and the low solubility of the gases in body tissues. The solubility coefficients are listed in Table I-3 [71]. In pulmonary studies the biological half-life of xenon is 1 to 10 minutes, much less than that of other radioactive tracers used in clinical applications. Estimates of the absorbed radiation does to body tissues that is associated with the use of xenon radioactive gas in the lungs have been published [66,72].

The tissue radiation dose from ^{133}Xe inhaled in one minute at a concentration of 1 $\mu Ci/cm^3$ corresponds to intravenous injection of 5 mCi of ^{133}Xe in an average normal subject [72]. Lassen has used the classical equations for computing absorbed dose,

$$D_\beta = 35.5 \cdot \bar{E}_\beta \cdot \int_{t_1}^{t_2} C(t)dt \quad \text{millirad}, \tag{1-1}$$

$$D_\gamma = 0.016 \cdot I_\gamma \cdot \rho \cdot g \cdot \int_{t_1}^{t_2} C(t)dt \quad \text{millirad}, \tag{1-2}$$

Table I-3. Solubility coefficients of ^{133}Xe.

Tissue	ml of gas/ml of tissue
Fat	1.70
Whole blood	0.18
Other tissues	0.13

where $\bar{E}_\beta$ is the mean energy of the beta particles in MeV,

$C(t)$ is the concentration of the isotope in microcuries for one gram of tissue as a function of time,

I_γ is the gamma dose factor in r/mCi-hr at 1 cm,

ρ is the specific gravity, and

g is the geometric factor.

Lassen has obtained the results summarized in Table I-4 [72].

A newer technique has been recommended by the Medical Internal Radiation Dose (MIRD) Committee of the Society of Nuclear Medicine [73-75]. This technique has been applied by Loken and Kush [66] to calculate the dose to lungs during rebreathing and wash-out of 30 mCi of ^{133}Xe from a 3-liter spirometer. The same technique has also been used to calculate the dose to body tissues during lung perfusion-ventilation studies after intravenous injection of 30 mCi of ^{133}Xe. The following expression was used to calculate the absorbed dose by the MIRD technique:

$$\bar{D} = A/m \sum_i \Delta_i \phi_i \quad \text{rads}, \tag{1-3}$$

where A is the cumulative activity in the source region (μCi-hr),

m is the mass of the organ for which the absorbed dose is being calculated (g),

Δ_i is the equilibrium absorbed-dose constant for radiation of type i (g-rads/μCi-hr), and

ϕ_i is the absorbed energy fraction for the i^{th} type of radiation (dimensionless).

Table I-4. Radiation dose in millirads for ^{133}Xe inhaled in a concentration of 1 $\mu Ci/cm^3$ for 1 min corresponding to intravenous injection of 5 mCi of ^{133}Xe [72].

Tissue	β Dose	γ Dose	Total Dose
Tracheal mucosa (mucus thickness 100 μ)	95.1	1.20	96.30
Lung	16.1	1.20	17.30
Adipose tissue (10%)	7.8	0.80	8.60
Other tissue	0.6	0.80	1.40
Gonads	0.6	0.33	0.96

Loken and Kush [66] assumed that an instantaneous equilibrium of xenon gas occurs between the spirometer and the subject, who has a tidal volume of 5 liters, a functional residual capacity of 3 liters, and a lung mass of 1000 g. Their results are summarized in Table I-5.

A complete comparison of the dosimetry calculations of ^{125}Xe, ^{127}Xe, and ^{133}Xe, as used for a regional pulmonary function study, has been made by Goddard and Akey [76]. Assuming an exponential model for wash-in and wash-out of gas, they showed that the integral value for the specific activity-time relationship is always equal to the product of the original spirometer concentration and the duration of the re-breathing period. The beta and electron doses to lungs, blood, fat, and gonads were calculated by using equation (1-1). The MIRD Committee calculation was used to determine the gamma radiation dose to different tissues. In their calculations they assumed the following: the lung mass is 1000 g; the lung mean density, 3 mg/cm^3; vital capacity, 5 liters; functional residual capacity, 2 liters; mean tidal volume, 1 liter; concentration of xenon in the spirometer, 1 cm^3/ℓ ; rebreathing time, 3 min.

The dose to mucosal surfaces has been calculated for a hemi-cylindrical airway, assuming a 1.5-cm radius, a length of 10 cm, and a mucus layer of 5 μm. Table I-6 summarizes doses in millirads to various tissues during rebreathing-washout, single breath-washout, and 10 mCi intravenous (I.V.) injection-washout of ^{125}Xe, ^{127}Xe, and ^{133}Xe. Total radiation doses received in various tissues (in millirads) from these isotopes used during a lung function investigation are also listed. Doses from ^{125}Xe and ^{127}Xe to the lung, blood, fat, and gonads differ by less than 10 percent.

Table I-5. Typical radiation dose in millirads during pulmonary function evaluation with ^{133}Xe [66].

Procedure		Lung	Fat (10%)	Blood	Other tissue
VENTILATION					
Rebreathing*	β	80.5			
	γ	2.7			
Washout	β	42.0			
	γ	1.4			
Total dose		126.6			
PERFUSION-VENTILATION†					
First breath-hold (20 sec)	β	34.8			
	γ	1.2			
Rebreathing to equilibrium (120 sec) and second breath-hold (20 sec) and washout	β	187.0	77.1	8.1	5.8
	γ	6.3	1.2	1.3	0.8
Third breath-hold (20 sec) and washout	β	25.2	4.9	0.5	0.4
	γ	0.8	0.8	—	—
Total dose		255.3	84.0	9.9	7.0

*One minute of rebreathing from a spirometer containing 30 mCi of ^{133}Xe.

†Intravenous injection of 30 mCi of ^{133}Xe.

Table I-6. Doses in millirads to various tissues for different procedures [76].

Isotope: Procedure		Lung	Blood	Fat	Gonads	Major airway	Mucosa
^{133}Xe:							
Rebreathing and washout	β	37.0	30.7	24.0	3.0	640.0	
	γ	2.0	0.7	0.7	0.7	2.0	
Single breath and washout	β	29.0	1.0	8.0	1.0	260.0	
	γ	1.0	0.3	0.3	0.3	1.0	
IV injection and washout	β	38.0	82.0*	10.0	1.0	256.0	
	γ	2.0	0.4	0.4	0.3	1.0	
Total dose		108.0	91.0	43.0	6.0	1160.0	
^{125}Xe or ^{127}Xe:						^{125}Xe	^{127}Xe
Rebreathing and washout	β	9.0	0.7	6.0	0.7	130.0	71.0
	γ	8.0	3.0	3.0	4.0	8.0	8.0
Single breath and washout	β	7.0	0.2	2.0	0.2	53.0	29.0
	γ	5.0	1.0	1.0	1.0	5.0	5.0
IV injection and washout	β	9.0	20.0*	3.0	0.3	52.0	29.0
	γ	6.0	2.0	2.0	2.0	5.0	5.0
Total dose		45.0	35.0	16.50	7.0	250.0	150.0

*Dose for 10 ml volume.

Because of the different methods and assumptions employed in each case, the results of estimates of absorbed radiation dose vary to some extent. Calculations indicate that fairly large quantities (millicuries) of a xenon radioisotope can be administered to a patient without excessive radiation exposure [62,72,76]. The dose to the cells lining the major airway is higher than that received by other tissues in the body. Of the three nuclides examined, ^{127}Xe gives the lowest radiation dose during a typical lung function study. Xenon-125 has the disadvantage that it decays to ^{125}I. It has been calculated [76] that for a typical lung investigation, approximately 1 μCi of ^{125}I would be deposited in the body, and would result in a radiation dose of 1500 mrad to the thyroid gland and 4 mrad to the whole body.

I-5. Release of Radioactive Xenon Gases

Unless properly contained or vented, expired radioactive xenon can be a source of radiation exposure. The usual disposal method is to exhaust the xenon gas to the atmosphere through the ventilation system.

The United States Nuclear Regulatory Commission, 10 CFR 20 [77], has set the following limits on the maximum concentrations of radioactive xenon gas that are permitted to be dispersed into the atmosphere through a stack, pipe, or similar structure (these concentrations are averaged over a one-year period):

Isotopes	Maximum Concentrations in Air (μCi/ml) Averaged Over a Year
$^{131m}_{54}Xe$	4×10^{-7}
$^{133}_{54}Xe$	3×10^{-7}
$^{135}_{54}Xe$	1×10^{-7}
Other xenon isotopes with half-life greater than 2 hr	1×10^{-10}

For a nuclear medicine laboratory that releases 50 mCi of radioactive xenon gas per week to the atmosphere, volumes of air contaminated to the above concentration levels are calculated to be 3.68×10^5 and 8×10^9 cubic meters for ^{133}Xe and ^{127}Xe respectively. Therefore, to minimize the atmospheric contamination caused by release of these isotopes, especially ^{127}Xe, it is preferable to confine and recycle them.

I-6. Methods Used for Containment of Radioactive Inert Gases

The widespread use of radioactive xenon gas in clinical applications as well as in medical research has led laboratories and industries to develop systems for delivering and containing xenon for these studies [60-68,78,79]. There are two methods for collection and containment of inert gases like xenon: One is the cryogenic technique, where radioactive gas is frozen out in a trap cooled with liquid nitrogen. The other method takes advantage of the high adsorbability of activated charcoal for xenon.

In the cryogenic trapping system [79], the exhaled air and radioactive xenon from the patient pass through a chemically activated trap, which removes the moisture and carbon dioxide from the gas mixture. The remaining gas is channeled to the trapping system composed of three different shells: The inner shell is a baffle assembly for freezing xenon; the middle shell contains pressurized liquid nitrogen, and the outer shell is a vacuumed Dewar vessel. Xenon is frozen inside the inner shell and the remaining gas mixture is pumped out with a high-volume pump. The major difficulty with this technique is the liquification of air in a static state which results in a dangerous condition where the trapped gas is allowed to return to room temperature.

Traps containing activated charcoal as the adsorbent have been investigated for use in pulmonary studies by directly collecting ^{133}Xe from the exhaled breath of patients [80]. The basic trap consisted of two cylindrical glass vessels each containing 100 g of loosely packed activated carbon granules. A moisture pretrap, consisting of a glass cylinder filled with Drierite ($CaSO_4$), was connected integrally to the inlet of the trap system at a flow rate of about 6 ℓ/min. A pulmonary bag was used as a damping volume to accommodate the nonuniform flow of exhaled air. The above setup was used to study fractional efficiency of xenon as a function of temperature [80]. Recently, commercial units containing charcoal-filled cartridges have been marketed by Atomic Development Corporation, Radiation-Medical Corporations, and others.

Although various designs have been developed for a delivery and trapping system to be used with radioactive xenon gas in these types of studies, no attention has been given to the design of a recycling

system. The high cost of production, long half-life, and hazardous release of radioactive effluents were incentives for the design of a recycling apparatus to be used with xenon isotopes, especially ^{127}Xe, in pulmonary function studies.

CHAPTER II.

THEORETICAL TREATMENT OF DYNAMIC ADSORPTION AND DESORPTION PROCESSES

II-1. Theory of Adsorption

The method often proposed for removing small amounts of radioactive noble gases from large volumes of carrier gas is by adsorption onto solid adsorbents. It is possible to achieve large decontamination and volume reduction factors by using solid adsorbents under proper conditions, thus reducing the problem of releasing these gases to the atmosphere.

When a gas molecule impinges against any solid surface from a random direction it can either bounce back from the surface elastically, with the angle of deflection equaling the angle of incidence, or it may stay at the surface for a period of time and come off in a direction unrelated to that from which it came. The latter is usually the case, the residence time depending on the type of molecule, its kinetic energy, and the nature and temperature of the surface. Clearly, when gas molecules strike continually upon a surface and remain there for a certain length of time before re-evaporating we shall find a higher concentration of the gas at this surface than in the bulk of gas. This tendency exhibited by all solids to condense upon their surface a layer of any gas with which they are in contact is termed adsorption.

The atoms or molecules constituting a solid are held together by different forces. Whatever the nature of the forces, an atom located inside the body of the solid is subjected to equal forces in all directions; whereas an atom in the plane of the surface is subjected to unbalanced forces, the inward pull being greater than the outward forces. This results in a tendency to decrease the surface area. Any process that tends to decrease the free surface energy (the product of surface tension and surface area) occurs spontaneously. An atom or a molecule of a gas adsorbed by the solid, saturates some of the unbalanced forces of the surface, thereby decreasing the surface tension. Thus all adsorption phenomena are spontaneous, and result in a decrease of the system's free energy. The process also involves loss of degrees of freedom; therefore there is also a decrease in entropy, and the adsorption process is always exothermic, regardless of the type of forces involved.

The forces that cause adsorption are the same ones that cause cohesion in solids and liquids, and are responsible for the deviation of real gases from the laws of ideal gases. The basic forces causing adsorption can be divided into two groups: intermolecular or van der Waals, and chemical, which generally involves electron transfer between the solid and the gas. Depending upon which of these two forces plays the major role in the adsorption process, it can be classified as either physical adsorption (van der Waals) or chemisorption. Thus, if in the process of adsorption the individuality of the adsorbed molecule (adsorbate) and the surface (adsorbent) are preserved, we have physical adsorption. If electron transfer or sharing occurs between the adsorbate

and the adsorbent, or if the adsorbate breaks up into atoms or radicals that are bound separately, then we are presented with chemisorption.

The number of molecules present on a surface at any one time depends on the number of molecules that strike the surface and the duration of their stay, "residence time." If n molecules strike a unit area of a surface per unit time, and remain there for an average time τ, then we shall find σ molecules per unit area of surface as

$$\sigma = n\tau \quad , \tag{2-1}$$

where cm^2 is a unit of area, the second is the unit of time, and n is the number of molecules striking 1 cm^2/sec.

By using Maxwell and Boyle-Gay Lussac equations, the following relation for n can be obtained [81]

$$n = \frac{NP}{\sqrt{2\pi MRT}} \quad , \tag{2-2}$$

where N = Avogadro number, giving the number of molecules/mole,

P = pressure in mm of Hg,

M = molecular weight,

T = absolute temperature, °K

R = molar gas constant.

Evaluation of this expression by using the known figures gives

$$n = \frac{3.52 \times 10^{22} \times P}{\sqrt{MT}} \quad . \tag{2-3}$$

The residence time τ is greatly dependent on temperature. Theoretically, from the Frenkel equation [81,82]:

$$\tau = \tau_o e^{Q/RT} \quad , \tag{2-4}$$

where τ_o is the time of oscillation of molecules in the adsorbed state. τ_o has a direct relation to the time of vibration of the constituent molecules or atoms of the adsorbing surface, and it will be of the same order of magnitude, namely 10^{-12} to 10^{-14} sec [83]. Q is the heat of adsorption, or the amount of heat that is liberated when the molecule changes from the gaseous to the adsorbed state.

II-1.1 Adsorption Equilibrium

Adsorption equilibrium is defined as when the number of molecules arriving on the surface is equal to the number of molecules leaving the surface in the gas phase. As discussed previously, the adsorbed molecules exchange energy with the structural atoms of the surface, and provided that the time of adsorption is long enough, they will be in thermal equilibrium with the surface atoms. In order to leave the surface, the adsorbed molecule has to take up sufficient energy from the fluctuations of the thermal energy at the surface so that the energy corresponding to the normal component of its vibrations surpasses the holding limit.

The amount of gas adsorbed when equilibrium is established at a given temperature and pressure is a function of the nature of the adsorbent and adsorbate. This includes on the one hand the physical structure of the adsorbent (the extent of its surface, the size, shape, and distribution of pores) and its chemical constitution -- and on the

other, the physical and chemical properties of the adsorbed gas molecules. Correlation of adsorption with certain physical properties of adsorbed gases has revealed [84] that the most easily condensable gases are adsorbed in the largest quantities by a given adsorbent. A study of the volumes of the different gases adsorbed by a given weight of adsorbent at a constant temperature and pressure shows that the adsorption increases as the boiling point of the gas increases. Table II-1 shows one study that demonstrates this [83].

II-1.2 Adsorption Isotherms

For a particular gas and a unit weight of a particular adsorbent, the amount of gas adsorbed at equilibrium is a function of the final pressure and temperature only:

$$a = f(p,T) \quad , \tag{2-5}$$

where a is the amount adsorbed per gram of adsorbent, p is the equilibrium pressure, and T is the absolute temperature. When true equilibrium is present it does not matter whether the initial pressure was higher or lower than the final pressure. At any specific final pressure, the amount of gas adsorbed is always the same. This is also true with respect to temperature. Usually either the pressure or temperature alone is varied, while the other is kept constant. When the pressure of the gas is varied and the temperature is kept constant, the plot of the amount adsorbed against the pressure is called the "adsorption isotherm," and the isotherm equation is

Table II-1. Absorption of gases by one gram of charcoal at 15°C [83].

Gas	Volume adsorbed (cm^3)	Boiling point (°C)
$COCl_2$	440	- 8
SO_2	380	- 10
CH_3Cl	277	- 24
NH_3	181	- 33
H_2S	99	- 62
HCl	72	- 83
N_2O	54	- 90
C_2H_2	49	- 84
CO_2	48	- 78
CH_4	16	- 164
CO	9	- 190
O_2	8	- 182
N_2	8	- 195
H_2	5	- 252

$$a = f(p) \quad , \text{ when } \quad T = \text{constant} \quad . \tag{2-6}$$

This is the most frequently determined experimental relation in the field of adsorption. Isotherms of xenon and krypton gases on charcoal are shown in Fig. II-1 [85]. Inserting the generalized value for n from equation (2-2) and values for τ from equation (2-4) into equation (2-1), we get

$$\sigma = \frac{NP}{\sqrt{2\pi MRT}} \tau_o e^{Q/RT} \quad . \tag{2-7}$$

For constant temperature, because the adsorbent and the adsorbate are defined, M and τ are constant. Thus we arrive at the simplest form of the adsorption isotherm: the linear adsorption isotherm

$$\sigma = k_o p \quad , \tag{2-8}$$

in which

$$k_o = \frac{N\tau_o e^{Q/RT}}{\sqrt{2\pi MRT}} \quad . \tag{2-9}$$

Equation (2-8) shows that the amount of gas adsorbed will be directly proportional to the pressure. Since the adsorption process is always exothermic, the amount adsorbed at equilibrium always decreases with increasing temperature. Fig. II-1 shows that this is actually the case: the lower the temperature the greater the adsorption.

A number of equations have been developed to follow the actual detail of the adsorption equilibrium process. The oldest and still widely used isotherm equation is the Freundlich [86] empirical equation

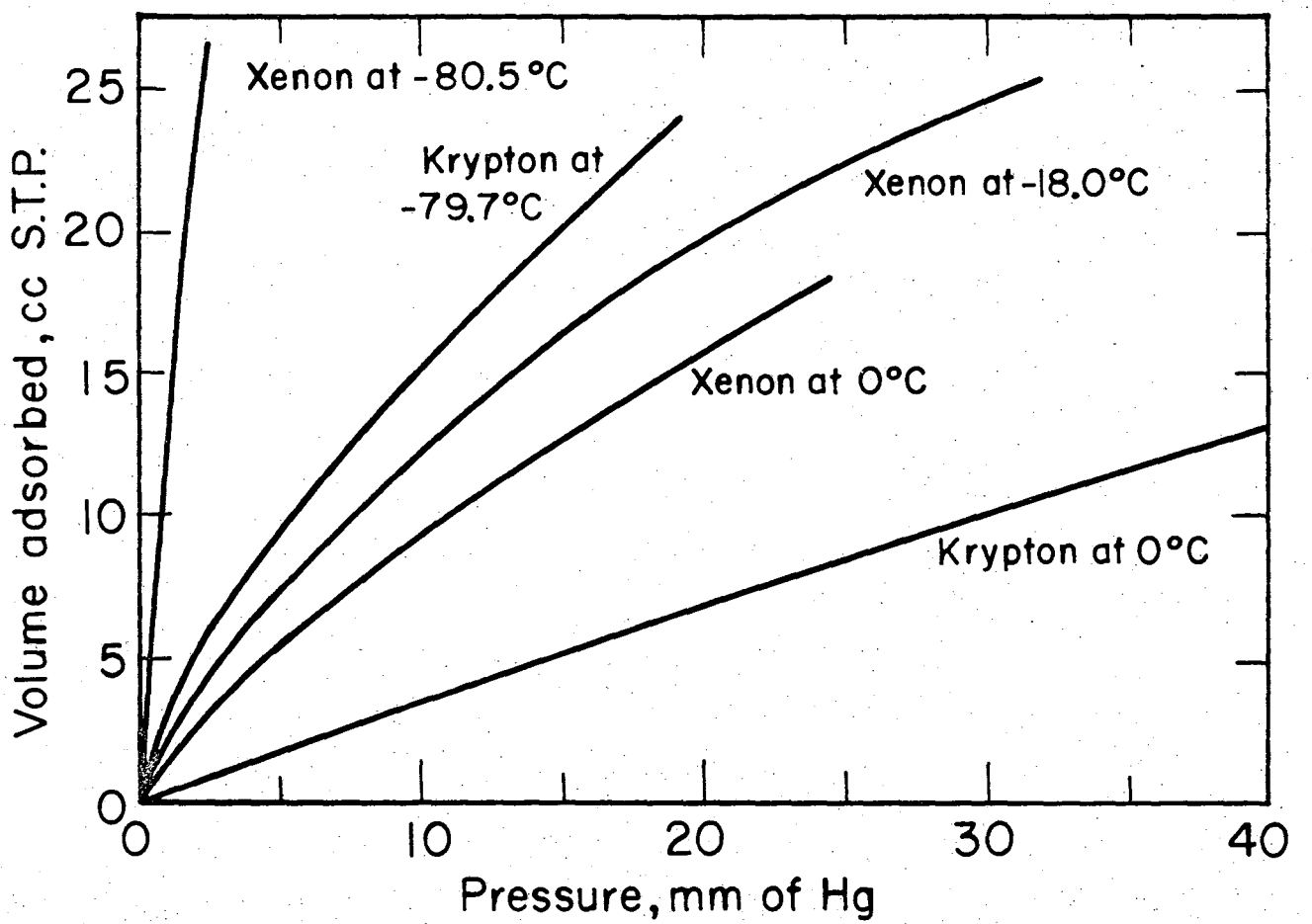

FIGURE II-1. Adsorption isotherms of xenon and krypton on charcoal.

$$V_a = \kappa p^{1/\nu} \tag{2-10}$$

where V_a is the volume adsorbed per unit weight of adsorbent, p is the equilibrium pressure, and κ and ν are constants. In general, a large number of experimental results in the field of van der Waal's adsorption can be expressed by means of the Freundlich equation in the middle pressure range. Adsorption of xenon on charcoal (Fig. II-1) is one of the examples where the Freundlich equation is obeyed.

The Freundlich equation is useful as an empirical formula but a better equation has been developed by Langmuir [87]. Derivation of the Langmuir isotherm is based on two assumptions: The first is that the probability of a molecule evaporating from the surface is the same whether or not the neighboring surface positions are occupied by other molecules. This is equivalent to assuming that the forces of interaction between the adsorbed molecules themselves are negligible. The second assumption is that any molecule coming from the gas phase and striking a molecule that is already adsorbed on the surface is elastically reflected, so that only those molecules that strike the bare surface condense. This assumption is equivalent to the postulation of a unimolecular layer of adsorption. The maximum amount of adsorption will be reached when the surface is covered with an adsorbed layer of molecules closely packed two-dimensionally, and no adsorption can take place upon the unimolecular adsorbed layer. If we denote by σ_o the number of adsorbed molecules per square centimeter of surface that would form a completely filled unimolecular layer, and by σ the number of molecules which are actually adsorbed, we see that the number of places available for adsorption will be $\sigma_o - \sigma$. If n molecules strike every square centimeter of surface each second, a frac-

tion, σ/σ_o , will strike on molecules that are already there, and will return to the gas phase immediately. It is, therefore, $1 - (\sigma/\sigma_o)$ which is available for adsorption. Equation (2-1) now modifies to

$$\sigma = n(1 - \sigma/\sigma_o)\tau \quad . \tag{2-11}$$

This may be written as

$$\sigma = \frac{\sigma_o n\tau}{\sigma_o + n\tau} \quad . \tag{2-12}$$

Instead of the surface concentration one may use the fraction of the surface covered,

$$\theta = \sigma/\sigma_o = \frac{n\tau}{\sigma_o + n\tau} \quad , \tag{2-13}$$

or

$$\theta = \frac{n\tau/\theta_o}{1 + n\tau/\theta_o} \quad . \tag{2-14}$$

Substituting equation (2-2) for n , one obtains the Langmuir isotherm equation

$$\theta = \frac{kp}{1 + kp} \quad , \tag{2-15}$$

where

$$k = \frac{N}{\sqrt{2\pi MRT}} \times \tau/\sigma_o \tag{2-16}$$

is the adsorption coefficient and a function of temperature only.

The limiting form of the Langmuir isotherm at high and low pressure is important. At low pressure the term kp of equation (2-15) becomes

small with respect to 1, and equation (2-15) reduces to

$$\theta = kp \quad .$$

Therefore, the adsorption varies linearly with pressure, as in equation (2-8); i.e., the Langmuir isotherm reduces to a linear isotherm at low pressure. In the high pressure range, the term kp becomes large with respect to 1, and θ approaches 1; i.e., the adsorbed monolayer will be completed or saturated.

The application of adsorbents for removal of radioactive inert gases such as xenon from a flowing gas stream involves the use of a dynamic system. Generally the gas mixture is passed through the adsorbent which is used in a fixed bed.

II-2. Dynamic Adsorption Process

In the process of dynamic adsorption, an adsorbate such as xenon is physically adsorbed from the carrier gas stream, air, onto the surface of a solid adsorbent such as activated charcoal. At every point, gas molecules will be desorbed from the surface at a lower rate as others are being adsorbed from the gas stream. This process effectively increases the time required for a noble gas molecule to pass through a portion of the adsorbed system relative to the passage time required for the carrier gas molecules, and results in the creation of a concentration wave front in the adsorbent bed. The wave front moves from the inlet end of the bed toward the outlet. This is an unsteady state process, the xenon concentration being a function not only of space but also of time.

Several theoretical treatments have been used to charactierize the dynamic adsorption process. Recent developments have included attempts to describe an adsorber bed in terms of the number of discrete theoretical stages that it represents under a given set of operating conditions [88,89]. In one of the later approacher, proposed by Browning and Bolta [89], it is assumed that a series of N theoretical chambers comprises the adsorber column, and that the gas flow into each chamber is instantly distributed and brought to adsorption equilibrium. For linear adsorption isotherms, which apply at low adsorbate concentrations, the mass balance for the adsorbate across each of the N stages is

$$dg_i/dt = - \frac{FN}{k_d M} (g_i - g_{i-1}) \quad , \tag{2-17}$$

where g_i = volume fraction of adsorbate gas phase leaving the i^{th} stage at time t ;

F = total gas flow rate;

M = total charcoal mass;

N = number of theoretical equilibrium stages,

t = time; and

k_d = dynamic adsorption coefficient.

Solution of the series of N differential equations for a unit input pulse at time $t = 0$, yield the following effluent concentration profile for the N^{th} stage:

$$g_N = \left[\frac{N^N F^{N-1} t^{N-1}}{(N-1)!(k_d M)^N} \right] e^{\left(- NFt/k_d M \right)} \quad . \tag{2-18}$$

By differentiating equation (2-18) with respect to time and setting the result equal to zero, an equation relating the number of theoretical plates to the time necessary to reach maximum concentration of the adsorbate in the effluent is found:

$$t_{max} = \left(\frac{N - 1}{N}\right)\left(\frac{k_d M}{F}\right) \quad . \tag{2-19}$$

This model, while predicting the distribution of the adsorbate in the effluent for a pulse input of noble gases, does not provide the spatial distribution of the concentration wave in the adsorption column.

The most general method available for the prediction and interpretation of adsorption column performance is that of Thomas [90,91]. He has developed, for cases of constant input rate of adsorbate, explicit general relations for the saturation of an initially empty adsorbent bed, as well as for the converse elution of a completely saturated column. Applying a modification of his adsorption kinetic approach to the case of exponential input of radioactive gas, general relations are developed for the adsorbed xenon concentration in a charcoal column and an air stream during the dynamic adsorption process.

II-2.1 Conservation Equations

Consider a stream of xenon and air flowing through a bed of charcoal with cross sectional area A cm^2 and length L cm, as indicated in Fig. II-2. The conservation condition for a quantity of xenon which enters a layer of charcoal of thickness dz in time dt may be expressed as follows:

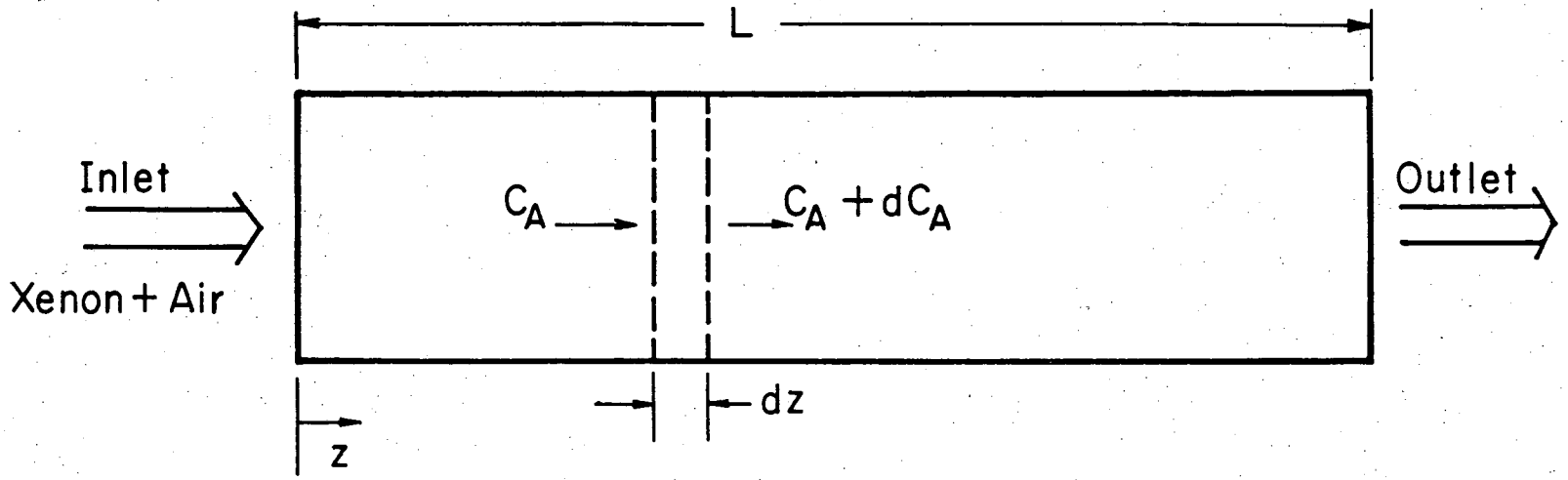

XBL764-5394

FIGURE II-2. Flow of gas through an adsorption column.

$$c_A F dt = \frac{\partial q_A}{\partial t} (A dz) dt + (c_A + dc_A) F dt \quad , \tag{2-20}$$

where c_A = concentration of xenon in air stream in adsorption process, μCi of xenon per cm^3 of air;

q_A = concentration of adsorbed xenon in bed during adsorption process, μCi of xenon per cm^3 of bed; and

F = volumetric flow rate of gaseous mixture cm^3/min .

Equation (2-20) may be arranged to give

$$- dc_A = \frac{A}{F} \frac{\partial q_A}{\partial t} dz \quad . \tag{2-21}$$

Because c_A is a function of the variables z and t , the total differential is

$$dc_A = \left(\frac{\partial c_A}{\partial z} \right)_t dz + \left(\frac{\partial c_A}{\partial t} \right)_z dt \quad . \tag{2-22}$$

Taking

$$dz/dt = u \quad , \tag{2-23}$$

and

$$F = uA\alpha \quad , \tag{2-24}$$

where u is the linear velocity through the interstices between charcoal particles and α is the porosity (i.e., the fraction of voids per unit gross volume of bed), one obtains

$$- \left[\left(\frac{\partial c_A}{\partial z} \right) dz + \left(\frac{\partial c_A}{\partial t} \right) dt \right] = \frac{1}{\alpha u} \frac{\partial q_A}{\partial t} dz \quad , \tag{2-25}$$

which can be arranged to give

$$\frac{u\partial c_A}{\partial z} + \frac{\partial c_A}{\partial t} + \frac{1}{\alpha}\frac{\partial q_A}{\partial t} = 0 \quad . \tag{2-26}$$

It is implicitly assumed in the derivation of equation (2-26) that the concentration of xenon in the air stream is small and that the diffusion in the direction of flow is negligible.

The solution to equation (2-26) depends on the mathematical relation one assumes for $\partial q_A/\partial t$, the local rate of removal of the gas by charcoal; the particular mathematical form to be chosen depends on the mechanism of the removal process. If xenon is adsorbed reversibly, the equation obtained for c_A depends on the character of the adsorption isotherm. For pure physical adsorption, as described by the Langmuir equation, the isotherm becomes linear when the concentration of adsorbate on the adsorbing surface is sufficiently low.

A way to introduce the time factor into the theory is to take explicit account of the finite rate of adsorption. Assuming that for a low xenon concentration, the rate of adsorption and desorption is first-order with respect to the xenon gas phase and adsorbed phase, we may write

$$\frac{1}{\alpha}\left(\frac{\partial q_A}{\partial t}\right)_z = k_1 c_A - k_2 q_A \quad , \tag{2-27}$$

where k_1 and k_2 are the rate constants in terms of which the process is described. The resulting equilibrium relation is

$$q_A = \frac{k_1}{k_2} c_A = k c_A \quad , \tag{2-28}$$

in which k, a constant, is proportional to the slope of the adsorption isotherm. The mechanism represented by equation (2-27) has been called by Thomas [91] the case of linear kinetics.

II-2.2 Boundary Conditions

The solution of the differential equations (2-26) and (2-27) for the case of constant input concentration of adsorbate is given by Thomas [91] in his treatment of chromatography. This initial condition is a special case for the exponential input concentration of xenon into a bed, which is encountered in experiments performed to determine the effectiveness of charcoal beds for trapping xenon gas in a high-velocity air stream.

For a well-mixed single open system of volume V_o and inflow-outflow rate of F, containing I amount of traces such as xenon at zero time, the concentration, c_A, of xenon leaving the pool at any time t is given by

$$c_A(t) = \frac{I}{V_o} e^{-\frac{Ft}{V_o}} \quad . \tag{2-29}$$

If $c_{Ao} = I/V_o$ is the concentration of tracer at time $t = 0$, then

$$c_A = c_{Ao} e^{-\frac{Ft}{V_o}} \quad , \tag{2-30}$$

and if the output of such a system flows into a charcoal adsorption column that is initially free of xenon, it would result in an exponential concentration input of xenon to the column.

II-2.3 Analytical Solution

The complete statement of the problem to be solved is

$$u \frac{\partial c_A(z,t)}{\partial z} + \frac{\partial c_A(z,t)}{\partial t} + \frac{1}{\alpha} \frac{\partial q_A(z,t)}{\partial t} = 0 \quad , \tag{2-26}$$

$$\frac{1}{\alpha} \frac{\partial q_A(z,t)}{\partial t} = k_1 c_A(z,t) - k_2 q_A(z,t) \quad , \tag{2-27}$$

$$c_A(0,t) = c_{Ao} e^{-(F/V_o)t} \quad , \tag{2-30}$$

$$q_A(z,0) = 0 \quad . \tag{2-31}$$

By making the following change of variables,

$$x = z/u \quad , \tag{2-32}$$

$$y = \alpha(t - z/u) \quad , \tag{2-33}$$

equations (2-26) and (2-27) simplify to

$$\frac{\partial q_A(x,y)}{\partial y} + \frac{\partial c_A(x,y)}{\partial x} = 0 \quad , \tag{2-34}$$

$$\frac{\partial q_A(x,y)}{\partial y} = k_1 c_A(x,y) - k_2 q_A(x,y) \quad ; \tag{2-35}$$

and equations (2-30) and (2-31) may be written as

$$c_A(0,y/\alpha) = c_{Ao} e^{-\left(\frac{Fy}{\alpha V_o}\right)} = c_{Ao} e^{-\left(\frac{uAy}{\alpha V_o}\right)} \quad , \text{ where } x = 0 \tag{2-36}$$

$$q_A(xu,0) = 0 \quad \text{when} \quad y = 0 \quad . \tag{2-37}$$

Let

$$\lambda = \frac{uA}{\alpha V_o} \quad , \tag{2-38}$$

then

$$c_A(0,y/\alpha) = c_{Ao}e^{-\lambda y} \quad , \text{ where } x = 0 \ . \tag{2-39}$$

Note that equation (2-34) is the necessary and sufficient condition for the existence of a function F_1 given by

$$dF_1(x,y) = q_A dx - c_A dy \quad , \tag{2-40}$$

in which dF_1 is a perfect differential. In terms of F_1 the relations for the calculation of the concentrations are

$$q_A = \frac{\partial F_1(x,y)}{\partial x} \quad , \tag{2-41}$$

$$c_A = -\frac{\partial F_1(x,y)}{\partial y} \ . \tag{2-42}$$

Then it follows from equation (2-35) that

$$\frac{\partial^2 F_1}{\partial x \partial y} + k_1 \frac{\partial F_1}{\partial y} + k_2 \frac{\partial F_1}{\partial x} = 0 \ . \tag{2-43}$$

If we make the simplifying substitution

$$F_1(x,y) = e^{-(k_1 x + k_2 y)} \phi(x,y) \quad , \tag{2-44}$$

then equation (2-43) reduces to

$$\frac{\partial^2 \phi(x,y)}{\partial x \partial y} - k_1 k_2 \phi(x,y) = 0 \ . \tag{2-45}$$

Combining equation (2-41) and (2-44) with equation (2-39), we obtain

$$-\frac{\partial F_1(0,y)}{\partial y} = -k_2 e^{-k_2 y}\phi(0,y) + e^{-k_2 y}\frac{\partial \phi(0,y)}{y} = c_{Ao}e^{-\lambda y} \quad . \tag{2-46}$$

Solving equation (2-46) for $\phi(0,y)$, we get

$$\phi(0,y) = \frac{c_{Ao}}{\lambda} e^{(k_2 - \lambda)y} + \left(1 - \frac{c_{Ao}}{\lambda}\right)e^{k_2 y} \equiv G_1(y) \quad , \tag{2-47}$$

in the same way combination of equation (2-41) and (2-44) with equation (2-37) gives

$$\frac{\partial F_1(x,0)}{\partial x} = -k_1 e^{-k_1 x}\phi(x,0) + e^{-k_1 x}\frac{\partial \phi(x,0)}{\partial x} = 0 \quad . \tag{2-48}$$

Thus, solving for $\phi(x,0)$, we get

$$\phi(x,0) = \phi(0,0)e^{k_1 x} = e^{k_1 x} \equiv H_1(x) \quad . \tag{2-49}$$

Equations (2-47) and (2-49) define functions $G_1(y)$ and $H_1(x)$. In these deductions, the expression $\phi(0,0)$ has been put equal to unity so that $c_A = c_{Ao}$ for $x = 0$ and $y = 0$.

It follows that the original problem is reduced to the solution of equations (2-45), (2-47), and (2-49). This system of equations may be further reduced to two others. Consider these two systems of equations:

$$\frac{\partial^2 \phi_1(x,y)}{\partial x \partial y} - k_1 k_2 \phi_1(x,y) = 0 \quad , \tag{2-50}$$

$$\phi_1(0,y) = G_1(y) \quad , \text{ where } x = 0 \quad , \tag{2-51}$$

$$\phi_1(x,0) = 1 \quad , \text{ when } y = 0 \quad ; \tag{2-52}$$

$$\frac{\partial^2 \phi_2(x,y)}{\partial x \partial y} - k_1 k_2 \phi_2(x,y) = 0 \quad , \tag{2-53}$$

$$\phi_2(0,y) = 0 \quad , \tag{2-54}$$

and

$$\phi_2(x,0) = H_1(x) - 1 \quad . \tag{2-55}$$

It may be easily shown that the sum $\phi_1 + \phi_2$ satisfies equation (2-45), as well as equation (2-47) and (2-49); therefore $\phi = \phi_1 + \phi_2$ is the desired solution.

The solution to the above systems may be found by the method of the Laplace transform. Let

$$\bar{\phi}_1(x,p) = L\left[\phi_1(x,y)\right] \quad , \tag{2-56}$$

then equations (2-50) and (2-51) become

$$p \frac{\partial \bar{\phi}_1(x,p)}{\partial x} - k_1 k_2 \bar{\phi}_1(x,p) = 0 \quad , \tag{2-57}$$

$$\bar{\phi}_1(0,p) = \bar{G}_1(p) \quad , \text{ when } x = 0 \quad . \tag{2-58}$$

Solving equation (2-57) with the boundary condition (2-58), we get

$$\bar{\phi}_1(x,p) = \bar{G}_1(p) e^{\frac{k_1 k_2 x}{p}} \quad . \tag{2-59}$$

It can be shown that the inverst transform of this expression is a convolution of $G'(y)$ and $I_0(2\sqrt{k_1 k_2 xy})$ where I_0 is the zeroth-order

Bessel function for an imaginary argument, or

$$\phi_1(x,y) = L^{-1}\left[\bar{\phi}_1(x,p)\right] = \int_0^y G'_1(\xi) I_0\left(2\sqrt{k_1 k_2 x(y-\xi)}\right) d\xi \qquad (2\text{-}60)$$

where

$$G'_1(\xi) = c_{Ao}\left(\frac{k_2}{\lambda} - 1\right) e^{(k_2 - \lambda)\xi} + k_2\left(1 - \frac{c_{Ao}}{\lambda}\right) e^{k_2 \xi} \qquad (2\text{-}61)$$

is the derivative of $G_1(y)$.

The solution of equation (2-53) may be obtained in the same way by taking the transform with respect to x. Let

$$\bar{\phi}_2(s,y) = L\left[\phi_2(x,y)\right] \quad , \qquad (2\text{-}62)$$

then equations (2-53) and (2-54) become

$$s\frac{\partial \bar{\phi}_2(s,y)}{\partial y} - k_1 k_2 \bar{\phi}_2(s,y) = 0 \quad , \qquad (2\text{-}63)$$

$$\bar{\phi}_2(s,0) = \bar{H}_1(s) - \frac{1}{s} \quad . \qquad (2\text{-}64)$$

The solution to equations (2-63) and (2-64) is

$$\bar{\phi}_2(s,y) = \left[\bar{H}_1(s) - \frac{1}{s}\right] e^{\frac{k_1 k_2 y}{s}} \quad . \qquad (2\text{-}65)$$

After some manipulation, the inverse transform of this expression may be written as

$$\phi_2(x,y) = \int_0^x H'_1(\eta) I_0\left(2\sqrt{k_1 k_2 y(x-\eta)}\right) d\eta + I_0\left(2\sqrt{k_1 k_2 xy}\right) \quad , \qquad (2\text{-}66)$$

where

$$H'_1(\eta) = k_1 e^{k_1 \eta} \tag{2-67}$$

is the derivative of $H_1(x)$. The final solution for ϕ is then

$$\phi(x,y) = \phi_1(x,y) + \phi_2(x,y) = I_0\left(2\sqrt{k_1k_2xy}\right) + \int_0^y G'_1(\xi) I_0\left(2\sqrt{k_1k_2x(y-\xi)}\right) d\xi$$

$$+ \int_0^y H'_1(\eta) I_0\left(2\sqrt{k_1k_2y(x-\eta)}\right) d\eta \quad . \tag{2-68}$$

It can be easily shown that this solution satisfies equation (2-45) and the boundary condition equations (2-47) and (2-49).

To compute $c_A(x,y)$ and $q_A(x,y)$, it is necessary first to compute the partial derivatives of $F_1(x,y)$ as shown in equations (2-41) and (2-42). After some manipulation with Bessel functions, the following expression for $c_A(x,y)$ and $q_A(x,y)$ may be obtained:

$$c_A(x,y) = -\frac{\partial F_1}{\partial y} = e^{-(k_1x + k_2y)} \Bigg\{ k_2 I_o\left(2\sqrt{k_1k_2xy}\right)$$

$$+ k_2 \int_0^x H'_1(\eta) I_0\left[2\sqrt{k_1k_2y(x-\eta)}\right] d\eta$$

$$+ k_2 \int_0^y G'_1(\xi) I_0\left[2\sqrt{k_1k_2x(y-\xi)}\right] d\xi - \sqrt{\frac{k_1k_2x}{y}}\, I_1\left(2\sqrt{k_1k_2xy}\right)$$

$$- \int_0^x H'_1(\eta) \sqrt{\frac{k_1k_2(x-\eta)}{y}}\, I_1\left[2\sqrt{k_1k_2y(x-\eta)}\right] d\eta - G'_1(y)$$

$$- \int_0^y G'_1(\xi) \sqrt{\frac{k_1k_2x}{y-\xi}}\, I_1\left[2\sqrt{k_1k_2x(y-\xi)}\right] d\xi \Bigg\} \quad ; \tag{2-69}$$

$$q_A(x,y) = \frac{\partial F_1}{\partial x} = e^{-(k_1x + k_2y)} \left\{ -k_1 I_0\left(2\sqrt{k_1k_2xy}\right) + \sqrt{\frac{k_1k_2y}{x}}\, I_1\left(2\sqrt{k_1k_2xy}\right) - k_1 \int_0^x H'_1(\eta) I_0\left[2\sqrt{k_1k_2y(x-\eta)}\right] d\eta \right.$$

$$- k_1 \int_0^y G'_1(\xi) I_0\left[2\sqrt{k_1k_2x(y-\xi)}\right] d\xi$$

$$+ \int_0^y G'_1(\xi) \sqrt{\frac{k_1k_2(y-\xi)}{x}}\, I_1\left[2\sqrt{k_1k_2x(y-\xi)}\right] d\xi + F'_1(x)$$

$$\left. + \int_0^x H'_1(\eta) \sqrt{\frac{k_1k_2y}{x-\eta}}\, I_1\left[2\sqrt{k_1k_2y(x-\eta)}\right] d\eta \right\} . \qquad (2\text{-}70)$$

Rather than convert equations (2-69) and (2-70) into the original z and t variables, it is generally easier to convert the experimental data z and t into the x and y coordinates.

II-3. Dynamic Desorption Process

During the dynamic desorption process, radioactive noble gas is flushed from the surface of the charcoal by passing through a stream of appropriate fluid under conditions that favor desorption of this gas. It will be shown later that steam is an effective fluid for removing xenon gas from charcoal surface. Water vapor influences the desorption of noble gases merely by increasing the kinetic energy of the gas molecules and by occupying the space on the surface of the charcoal. Theoretical analysis of this case is similar to the one in the adsorption process. By

using a linear kinetic approach, general relations for the xenon concentration in the effluent and in the adsorbed phase are developed for cases of elution of arbitrary and Gaussian xenon distributions in the charcoal bed. The Gaussian distribution was chosen because it best fitted the experimental xenon distribution found in charcoal columns at the end of the adsorption process.

II-3.1 Solution for an Arbitrary Xenon Distribution on Charcoal

Consider the same charcoal column having an arbitrary distribution of xenon, $q_o(z)$, adsorbed on it at equilibrium. Suppose this column is purged with steam folwing with a linear velocity u_s cm sec^{-1}. The conservation equation (2-26) relating the concentration of xenon in the gas phase to the adsorbed phase is valid in this case, as is the kinetic equation (2-27) with different rate constants. Thus we get the solution to the following set of equations

$$u_s \frac{\partial c_D(z,t)}{\partial z} + \frac{\partial c_D(z,t)}{\partial t} + \frac{1}{\alpha} \frac{\partial q_D(z,t)}{\partial t} = 0 \quad , \qquad (2\text{-}71)$$

$$\frac{1}{\alpha}\left(\frac{\partial q_D(z,t)}{\partial t}\right) = L_1 c_D(z,t) - L_2 q_D(z,t) \qquad (2\text{-}72)$$

with the following boundary conditions

$$c_D(0,t) = 0 \quad , \text{ at } \quad z = 0 \qquad (2\text{-}73)$$

$$q_D(z,0) = q_o(z) \quad , \text{ for } \quad t \leqslant \frac{z}{u_s} \qquad (2\text{-}74)$$

must be obtained. The subscript D indicates the concentration during

the desorption process. L_1 and L_2 are the new rate constants for the case of column elution by steam.

We proceed in the solution, as in the first case (2-40), by making the same change of the variable. A function $F_2(x,y)$ may be defined such that

$$\frac{\partial^2 F(x,y)}{\partial x \partial y} + L_1 \frac{\partial F_2(x,y)}{\partial y} + L_2 \frac{\partial F_2(x,y)}{\partial x} = 0 \quad . \qquad (2\text{-}75)$$

As before, this can be reduced to

$$\frac{\partial^2 \psi(x,y)}{\partial x \partial y} - L_1 L_1 \psi(x,y) = 0 \quad , \qquad (2\text{-}76)$$

by the following change of variables;

$$F_2(x,y) = e^{-(L_1 x + L_2 y)} \psi(x,y) \quad . \qquad (2\text{-}77)$$

By using the same change of variables given by equations (2-32) and (2-33), equations (2-73) and (2-74) reduce to

$$c_D(0,y) = 0 \quad , \text{ where } x = 0 \quad , \text{ and} \qquad (2\text{-}78)$$

$$q_D(x,0) = q_1(x) \quad , \text{ when } y = 0 \quad . \qquad (2\text{-}79)$$

The corresponding boundary values for ψ follow from equations (2-41), (2-42), (2-78), and (2-79):

$$\psi(0,y) = e^{L_2 y} \equiv G_2(y) \quad , \qquad (2\text{-}80)$$

$$\psi(x,0) = e^{L_1 x}\left[1 + \int_0^x q_1(\gamma)\,d\gamma\right] \equiv H_2(x) \quad . \qquad (2\text{-}81)$$

These equations define $G_2(y)$ and $H_2(x)$. Hence the problem to be solved is analogous to that of the adsorption process, except for the boundary condition function, which is not analytically defined. Similar to equation (2-68), the solution for ψ is as follows:

$$\psi(x,y) = I_0\left(2\sqrt{L_1L_2xy}\right) + \int_0^y G'_2(\xi) I_0\left[2\sqrt{L_1L_2x(y-\xi)}\right] d\xi$$

$$+ \int_0^x H'_2(\eta) I_0\left[2\sqrt{x-\eta)}\right] d\eta \quad ; \tag{2-82}$$

and expressions for $c_D(x,y)$ and $q_D(x,y)$, similar to equations (2-69) and (2-70), may be written as:

$$c_D(x,y) = -\frac{\partial F_2(x,y)}{\partial y} = e^{-(L_1x + L_2y)}\left\{L_2 I_0\left(2\sqrt{L_1L_2xy}\right)\right.$$

$$+ L_2 \int_0^x H'_2(\eta) I_0\left[2\sqrt{L_1L_2y(x-\eta)}\right] d\eta$$

$$+ L_2 \int_0^y G'_2(\xi) I_0\left[2\sqrt{L_1L_2x(y-\xi)}\right] d\xi - \sqrt{\frac{L_1L_2x}{y}}\, I_1\left(2\sqrt{L_1L_2xy}\right)$$

$$- G'_2(y) - \int_0^x H'_2(\eta)\sqrt{\frac{L_1L_2(x-\eta)}{y}}\, I_1\left[2\sqrt{L_1L_2y(x-\eta)}\right] d\eta$$

$$\left. - \int_0^y G_2(\xi)\sqrt{\frac{L_1L_2x}{y-\xi}}\, I_1\left[2\sqrt{L_1L_2x(y-\xi)}\right] d\xi \right\} \quad ; \tag{2-83}$$

$$q_D(x,y) = \frac{\partial F_2(x,y)}{\partial x} = e^{-(L_1 x + L_2 y)} \left\{ - L_1 I_0\left(2\sqrt{L_1 L_2 xy}\right) \right.$$

$$+ \sqrt{\frac{L_1 L_2 y}{x}}\, I_1\left(2\sqrt{L_1 L_2 xy}\right) - L_1 \int_0^x H'_2(\eta) I_0\left[2\sqrt{L_1 L_2 y(x-\eta)}\right] d\eta$$

$$- L_1 \int_0^y G'_2(\xi) I_0\left[2\sqrt{L_1 L_2 x(y-\xi)}\right] d\xi$$

$$+ \int_0^y G'_2(\xi) \sqrt{\frac{L_1 L_2 (y-\xi)}{x}}\, I_1\left[2\sqrt{L_1 L_2 x(y-\xi)}\right] d\xi + H'_2(x)$$

$$\left. + \int_0^x H'_2(\eta) \sqrt{\frac{L_1 L_2 y}{x-\eta}}\, I_1\left[2\sqrt{L_1 L_2 y(x-\eta)}\right] d\eta \right\} ; \qquad (2\text{-}84)$$

where

$$G'_2(y) = L_2 e^{L_2 y} , \qquad (2\text{-}85)$$

$$H'_2(x) = e^{L_1 x}\left[L_1 + q_1(x) + L_1 \int_0^x q_1(\gamma) d\gamma\right] , \qquad (2\text{-}86)$$

are the derivatives of functions $G_2(y)$ and $H_2(y)$.

II-3.2 Solution for a Gaussian Distribution of Xenon on Charcoal

Expressions given for $c_D(x,y)$ in equation (2-83) and $q_D(x,y)$ in equation (2-84) are perfectly general. They were developed for the desorption process in beds of charcoal having an arbitrary distribution of xenon. For a Gaussian distribution of xenon adsorbed on charcoal these

expressions are still valid, except the boundary condition functions $G_2(y)$ and $H_2(x)$, which have to be obtained for this case.

Equation (2-74) for a Gaussian distribution function may be written as

$$q_D(z,y) = q_D(z) = Q_{Do} e^{-\frac{(z - m)^2}{2\sigma^2}} , \qquad (2\text{-}87)$$

where Q_{Do} is the peak concentration at equilibrium; m is the mean, an arithmetic average of the distances; and σ is the standard deviation, a parameter that describes the breadth of distribution of deviation $(z - m)$ from the mean. When we use the change of variables given by equations (2-29) and (2-30), the boundary conditions given by equations (2-78) and (2-79) become

$$c_D(0,y) = 0 \quad , \text{ where } x = 0 \qquad (2\text{-}88)$$

$$q_D(x,0) = q_1(x) = Q_{Do} e^{-\frac{(u_s x - m)^2}{2\sigma^2}} , \text{ where } y = 0 . \qquad (2\text{-}89)$$

The corresponding functions $G'_2(y)$ and $H'_2(x)$ given by equations (2-85) and (2-86) may then be written as

$$G'_2(y) = L_2 e^{L_2 y} \qquad (2\text{-}90)$$

$$H'_2(x) = e^{L_1 x}\left[L_1 + Q_{Do} e^{-\frac{(u_s x - m)^2}{2\sigma^2}} + L_1 Q_{Do} \int_0^x e^{-\frac{(u_s \gamma - m)^2}{2\sigma^2}} d\gamma \right] \qquad (2\text{-}91)$$

The integral of a Gaussian distribution function does not have a simple analytical form; however, the last term in equation (2-91) may be written in terms of error functions. By making the following change of the variable

$$t = \frac{u_s\gamma - m}{\sqrt{2\sigma}} \tag{2-92}$$

and after some manipulation, we obtain

$$H'_2(x) = e^{L_1 x}\left\{ L_1 + Q_{Do} e^{-\frac{(u_s x - m)^2}{2\sigma^2}} + \left(\sqrt{\frac{\pi}{2}}\right)\left(\frac{\sigma L_1 Q_{Do}}{u_s}\right)\left[\operatorname{erf}\left(\frac{u_s x - m}{\sqrt{2\sigma}}\right) + \operatorname{erf}\left(\frac{m}{\sqrt{2\sigma}}\right)\right]\right\} , \tag{2-93}$$

where erf(s) is the error function defined by the integral

$$\operatorname{erf}(s) = \frac{2}{\sqrt{\pi}} \int_0^s e^{-t^2}\, dt \quad . \tag{2-94}$$

Hence, expressions given by equations (2-83) and (2-84), with equations (2-90) and (2-93) substituted for $G'_2(y)$ and $H'_2(y)$, would give a xenon concentration in the effluent and in the charcoal bed during elution of a column in which the xenon has been initially adsorbed in a Gaussian distribution.

II-4. Numerical Evaluations

The equations developed for determining the concentration of xenon in the effluent and in the charcoal bed for both processes are rather complex for analytical integration; however, numerical integration is relatively easy. Simpson's method of integration is used to integrate equation (2-70). Successive approximations are made until the absolute fractional error between two integrals is less than 1 percent. Listing of the FORTRAN program used may be found in Appendix A.

The last term in the equation has a singularity, which is removable by the following change of variable:

let

$$w = 2\sqrt{k_1 k_2 y(x - \eta)} \quad , \tag{2-95}$$

then

$$d\eta = \frac{-\, dw}{\sqrt{\frac{k_1 k_2 y}{x - \eta}}} \tag{2-96}$$

and the last term in equation (2-70) becomes

$$\int_0^x H'_1(\eta)\ \frac{k_1 k_2 y}{x - \eta}\ I_1\left[2\sqrt{k_1 k_2 y(x - \eta)}\right] d\eta = \int_0^{2\sqrt{k_1 k_2 xy}} H'_1(w) I_1(w)\, dw \quad . \tag{9-97}$$

The same type of change in the variables is applied to equation (2-84) for numerical evaluation.

For illustration, the xenon distribution in the charcoal column, $q_A(z,t)$, for constant flow time, is found for specific values given in

Table II-2. In Fig. II-3, normalized spatial variations of xenon concentration in the charcoal column are shown after flows of 10, 20, and 30 minutes, and in Table II-3 locations of maximum concentration and widths of concentration distribution at half maximum, denoted by $W_{1/2}$, are listed for each flow time. From these results we find, at least for the times and distances of interest, that adsorption waves travel through the column with a constant speed. As the flowing time increases, peak xenon concentration in the bed decreases, and the distribution curves broaden.

II-4.1 Factors Affecting Behavior of the Adsorption Column During the Adsorption Process

An experimental approach was employed to find how the location and shape of the xenon distribution in the column varied with the rate constants and the carrier gas flow rate. Fig. II-4 shows the distribution of xenon in the adsorption column after 30 minutes, as a function of k_2 for a constant k_1. After 30 minutes of flow, the distribution, as a function of k_1 for a constant k_2, is illustrated in Fig. II-5. Figure II-6 shows xenon distribution in the column when k_1 and k_2 are both varied, but the ratio is held constant.

The variations in the location of peak xenon concentration, Z_{Amax}, and in full width at half maximum of the distribution, $W_{1/2}$, were found to have particularly simple functional dependencies in the time span of interest:

$$Z_{Amax} \propto (k_2/k_1) \equiv k^{-1}$$

as in Fig. II-7 and Table II-4; and

Table II-2. Values of parameters used in plot of Fig. II-3.

Parameter	Value
Adsorption time constant	$k_1 = 295\ sec^{-1}$
Desorption time constant	$k_2 = 0.1\ sec^{-1}$
Linear velocity in the column for a flow rate of 8 liters/min	$u = 37.556$ cm/sec
Void fraction	$\alpha = 0.71$
Xenon concentration entering adsorption column at time t = 0	$c_{A_o} = 0.270\ \mu Ci/cm^3$ $= 10{,}000$ dia/sec-cm^3
Column cross section	$A = 5\ cm^2$

Table II-3. Location of maximum concentration, Z_{Amax}, and width at half maximum, $W_{1/2}$, of concentration curves at different times during flow.

Time (min)	Z_{Amax} (cm)	$W_{1/2}$ (cm)
10	5.0 ± 0.25	2.6
20	10.5 ± 0.25	4.0
30	16.0 ± 0.25	4.9

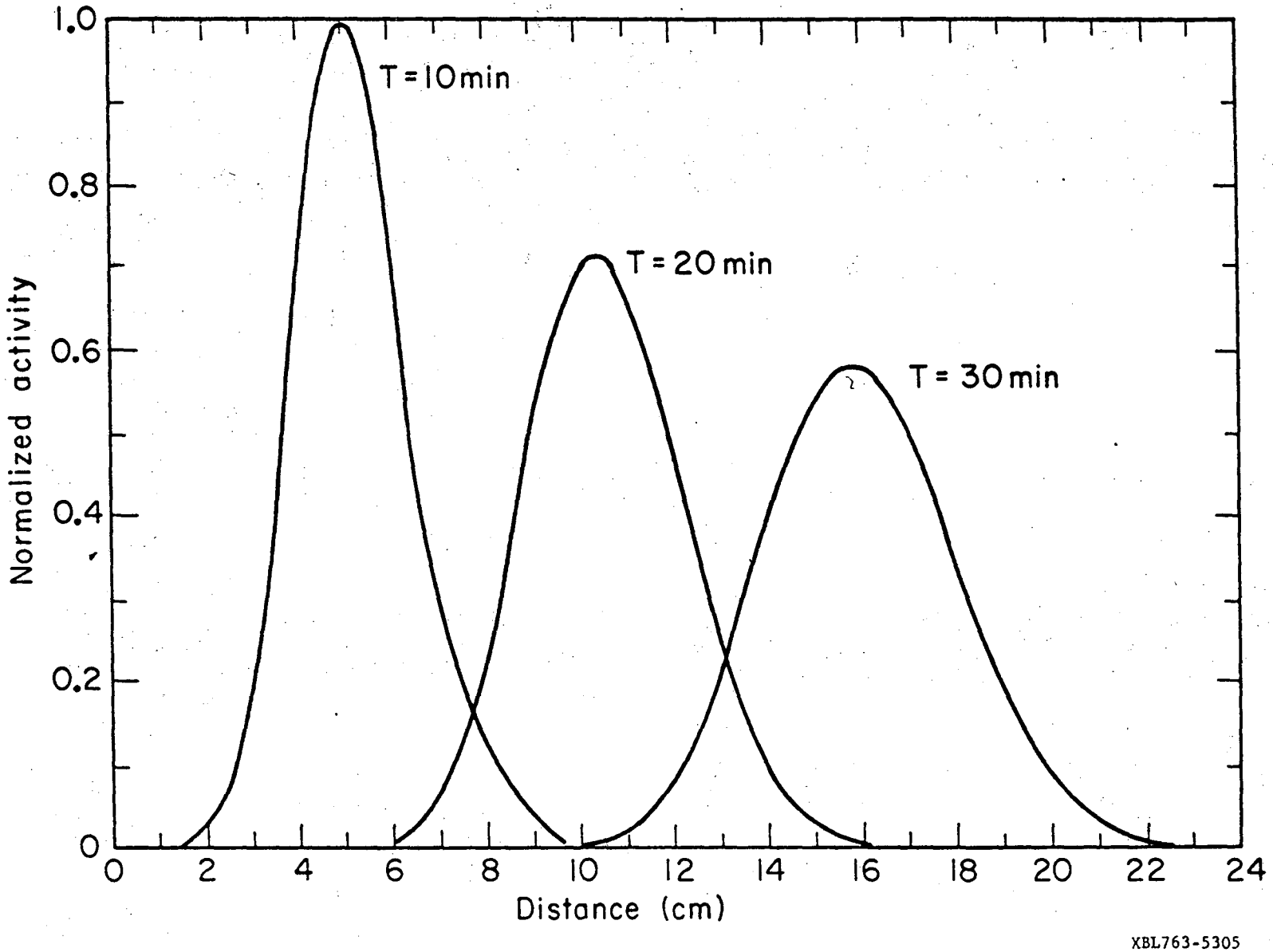

XBL763-5305

FIGURE II-3. Xenon distribution in the adsorption column for input data listed in Table II-2.

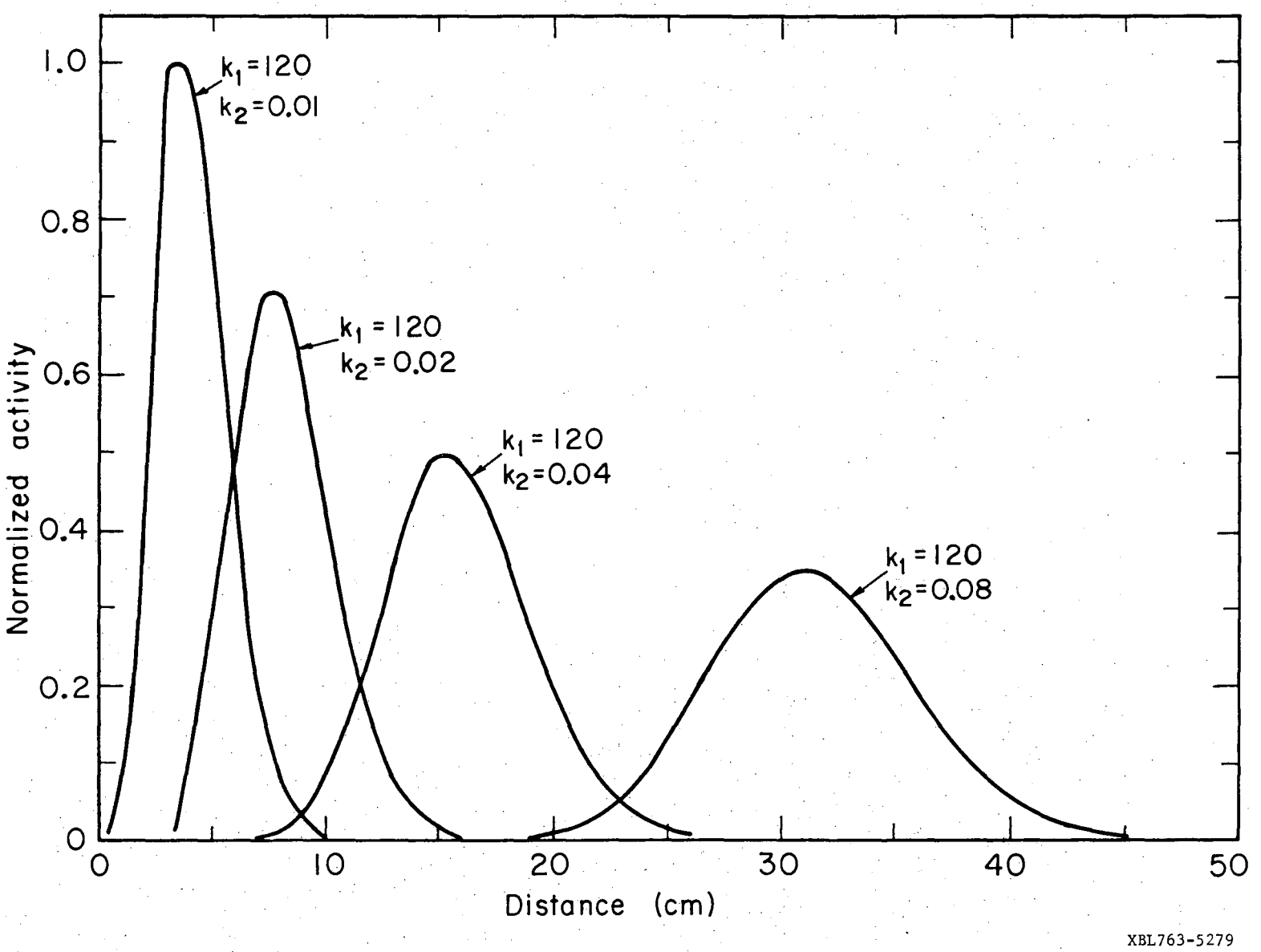

XBL763-5279

FIGURE II-4. Distribution of xenon in the charcoal column obtained by increasing the adsorption rate constant. Flow time = 30 minutes.

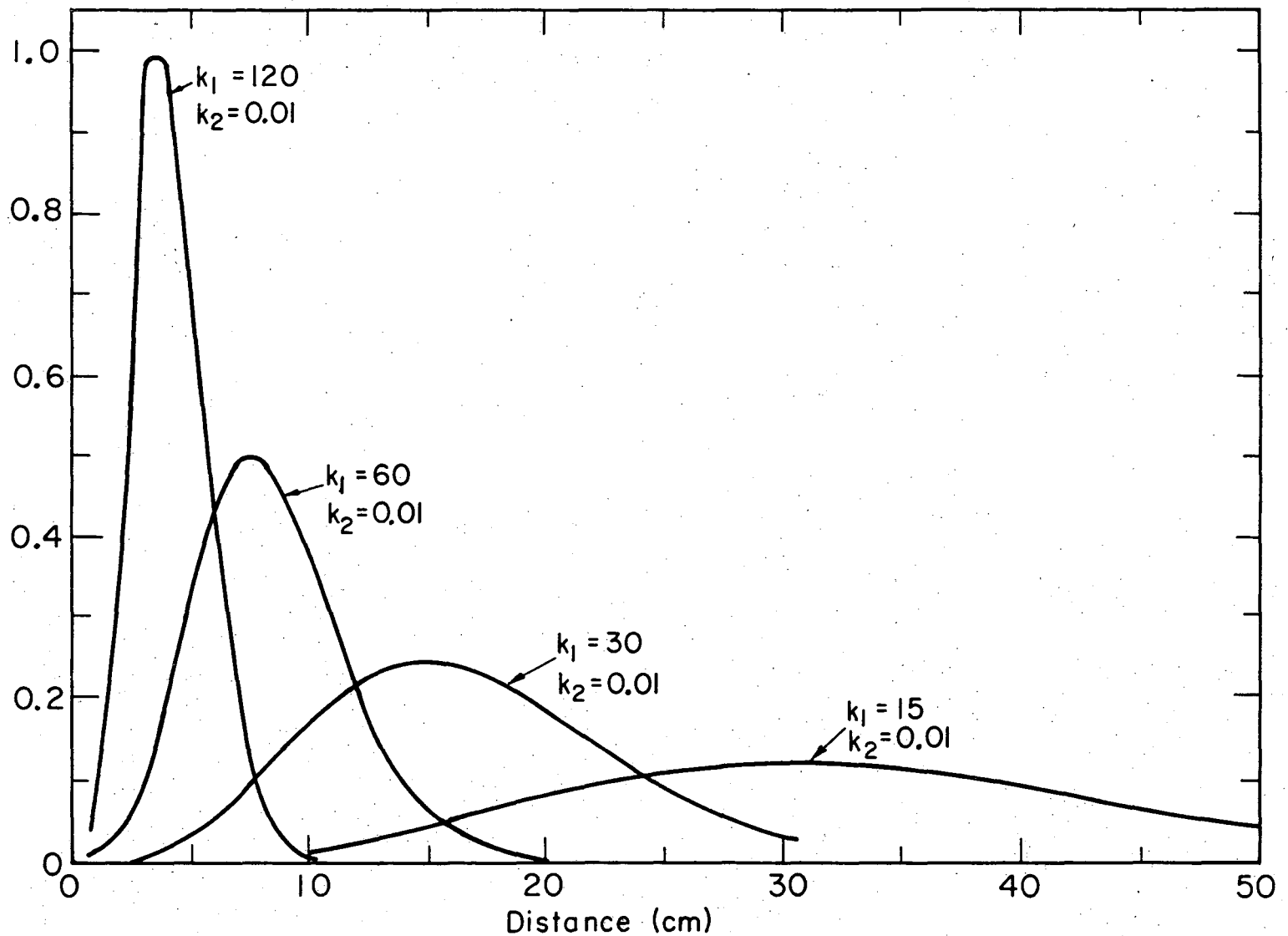

FIGURE II-5. Distribution of xenon in the charcoal column obtained by increasing the desorption rate constant. Flow time = 30 minutes.

XBL763-5280

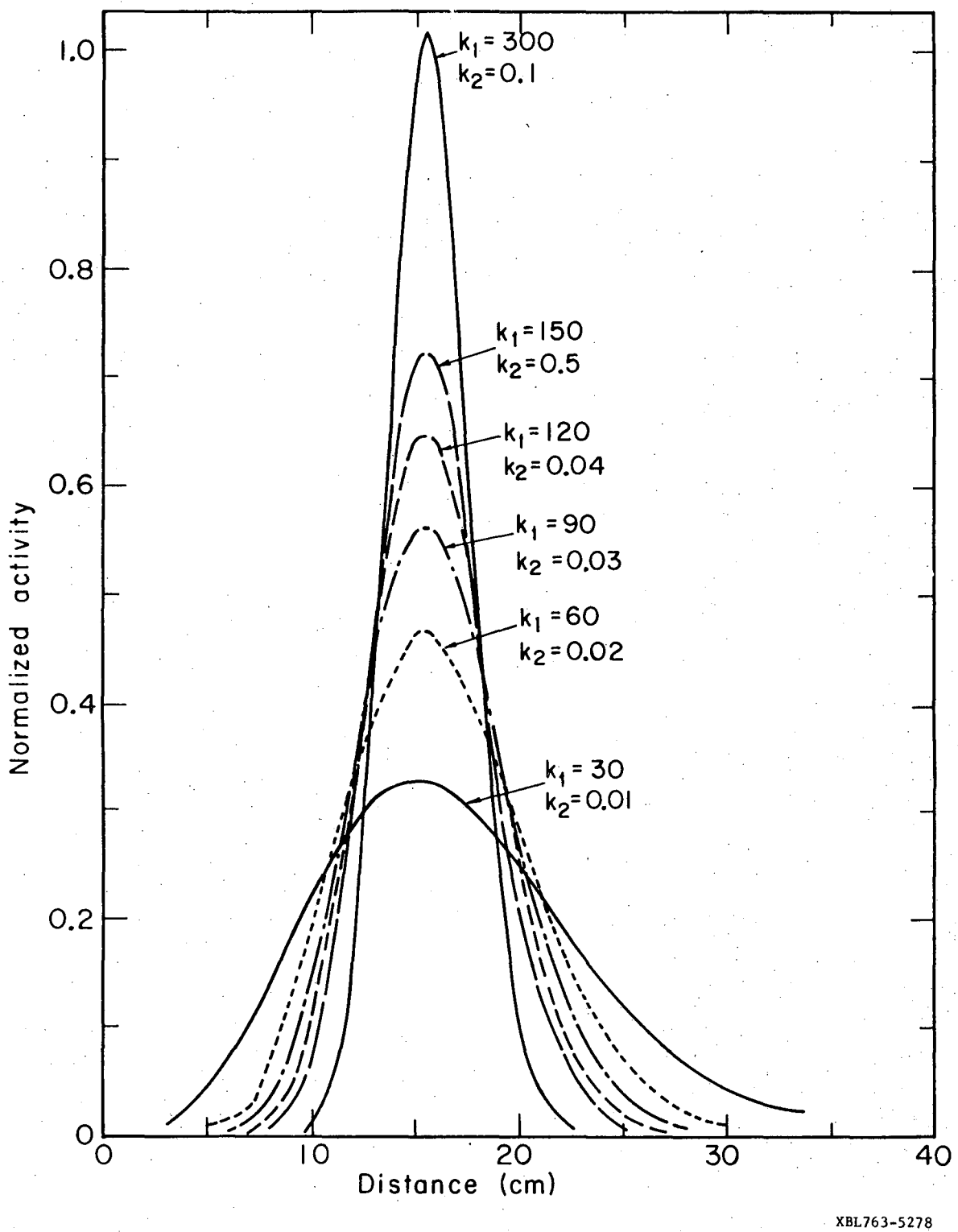

FIGURE II-6. Xenon distribution in the column for constant ratio of k_1/k_2. Flow time = 30 minutes.

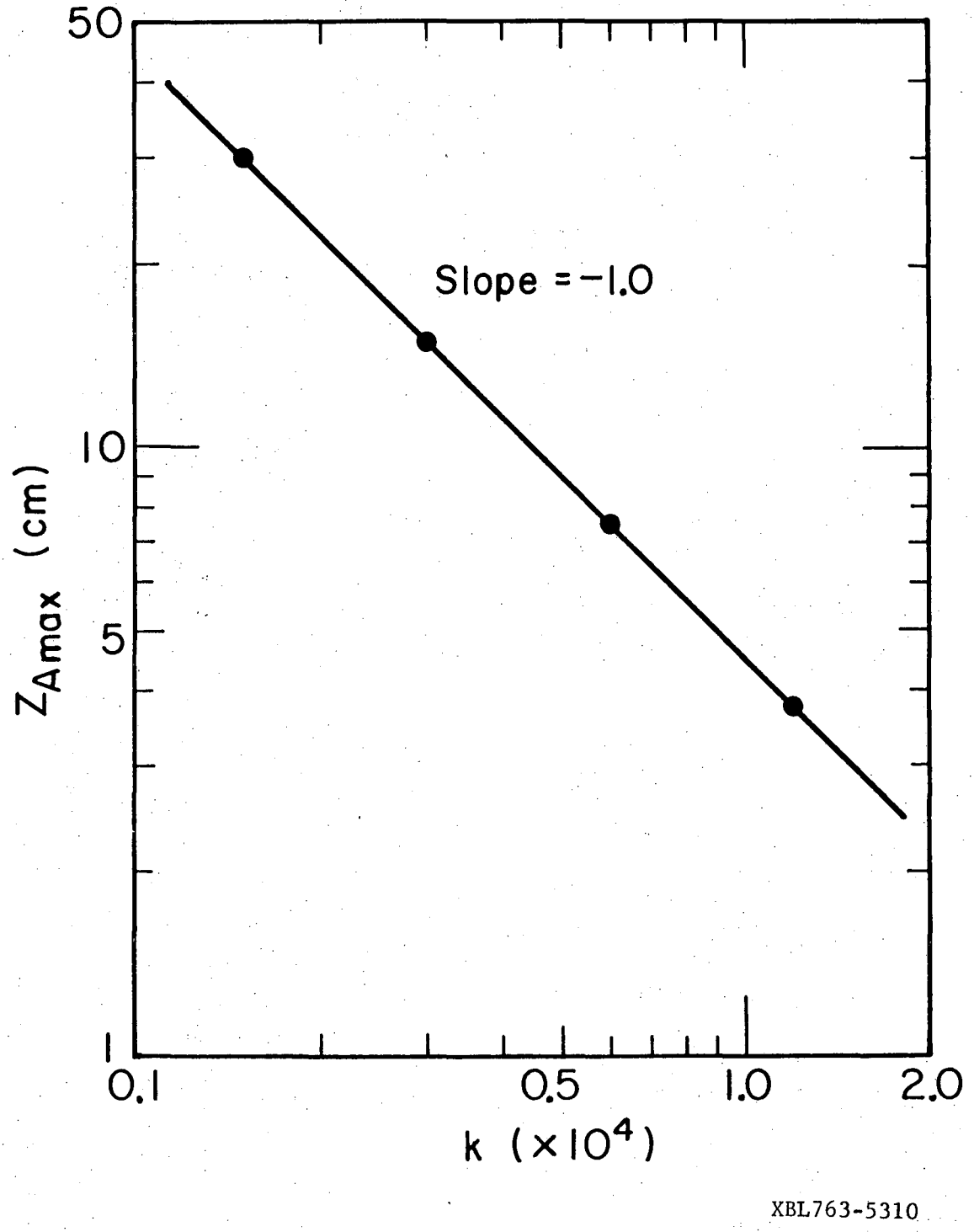

XBL763-5310

FIGURE II-7. Variation of the location of peak xenon concentration in the column with the ratio of rate constants, $k = k_1/k_2$.

Table II-4. Effect of rate constants on behavior of charcoal adsorption column.

k_1	k_2	$k = k_1/k_2$	Z_{Amax} (cm)	$W_{1/2}$ (cm)
120	0.01	12,000	3.75	3.750
120	0.02	6,000	7.50	5.250
120	0.04	3,000	15.00	7.500
120	0.08	1,500	30.00	10.500
60	0.01	6,000	7.50	7.125
60	0.02	3,000	15.00	10.500
60	0.04	1,500	30.00	15.000
60	0.08	750	60.00	20.500
15	0.01	1,500	30.00	28.500
30	0.01	3,000	15.00	14.250
60	0.01	6,000	7.50	7.125
120	0.01	12,000	3.75	3.750
15	0.02	750	60.00	—
30	0.02	1,500	30.00	21.000
60	0.02	3,000	15.00	10.500
120	0.02	6,000	7.50	5.250

$$W_{1/2} \propto (k_2/k_1^2)$$

as in Fig. II-8 and Table II-5. A similar analysis shows that for the same flow time of half an hour, the concentration wave moves forward and broadens as the carrier gas flow rate or linear velocity increases. The location of the peak, Z_{Amax}, and width, $W_{1/2}$, both increase linearly with gas velocity (Table II-6 and Fig. II-9).

II-4.2 Empirical Gaussian Distribution Fit of Xenon Activity Profiles

In Fig. II-3 it appears that the xenon concentration profile in the column becomes symmetrical as the chromatographic zone migrates further along the column, suggesting a Gaussian distribution fit of those curves. Using the following expressions for the mean and the standard deviation,

$$\bar{z} = \int_0^L zq(z)dz = \sum_i z_i q_i(z)\Delta z_i \quad , \tag{2-98}$$

$$\sigma^2 = \int_0^L (z - \bar{z})^2 q(z)dz = \sum_i (z_i - \bar{z})^2 q_i(z)\Delta z_i \quad ; \tag{2-99}$$

normalized xenon concentrations in the column obtained from expression (2-70) were approximated to a Gaussian distribution function

$$q(z) = e^{-\frac{(z - \bar{z})^2}{2\sigma^2}} \quad ,$$

where $\bar{z} = Z_{Amax}$ is the axis of the concentration zone, and $\sigma = W_{1/2}/1.177 \times 2$ is the standard deviation of the resulting Gaussian

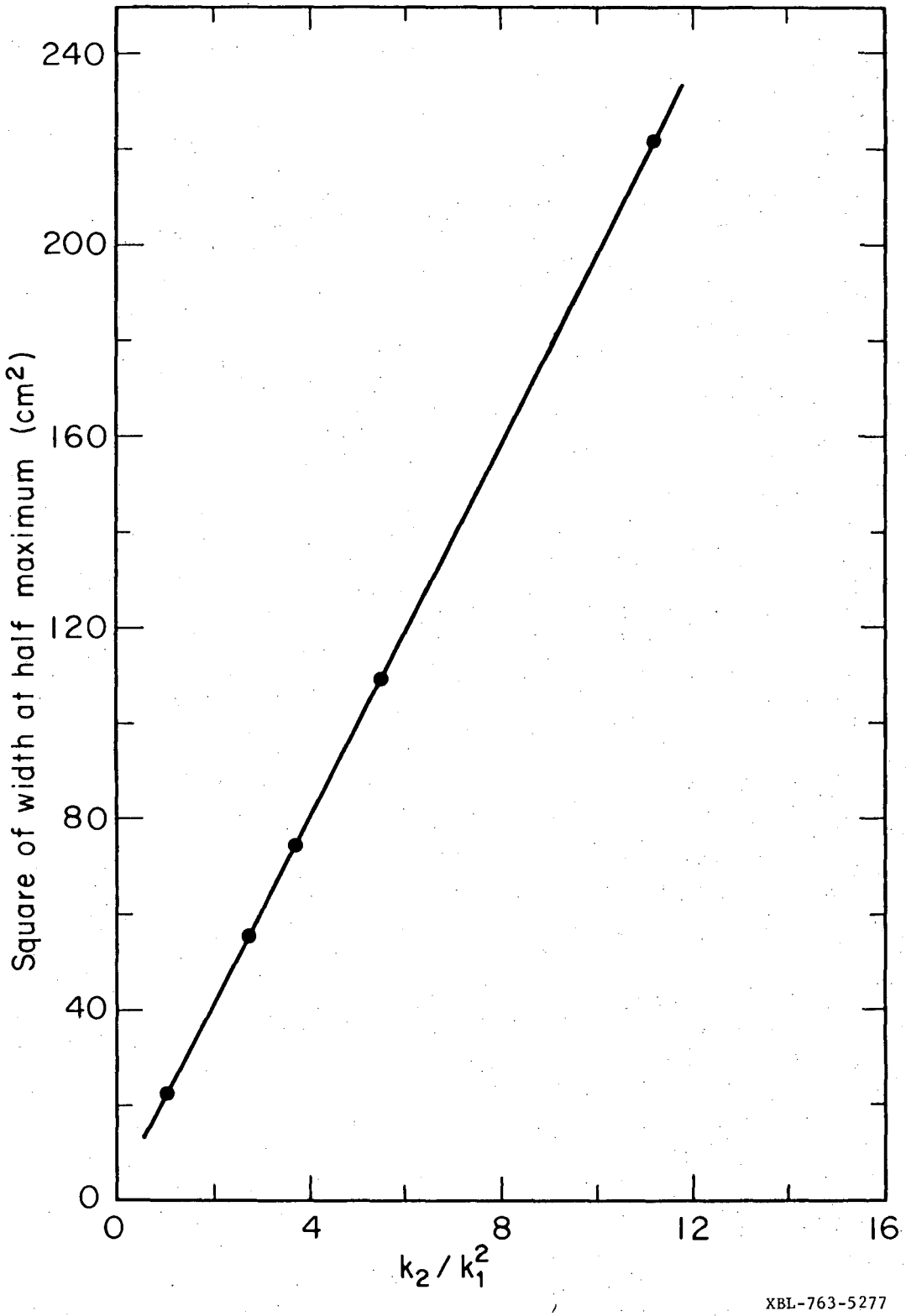

FIGURE II-8. Variation of full width at half maximum of xenon distribution in the column with k_2/k_1^2 .

Table II-5. Effect of varying k_1 and k_2, for a constant ratio of k_1/k_2, on behavior of charcoal adsorption column.

k_1	k_2	Z_{Amax} (cm)	$W_{1/2}$ (cm)
30	0.01	15	14.25
60	0.02	15	10.50
90	0.03	15	8.70
120	0.04	15	7.61
150	0.05	15	6.75
300	0.10	15	4.75

Table II-6. Effect of flow rate on behavior of the charcoal column during the adsorption process.

Linear velocity (cm)	Flow rate (liters/min)	Z_{Amax} (cm)	Velocity of the peak concentration (cm/min)	$W_{1/2}$ (cm)
9.389	2	4	0.113	1.2
18.779	4	8	0.266	2.6
28.169	6	12	0.400	3.7
37.559	8	16	0.533	4.9
46.948	10	20	0.666	6.0
56.338	12	24	0.800	7.2
65.727	14	28	0.933	8.2
75.117	16	32	1.066	9.5
84.507	18	36	1.200	10.4
93.896	20	40	1.330	11.4

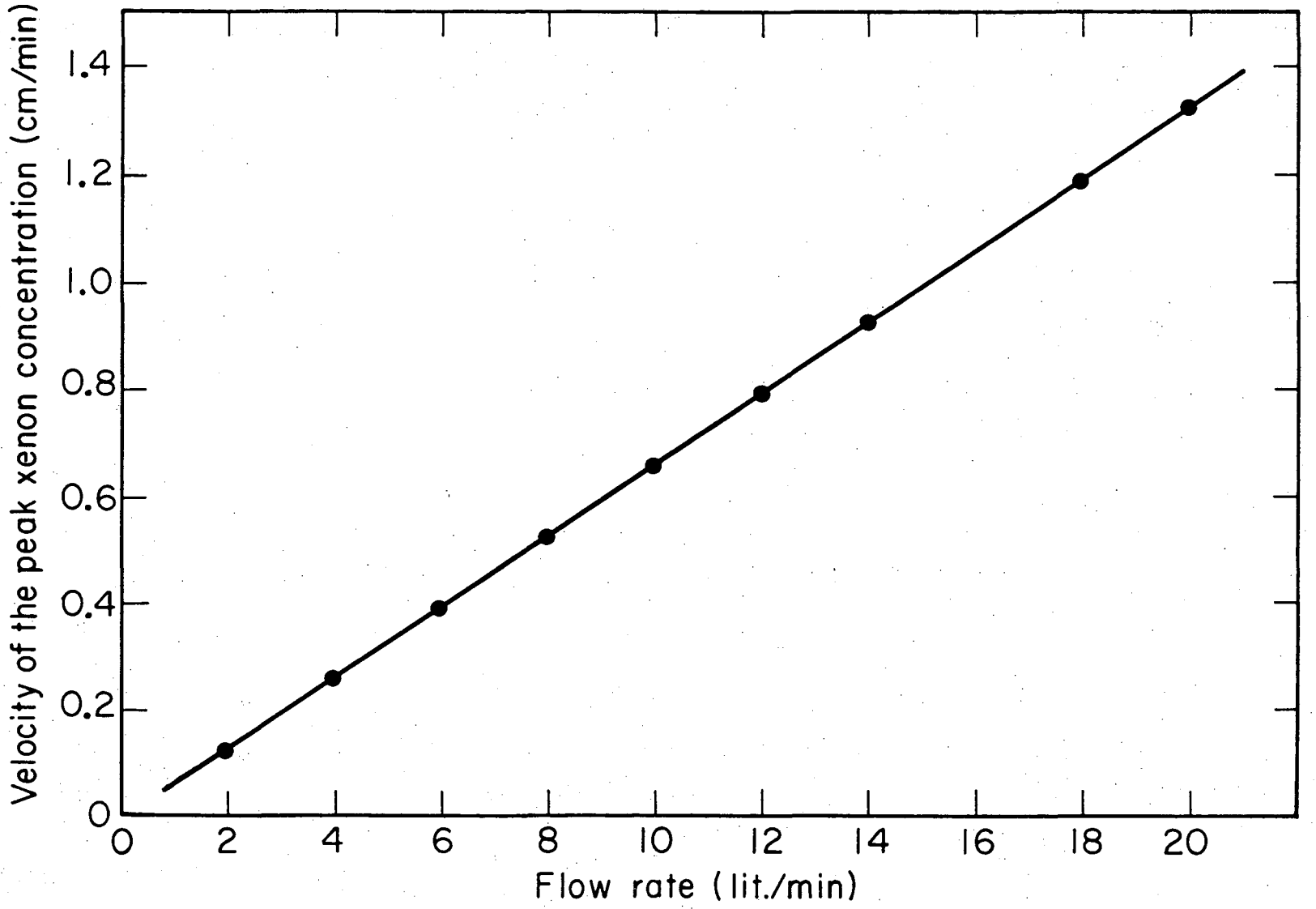

XBL763-5306

FIGURE II-9. Variation of the peak xenon concentration in the adsorption column with carrier gas flow rate.

concentration profile. For a flow time of 30 minutes, the normalized xenon concentration, calculated by both methods, is plotted against distance in Fig. II-10. It illustrates that the xenon profile in the column follows closely a Gaussian distribution function.

In order to facilitate the analysis of the experimental xenon activity profile in the adsorption column, results of the preceeding section were used to obtain the following empirical expressions relating constants of the Gaussian distribution function, $\bar{z}$ and σ, to the adsorption column characteristics

$$\bar{z} = \frac{k_2}{k_1} \frac{Ft}{A} \quad , \tag{2-100}$$

$$\sigma^2 = \frac{2}{\alpha} \frac{k_2}{k_1^2} \left(\frac{F}{A}\right)^2 t \quad , \tag{2-101}$$

where, as before,

k_1 = adsorption rate constant, sec^{-1} ;

k_2 = desorption rate constant, sec^{-1};

$k = k_1/k_2$;

F = total flow rate, cm^3/sec ;

A = cross-sectional area of the column, cm^2 ;

α = void fraction ; and

t = flow time, sec .

For the input data given in Table II-2, values of $\bar{z}$, σ, and $W_{1/2} = 1.177 \times 2 \times \sigma$, obtained from expression (2-70) and calculated as above are listed in Table II-7. A comparison of the corresponding values shows that by using expressions (2-100) and (2-101) it is possible to predict, within a few percent error, the location and shape of the distribution of the xenon activity in the adsorption column.

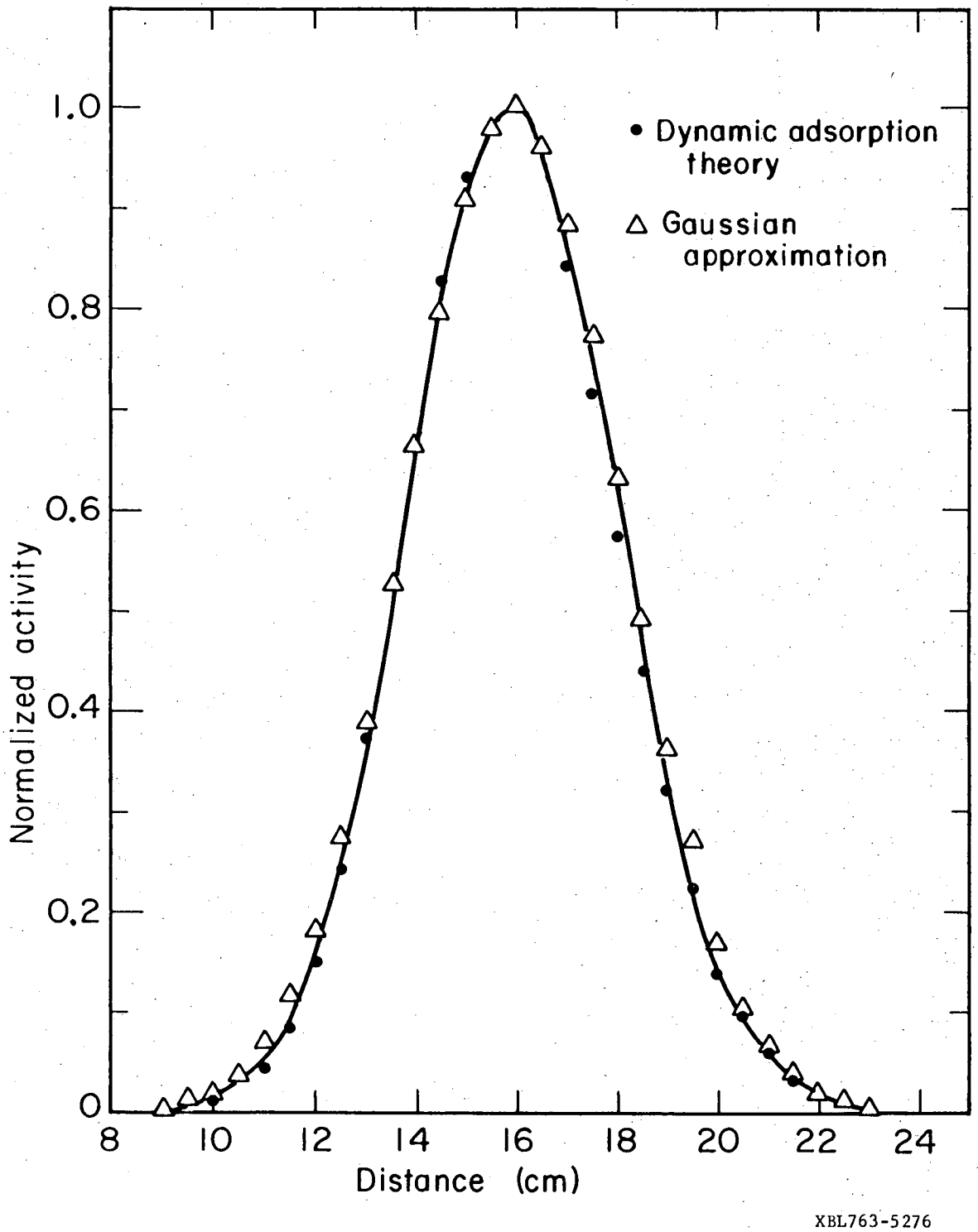

FIGURE II-10. Normalized activity distribution in the column after 30 minutes of flow.

Table II-7. Values obtained by rigorous dynamic adsorption method and calculated by empirical equations.

Flow time (min)	Z_{Amax}* (cm)	$W_{1/2}$* (cm)	$\bar{z}$† (cm)	σ† (cm)	$W_{1/2}$ (cm)
10	5.0 ± 0.25	2.6 ± 0.5	5.42	1.175	2.76
20	10.5 ± 0.25	4.0 ± 0.5	10.84	1.66	3.91
30	16.0 ± 0.25	4.9 ± 0.5	16.26	2.035	4.79

*Using expression (2-70).

†Using equations (2-100) and (2-101).

It can also be shown that the concentration-time profile in the effluent may be presented by a Gaussian distribution function with time as the variable:

$$c(t) = e^{-\frac{(t - \bar{t})}{2\tau^2}} , \qquad (2\text{-}102)$$

where $\bar{t}$ and τ, analogous to $\bar{z}$ and σ except having dimensions of time, are respectively the mean and the standard deviation of the xenon concentration profile in the effluent. By considering the fact that a given length of the concentration zone is swept off the column in a time equal to that length divided by the zone velocity, a corresponding pair of variables can be related to each other. For a charcoal column of length L cm, the following expressions are found for the mean and the standard deviation:

$$\bar{t} = \frac{k_1}{k_2} \frac{AL}{F} , \qquad (2\text{-}103)$$

$$\tau^2 = \frac{2}{\alpha} \frac{k_1}{k_2^2} \frac{AL}{F} . \qquad (2\text{-}104)$$

Input data from Table II-2 were used to calculate the values of time-to-peak, t_{max}, and full width at half maximum of the concentration-time distribution of xenon in the effluent; the same values are obtained from expression (2-69) and empirical equations (2-103) and (2-104), and are tabulated in Table II-8 for comparison.

For a charcoal column of 10-cm length, the normalized xenon activity profile in the effluent is determined, based on the dynamic adsorption approach and the Gaussian function approximation. These findings are plotted against time in Fig. II-11 and show that experimental data may well be correlated to the above empirical relation.

Table II-8. Calculated values of time-to-peak and full width at half maximum of the concentration——time distribution of xenon in the effluent for charcoal columns of variable length.

L (cm)	t_{max}* (min)	$W_{1/2}$* (min)	$\bar{t}^{\dagger}$ (min)	$\tau^{\dagger}$ (min)	$W_{1/2}^{\ddagger}$ (min)
10	19 ± 0.5	7.1 ± 0.7	18.437	2.954	6.957
20	37 ± 0.5	9.5 ± 0.7	36.875	4.160	9.792
30	56 ± 0.5	11.2 ± 0.7	56.312	5.090	11.993

*Using expression (2-69).

†Using expression (2-103) and (2-104).

‡$W_{1/2} = 2 \times 1.177 \times \tau$.

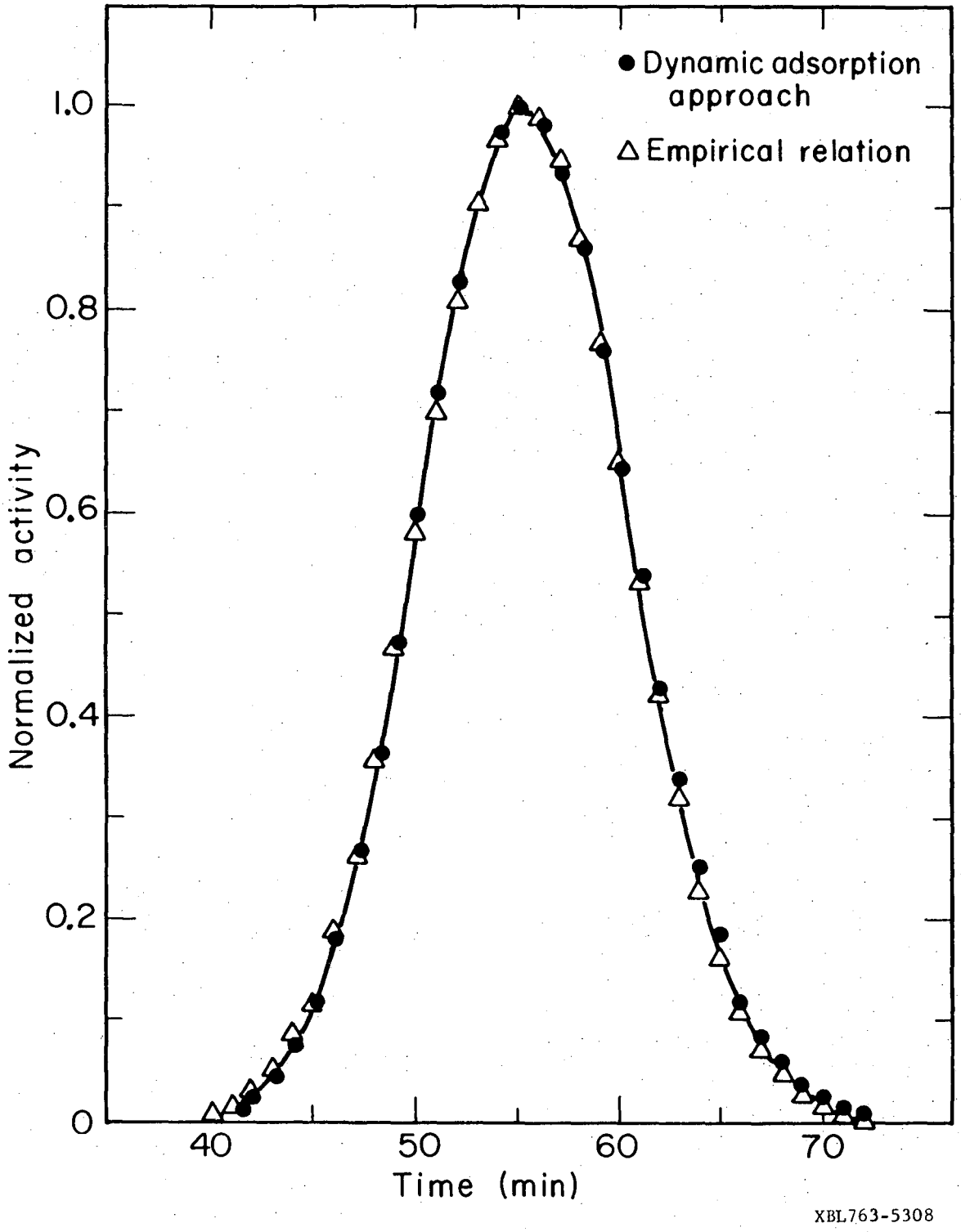

FIGURE II-11. Comparison of xenon activity distribution in the effluent for a charcoal column of length 10 cm as determined by dynamic adsorption and empirical results.

CHAPTER III.

ANALYSIS OF THE HOLDUP AND REMOVAL OF RADIOACTIVE XENON GAS FROM CHARCOAL TRAPS

III-1 Xenon Holdup by Charcoal Traps

One of the few satisfactory methods developed to reduce release of radioactive noble gases, particularly the fission products krypton and xenon, to the atmosphere from the off-gas streams of reactors and nuclear fuel reprocessing plants is the use of fixed-bed adsorption systems [92-105]. To achieve this reduction, two modes of operation have been considered: The first method is the conventional one, in which the process gas stream is passed through an adsorber bed until breakthrough occurs. The adsorbent is then either regenerated or removed. A charcoal bed, cooled with liquid nitrogen, has been used in this manner to remove radioactive krypton from the dissolved off-gas stream at the Chemical Processing Plant, National Reactor Testing Station, Arco, Idaho [106]. The alternative mode of operation is to use the adsorber as a "delay bed." In this case, breakthrough is allowed to occur, but the adsorber bed is sized to provide adequate chromatographic delay of the radioactive krypton and xenon isotopes. In other words, krypton and xenon are delayed in passage through the adsorber by the continuous process of adsorption and desorption, and the radioactive isotopes are allowed to decay before they escape from the adsorber. A water-cooled charcoal delay bed has been used in this way to remove krypton and xenon from the off gas stream of the

Homogeneous Reactor Test at Oak Ridge National Laboratory [107].

The effectiveness of a delay bed in holding up radioactive xenon gas is dependent on the geometry of the bed, the type and amount of charcoal, the bed temperature, and the total flow rate; it is independent of xenon concentration in the carrier gas as long as the concentration falls under the linear portion of the adsorption isotherm. If the concentration becomes sufficiently high, the adsorption isotherm will become appreciably nonlinear and the effectiveness of the delay bed will start to decrease with increasing concentration. This loss of effectiveness occurs because the adsorbate occupies an appreciable fraction of the adsorbate surface, and thus interfers with further adsorption. In the preceding chapter a theoretical treatment of the dynamic adsorption-desorption process in charcoal bed has been developed. From this analysis it appears possible to predict the shape and position of the xenon distribution in the bed and in the effluent when one knows the bed geometry, flow rate, and rate constants for the adsorption and desorption of xenon on charcoal, from a flowing air stream. To gain the necessary information on holdup behavior of a charcoal trap to be used in an apparatus for recycling trace amounts (10 to 50 mCi) of radioactive xenon gas in pulmonary function studies, a series of experiments was carried out to determine the shape and position of holdup and breakthrough curves when the gas fed into the trap has an exponential fall in xenon concentration. These curves were then compared to the ones obtained from expressions (2-69) and (2-70) to find rate constants suitable to the design of the trapping system.

III-1.1 Adsorption Capacity of Adsorbent Used

One of the important parameters in the design of an adsorber for the removal of a trace amount of a gas is the capacity of the adsorbent for that gas. Generally, the greater the surface area of the adsorbent, the higher its adsorption capacity for any compound. The range of surface area for commercial adsorbents capable of adsorbing inert gases is listed in Table III-1. These values reflect the relative effectiveness of these adsorbents. Experiments have also been carried out which confirm that activated charcoal is significantly better than inorganic materials [109-113] for removal of radioactive xenon from a flowing gas stream. Fig. III-1 shows the adsorption isotherm at 2°C for xenon on various adsorbers [109].

The adsorbent used in the experiments to be discussed is coconut charcoal, 6-14 mesh, from Fisher Scientific Company. The physical properties of this activated charcoal are listed in Table III-2 [112].

III-1.2 Apparatus

The apparatus used is shown schematically in Fig. III-2. The essential portions of the flow system include a spirometer, a water adsorber (Drierite), a pump, a charcoal trap with dry-ice bath, and a flow meter. The connecting lines are constructed of copper tubing with 1-in. i.d. and 1/16-in. thick walls. The trap is a 22-inch long adsorbent bed holding about 140 g of charcoal and connected to the system with vacuum fittings. Small-mesh copper-screens fitted inside the trap prevent dispersion of charcoal through the system. Trap temperature is measured

Table III-1. Surface area of commercial adsorbents.

Adsorbent	Surface area
Activated alumina	50-400 m^2/g
Silica gel	200-600 m^2/g
Molecular sieve	600-800 m^2/g
Activated carbon	500-1600 m^2/g

Table III-2. Physical properties of coconut charcoal used.

Property	Range of effectiveness
Surface area	1100-1200 m^2/g
Pore volume (N_2)	0.55-0.65 ml/g
Pore volume (He or Hg)	0.70-0.75 ml/g
Apparent density	0.48-0.53 g/ml

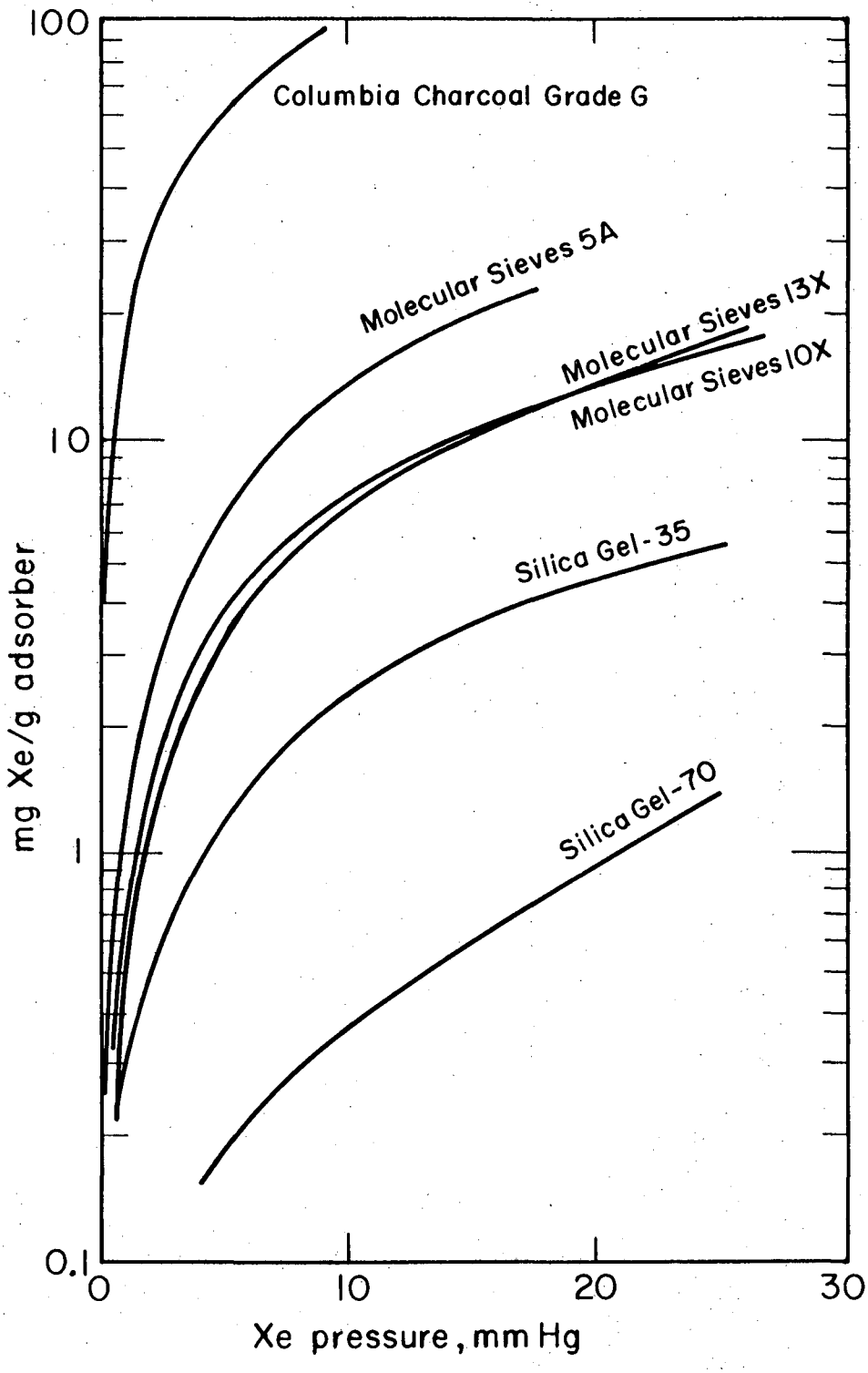

FIGURE III-1. Adsorption of xenon by various materials at 2°C [105].

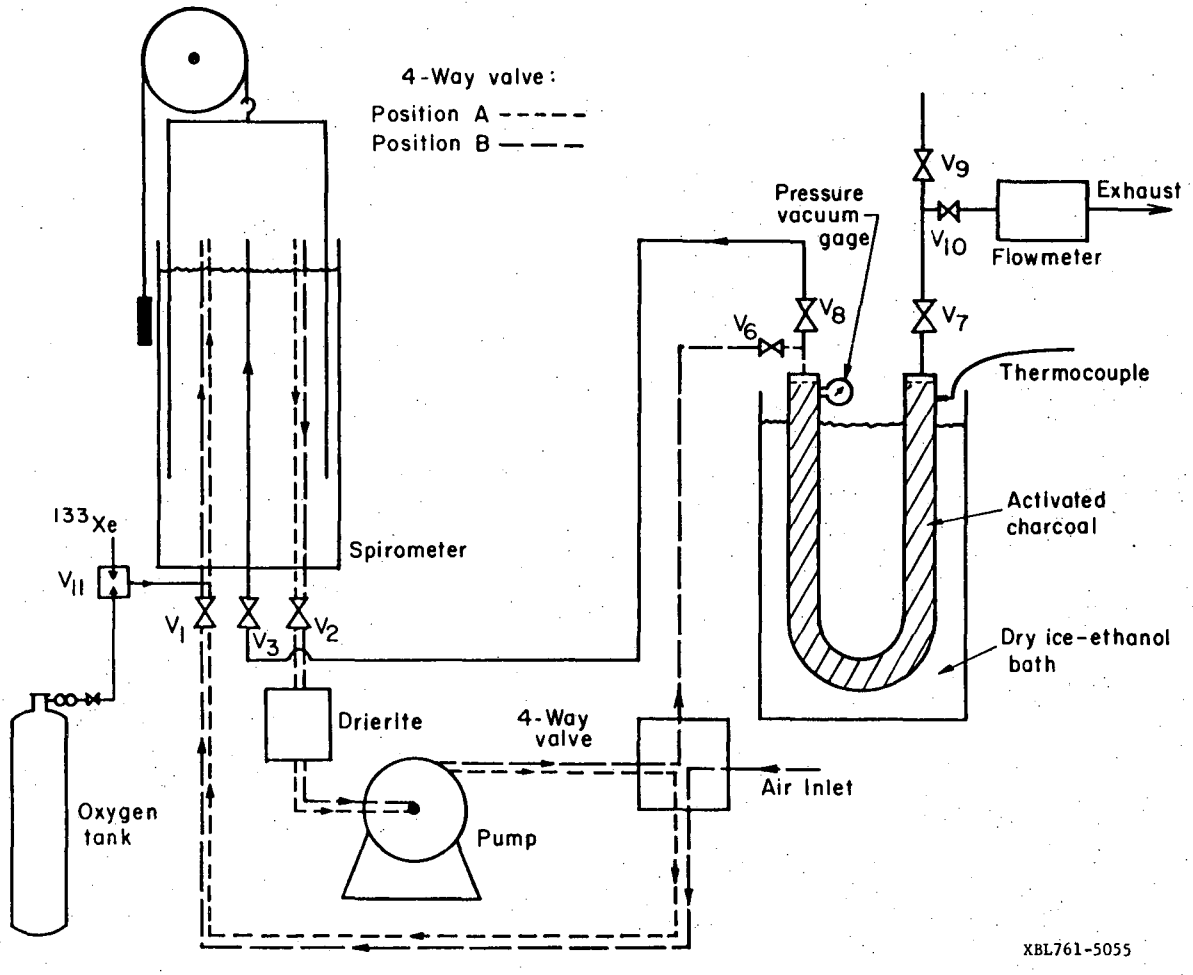

FIGURE III-2. Apparatus used in the experiments on holdup and removal of xenon.

with a stainless-steel clad, copper constantan thermocouple.

A NaI crystal, 1- in. thick by 3-in. diam., in conjunction with a photomultiplier, served as detector for measuring ^{133}Xe activity in the spirometer. The spirometer was shielded from the remainder of the apparatus so that activity present elsewhere in the system would not influence the counts obtained over the spirometer. A fan was installed inside the spirometer to insure complete mixing of the xenon with air. The output from the detector was recorded by a scaler and a rate meter. A continuous plot of rate meter output, and hence the gas activity level in the spirometer, was obtained using a strip chart recorder.

An Anger scintillation camera fitted with a low-energy collimator was used to detect gamma radiation emitted from ^{133}Xe inside the trap. The camera is interfaced to a digital system, the Hewlett-Packard Model 5407A Scintillation Data Analyzer, which stores and processes the basic information. The main components of the system consist of a 3-μ sec analog-to-digital converter, the Hewlett-Packard 2100A computer (16-bit words), movable head discs (2.4 million words), magnetic tape storage system, CRT display with light fan, and a teletype. Detailed information on the system is reported elsewhere [114].

III-1.3 Data Collection

The distribution of ^{133}Xe activity in the trap as well as the time-activity curves for any region of the trap are obtained with an Anger camera and the on-line data analyzer. The camera output in the form

of sequential 64 × 64 matrices is acquired and transferred onto the raw data file of the disc by the digital computer system at preselected time intervals (minimum 10 msec). At the end of an experiment the accumulated raw data are processed by selecting preset programs provided by the system. Each program is initiated by depressing the appropriate keys of a standard teletype and entering the relevant parameters.

Data processing begins by framing the accumulated raw data. During this operation, the raw data file is played back, and the data are regrouped into virtual images called frames and recorded on the frame file. Any frame from the frame file can be manipulated by a choice of arithmetic operations, or viewed in three different modes: contour, isometric, and slice. The contour mode is closest to a conventional scan or scintigram; each display point is intensified as a function of the counts present. The isometric mode gives a pseudo three-dimensional effect of the image; each point is displaced vertically and intensified as a function of the count present. The slice mode shows both a vertical and a horizontal slice in cross section, each point is displaced vertically as a function of the counts.

Once the sequence of frames representing the dynamic study has been created, time-activity curves of selected frames and areas can be generated. Markers or light pen are used to identify areas for determining integral counts. Total counts in each area, for each frame, are plotted vertically against frames horizontally. Generated time-activity curves can be called or operated on arithmetically. After manipulation, the curves can be stored on the disc. When data processing has been completed, the entire study -- including raw data -- is saved on magnetic tape for viewing or further analysis.

III-1.4 Adsorption and Desorption of Air from Charcoal

One of the problems associated with holdup of trace amounts of inert gases in an air stream is the adsorption of air on charcoal at low temperatures. Experiments were carried out to measure the volume of air adsorbed on charcoal during cooling to dry ice temperature of -78°C, as well as the volume and composition of gas desorbed from the charcoal while warming up to room temperature of 20°C. Part of the apparatus shown in Fig. III-1 was used in these experiments.

When the trap, previously at room temperature, was immersed in the dry-ice bath with all valves closed, the pressure inside the trap decreased and by the time the trap reached dry-ice temperature (about two hours), the gauge on the trap showed a vacuum of 18 mm Hg below atmospheric pressure. This was an indication that air inside the trap was adsorbed on the charcoal while being cooled down. To measure the volume of air adsorbed on the charcoal, valves V_1, V_2, and V_3 at the bottom of the spirometer were closed; air was introduced inside the spirometer through valve V_{10}; and by opening valves V_3 and V_8, air was allowed to flow from the spirometer to the trap. Volume displacement of 3 liters out of the spirometer brought the trap pressure to atmospheric level, and no noticeable change of volume in the spirometer occurred by leaving the trap in dry ice for another hour.

A variation of this experiment, giving a similar result, was also performed. With the same trap at 20°C, air was introduced into the spirometer, and after closing all the valves except V_3 and V_8, the trap was immersed into the dry-ice bath. When the trap temperature reached -78°C, the spirometer volume was decreased by 3 liters.

When the trap was warned to room temperature of 20°C, the pressure inside the trap increased due to excess air adsorbed on the charcoal during cooling down to -78°C. For 140 g of charcoal in the trap, the pressure rose to 15 psi above atmospheric. The volume of this excess gas was measured by first discharging the remaining air in the spirometer and then opening valves V_8 and V_3. The pressure gradient of the gas in the trap increased the volume of the spirometer by about 3 liters -- exactly the same amount of air that entered the trap during cooling.

The composition of gas released by charcoal while warming from -78 to 20°C was also determined by gas chromatography. With all valves closed, the trap was taken out of the dry-ice bath and allowed to warm up to room temperature. Then a syringe with a Luer-lock adapter was used to withdraw samples of excess gas from the trap. The gas released from the trap has the composition of atmospheric air. Hence, no selective adsorption exists at -78°C when a mixture of nitrogen and oxygen is adsorbed on charcoal.

III-1.5 Procedure

The operating procedure to analyze the dynamic adsorption of xenon on charcoal is divided into two sections: preparation and xenon collection. Each section is described in detail below.

A. Preparation

The four-way valve is set in position A (Fig. III-2); all connections are secured, valves V_8 and V_9 are closed; valves V_6, V_7, and V_{10} are opened, and the trap is immersed in the dry-ice bath. The

experimental system is positioned so that the xenon trap is in the camera field, as close as possible to the collimator. The camers is adjusted to the proper setting after shielding the back and the sides of the trap with 1/2-in.-thick lead sheet. Then the computer and peripheral systems are set to the desired mode to store data from the camera. Following these operations, the fan inside the spirometer is turned on, and with valves V_1, V_2, and V_3 closed, ^{133}Xe is introduced into the spirometer through valve V_{11}, and flushed by oxygen from a tank supply. Sufficient oxygen is added to the spirometer so that the volume of gas inside is about 5 liters. The amount of xenon introduced was not calibrated, so a scintillation collimator with variable collimation was used to monitor the initial count rate in the range of 300,000 to 500,000 counts per minute. The chart recorder was started, once a satisfactory initial count rate was achieved, and allowed to run continuously during the experiment to provide a plot of the activity level in the spirometer.

B. Xenon Collection

After the trap has reached dry-ice temperature, the count rate and volume of the gas in the spirometer is recorded; valves V_1 and V_2 are opened, and the pump is turned on. The xenon-air mixture is circulated in the closed circuit until the count rate in the spirometer reaches a steady-state level, at which point the flow is directed toward the trap by switching the four-way valve to position B. In this open circuit, atmospheric air enters the spirometer through the four-way valve and valve V_1; and after mixing with xenon, the gas flows out of the spirometer through valve V_2. The xenon-air mixture then passes through the Drierite, pump, and four-way valve to enter the charcoal trap. The

remaining gas leaves the trap through valves V_7 and V_{10} to enter the flowmeter. The flow is continued in this manner for 20 to 30 min while data are collected. At the end of this period, the pump is turned off and the trap is taken out of the bath to be warmed up to room temperature. In the principal experiment the flow rate was between 8 - 9 liters/min.

III-1.6 Experimental Results

The arrival and movement of the ^{133}Xe gas in the trap for a flow rate of 8 liters/minute is shown in Fig. III-3 as a series of displays in isometric mode. The duration of each displayed frame is 15 sec. In Fig. III-4, plotted simultaneously against time, are the counts in each frame (normalized to the frame with maximum counts) and the normalized activity level in the spirometer, obtained from the tracing of the chart recorder.

The time-activity curves (Fig. III-5) of four adjacent areas of the trap and the sum of these areas were obtained after regrouping the raw data into frames of one-minute duration. These curves were generated by dividing one leg of the "U" tube on the CRT display into four equal areas and adding counts in each area for all the frames. Figure III-6 shows locations and assigned numbers to each area of the trap. Counts in each area as well as the total count in all areas is tabulated in Table III-3. By taking the ratio of total counts in the areas of frame 12 (the frame with the maximum count) to those of frame 30, it was found that after 30 minutes of flow, less than 8 percent of the xenon activity had passed through 20 cm of the charcoal column. The percent activity in each section of the trap at different times

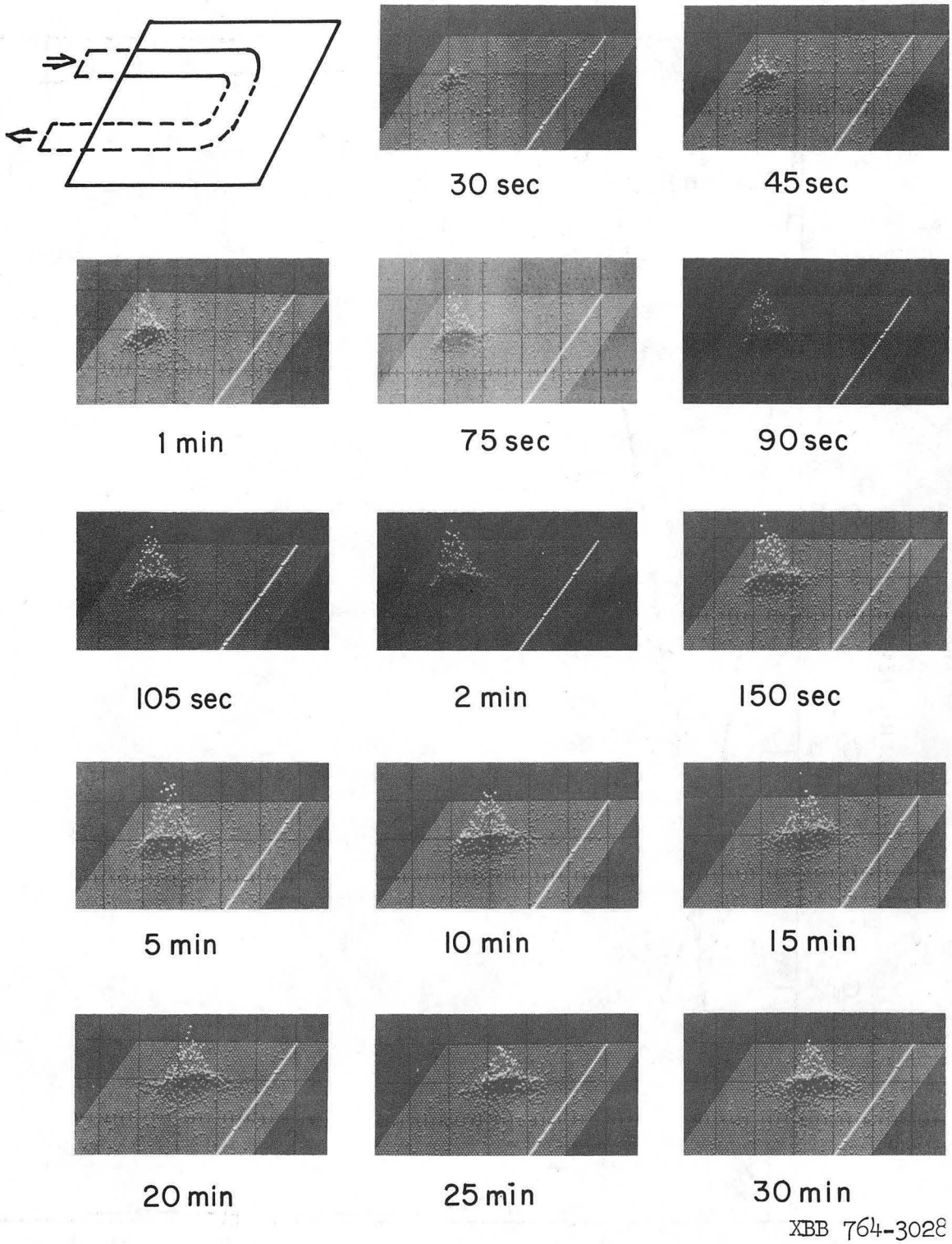

Fig III-3. Isometric display of activity in the trap during flow.

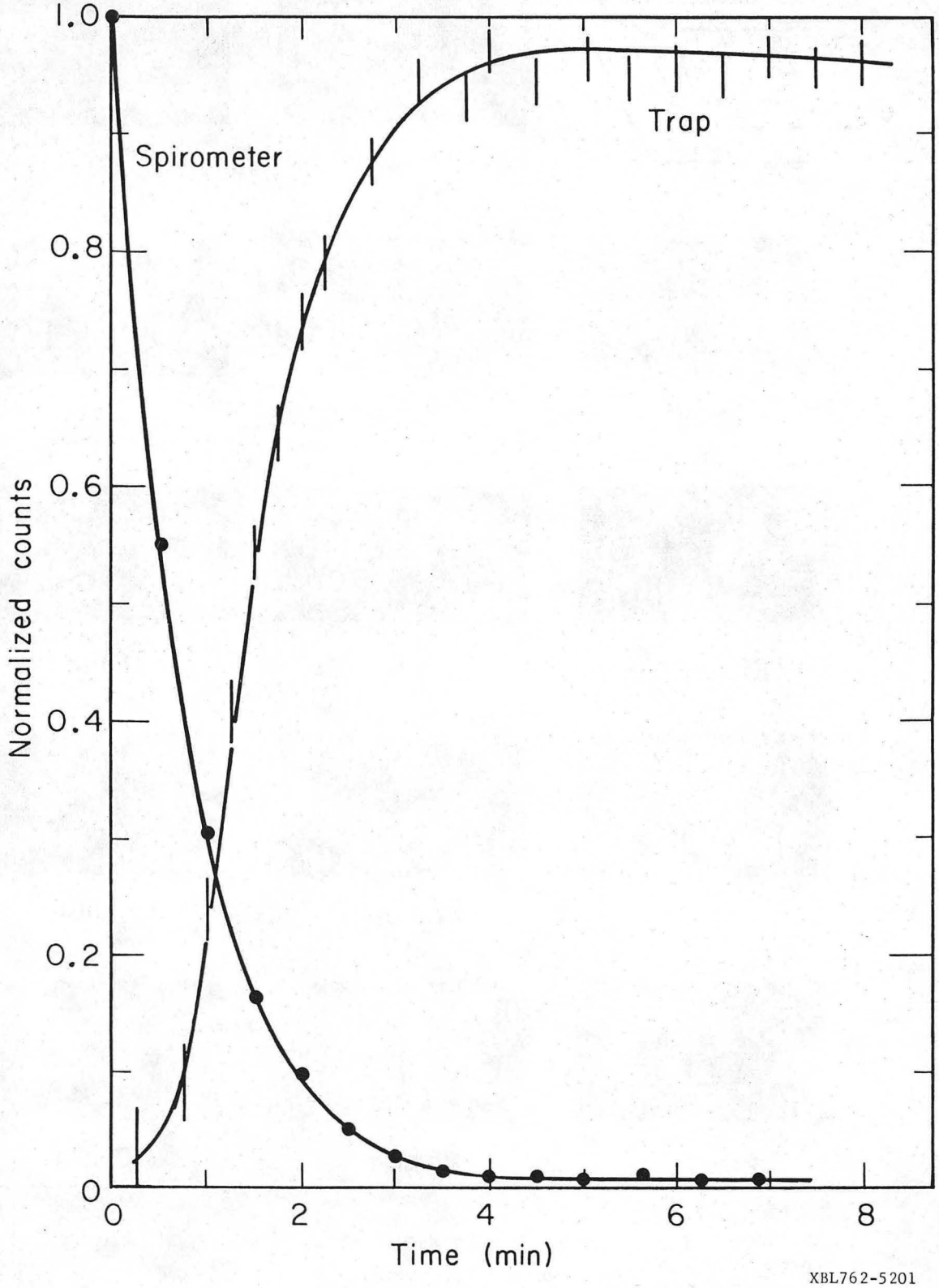

FIGURE III-4. Normalized activity level in the spirometer and in the trap during arrival of xenon into trap.

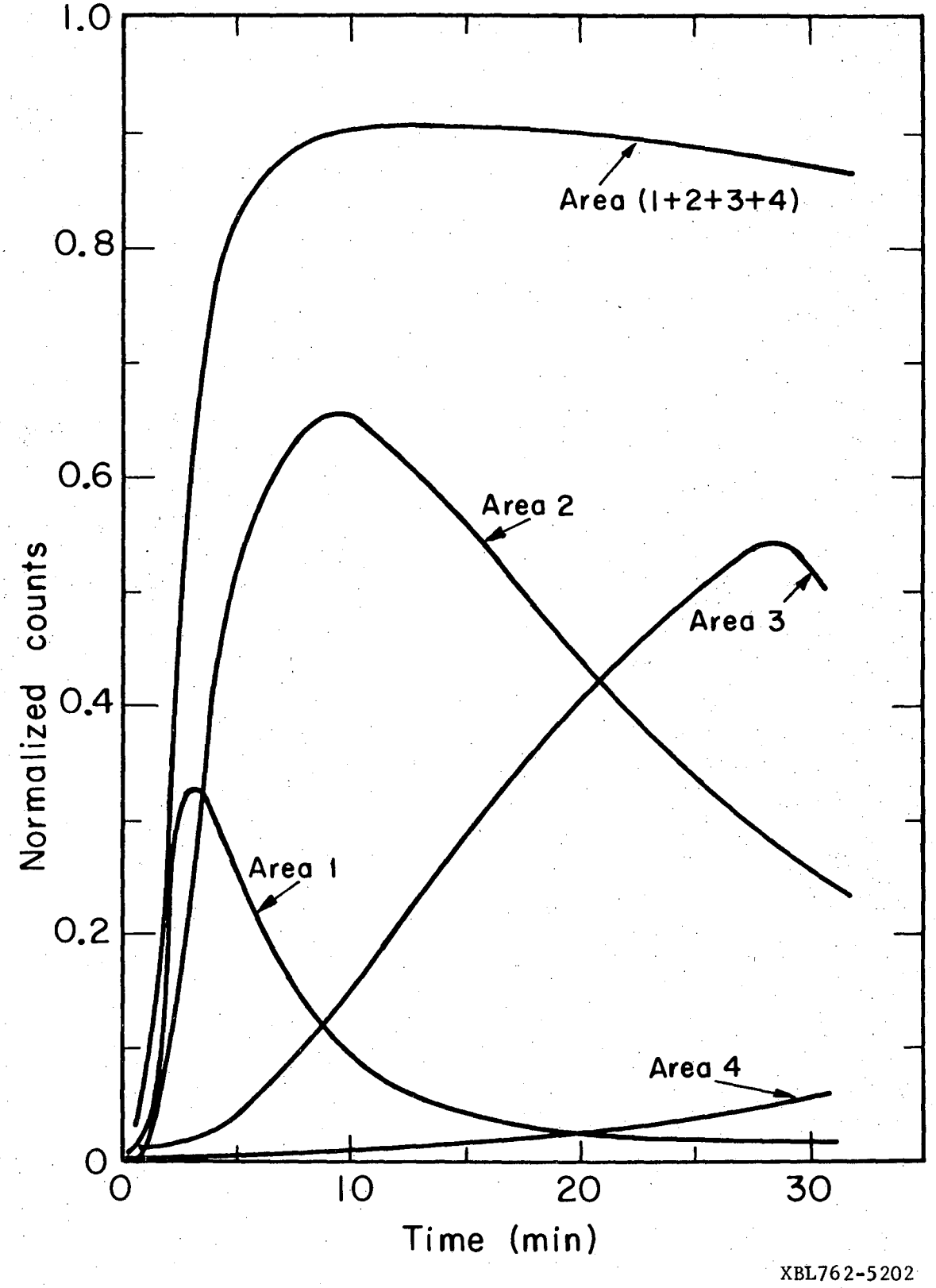

FIGURE III-5. Time-activity for selected area shown in Figure III-6.

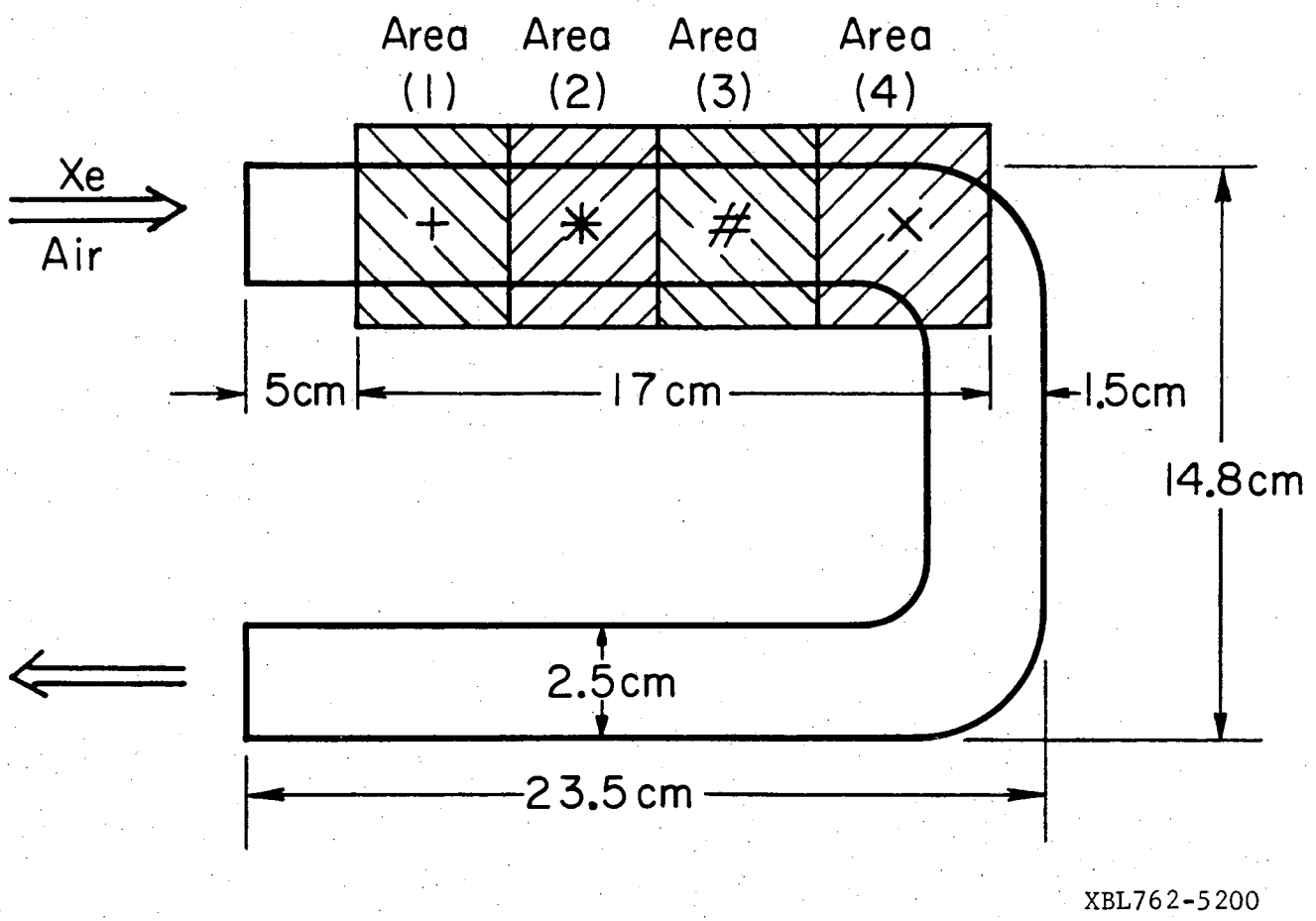

FIGURE III-6. Areas selected on CRT tube for time-activity plots.

Table III-3. Counts in designated sections of the trap (Fig. III-6), at various times during flow.

Time (min)	Area (1)	Area (2)	Area (3)	Area (4)	Area (1 + 2 + 3 + 4)
1	114	39	53	28	234
2	1118	403	70	35	1626
3	1634	1323	82	33	3072
4	1499	2128	126	41	3794
5	1265	2628	220	38	4150
6	1058	2845	341	35	4279
7	921	3088	389	42	4440
8	663	3206	508	44	4421
9	576	3269	630	37	4512
10	470	3267	734	50	4521
11	383	3190	844	65	4482
12	329	3167	1056	71	4623
13	302	3008	1150	55	4515
14	249	2956	1298	72	4575
15	226	2922	1384	73	4605
16	219	2666	1518	82	4485
17	177	2543	1714	111	4545
18	154	2424	1814	118	4510
19	125	2382	1933	125	4565
20	119	2194	1901	119	4336
21	138	2105	2095	158	4496
22	135	1993	2176	162	4466
23	114	1869	2323	162	4468
24	90	1791	2222	163	5266
25	95	1645	2410	192	4342
26	113	1602	2560	217	4492
27	125	1527	2521	226	4398
28	88	1456	2697	273	4514
29	109	1373	2698	250	4430
30	95	1277	2604	298	4274

during the flow is listed in Table III-4. These values reflect the relative xenon activity in different sections of the trap.

III-1.7 Comparison with Theoretical Results

The spatial distribution of the activity in the trap was obtained at different times during the flow by adding the counts in the elements constituting the trap cross section. Normalized activity distributions in the trap for a flow rate of 8 liters/min are plotted for 10, 20, and 30 minutes of flow in Fig. III-7. It can be seen that as xenon moves longitudinally in the trap, the height of central maximum decreases and the distribution curve spreads out progressively.

Values of the centroid and standard deviation of the activity distributions in the trap are listed in Table III-5 for each flow time. In Fig. III-8, values for the centroid or the average distance migrated by the activity zone are plotted against time. It can be seen that as the xenon moves through the trap, the velocity of the activity zone rapidly decreases, and then levels off to a steady-state value. Because the trap legs stood about 9 cm above the alcohol level in the dry-ice bath during holdup experiments, this variation of zone velocity is the result of nonuniform temperature distribution in the trap. Hence, according to the migration rate of the activity zone in the trap, two regions may be distinguished along its length: one where there is an axial temperature gradient, and the other where the temperature is practically uniform.

By fitting the last four points in the curve to a straight line, the steady-state velocity of the activity zone in the trap was found

Table III-4. Percent activity in designated sections of the trap (see Fig. III-6) at different times during flow.

Time (min)	Area (1)	Area (2)	Area (3)	Area (4)	Area (1 + 2 + 3 + 4)
5	27.3	56.8	4.7	0.8	89.6
10	10.1	70.6	15.8	1.0	97.5
15	4.8	63.2	29.9	1.5	99.4
20	2.5	47.5	41.1	2.6	93.9
25	2.0	35.5	52.1	4.1	93.7
30	2.0	27.6	56.3	6.4	92.3

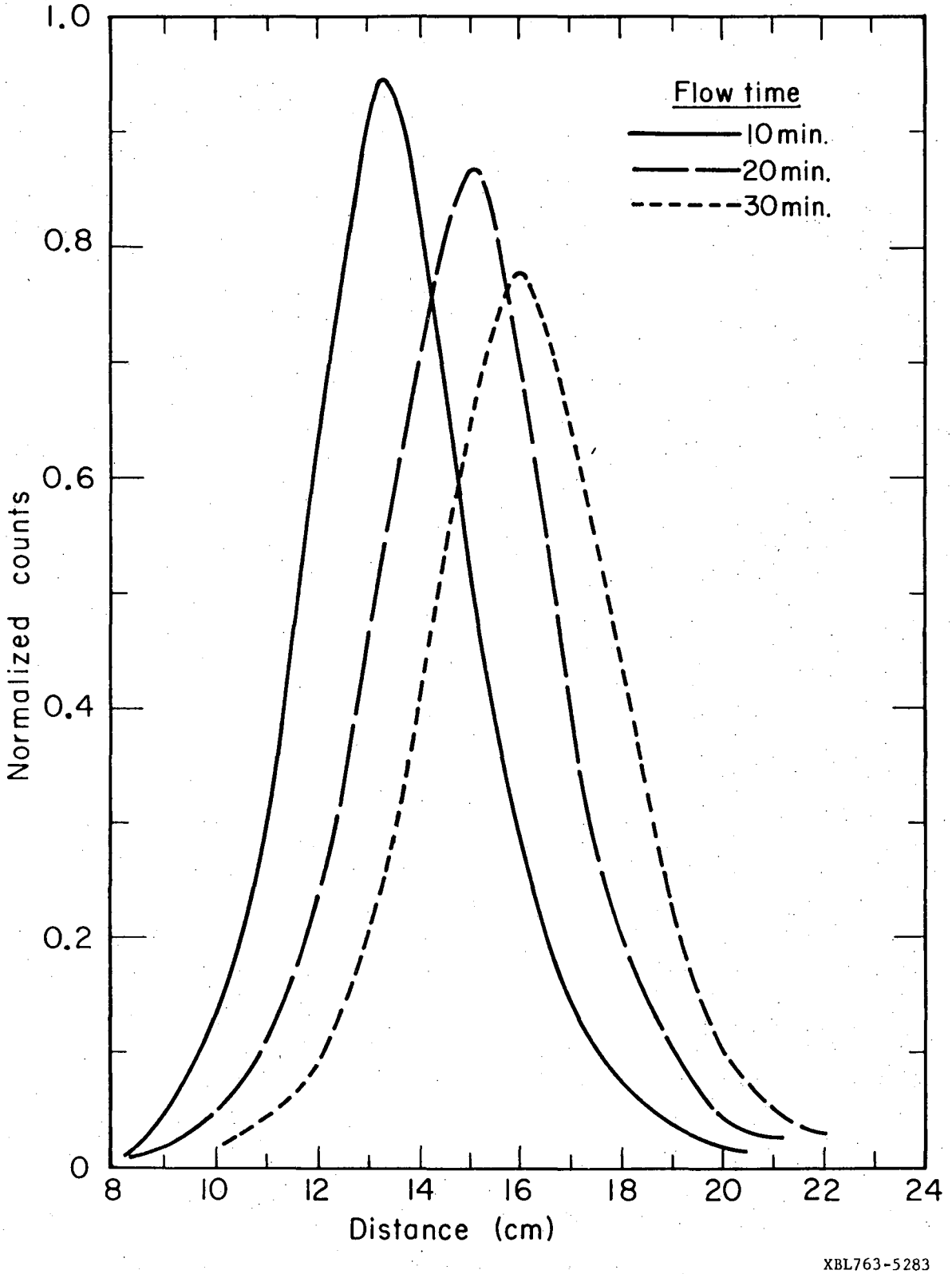

FIGURE III-7. Normalized activity distributions in the trap for a flow rate of 8 liters/min.

Table III-5. Measured and calculated values of average distance traveled and standard deviation of activity zones in the trap at different time during flow.

Flow time (min)	Mean (cm)		Standard deviation	
	Measured	Calculated	Measured	Calculated
5	11.67	13.51	1.714	1.794
10	13.24	14.02	1.883	1.884
15	14.18	14.53	1.976	1.971
20	14.97	15.04	2.070	2.053
25	15.62	15.56	2.133	2.133
30	16.04	16.07	2.224	2.209
35	16.53	16.58	2.272	2.283

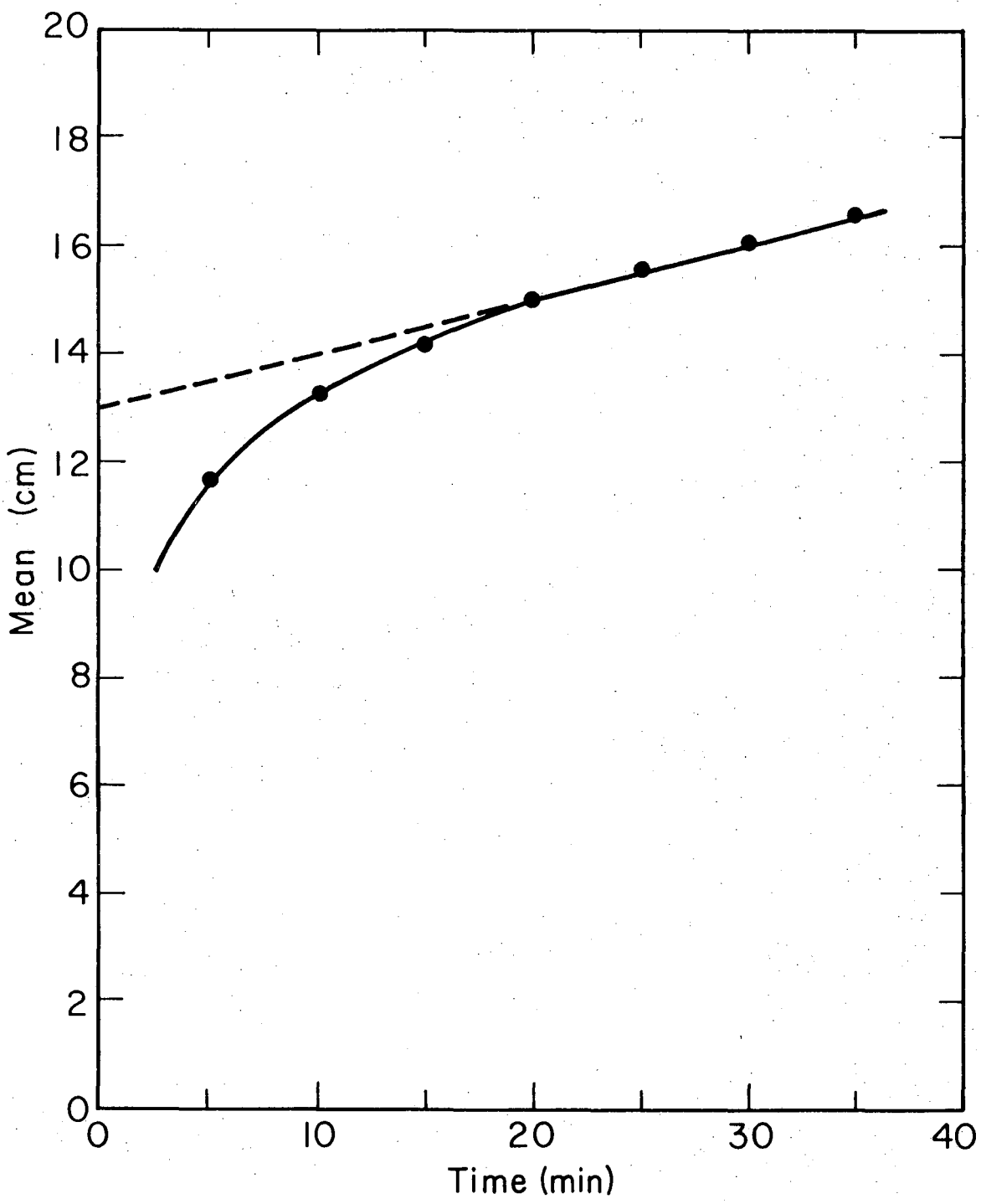

FIGURE III-8. Variation of the centroid of xenon activity distribution in the trap with flow time.

to be 0.102 cm/min. Extrapolation of this line to time zero resulted in an intercept value of 13 cm. This distance, denoted by z_o, reflects that length of trap that is partially ineffective in delaying xenon movement during the adsorption process. By knowing this steady-state velocity, the ratio of the adsorption to desorption rate constant, k, in the part of the trap where the temperature is uniform, may be calculated from the empirical relation (2-100). For a volumetric air flow rate of 8 liters/min, the ratio of k_1/k_2 was found to be equal to 15625.

It can easily be shown that $k = k_1/k_2$ and the dynamic adsorption coefficient, k_d, defined by Browning and Bolta [89], are related as

$$k_d = \frac{k}{\rho(1 - \alpha)} \quad ,$$

in which ρ is the charcoal density, and α is the void fraction. For an average charcoal density of 0.5 g/cm^3 (Table III-2), and a void fraction of 0.71, the above relation would give a k_d value of 107758 cm^3/g. In the literature no mention could be found of the dynamic adsorption coefficient of xenon in an air carrier gas at -78°C, so the obtained k_d value may only be compared to those measured in helium or argon gas.

Burnette et al [99] have given the variation of the ^{133}Xe dynamic adsorption coefficient with inverse temperature, in temperatures ranging from -45°C to 90°C, for Barnebey-Chaney Grade 107 activated coconut charcoal with helium as the carrier gas. Extrapolation of their data to -78°C gives a k_d value of 3.7×10^5 cm^3/g. Forster [102] has plotted

the xenon dynamic adsorption coefficient against temperature, between 175°K and 350°K for a variety of charcoals in argon carrier gas. His value of k_d at 195°K, corresponding to -78°C, is approximately 2×10^5 cm^3/g. Finally, First et al. [103] have measured the xenon dynamic adsorption coefficient at -78°C for two types of coconut base charcoal in argon carrier gas. For the one with surface area of 1150 m^2/g, k_d = 92,000 cm^3/g; and for the other with surface area 1200 m^2/g; k_d = 98,200 cm^3/g. If one considers the differences between the sources of charcoal, the carrier gas, and the experimental techniques, the obtained value of the dynamic adsorption coefficient agrees reasonably well with those reported in the literature.

In Fig. III-9, the square of the standard deviation of the activity profiles are plotted against time. This figure shows that in the region where the trap temperature is uniform, the square of the standard deviation increases linearly with time. As summarized in the empirical relation (2-101), similar results were reached by a theoretical analysis of the dynamic adsorption process. Therefore, the slope of this line (0.0672 cm^2/min) may be set equal to the ratio of $d\sigma^2/dt$ in equation (2-101) in order to find a second relation between k_1 and k_2; and hence the value of the adsorption and desorption rate constants can be estimated within this region.

Values of the adsorption and desorption rate constants resulting from this approach are 114 ± 2 sec^{-1} and $73 \times 10^{-4} \pm 1 \times 10^{-4}$ sec^{-1} respectively. For these values of k_1 and k_2, the mean and standard deviation of activity distributions, corrected for the intercept value z_o = 13 cm and σ^2 = 2.886 cm^2, were calculated by using the empirical relations

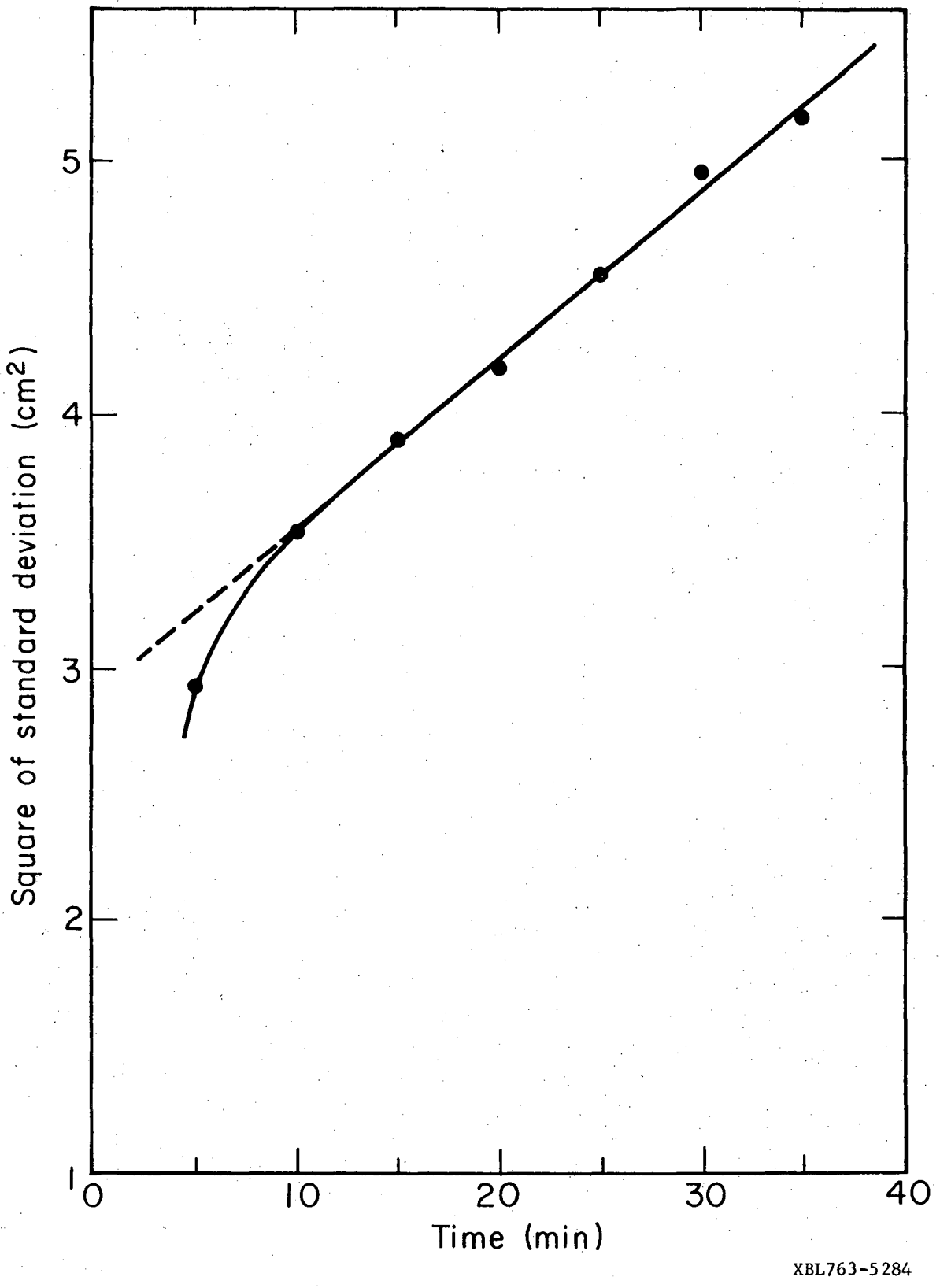

FIGURE III-9. Variation of the square of the standard deviation of the activity distribution in the trap with flow time.

(2-100) and (2-101). A summary of the results are given in Table III-5.

Since there is an axial temperature gradient present in the inlet port of the trap, the adsorption and desorption rate constants in this region of the trap vary with the trap position. However, an average value may be estimated for each of the rate constants within this region. By using the standard deviation of the xenon activity distribution in the trap in relation (2-101) and the average velocity of the activity zone during the first five minutes of flow in equation (2-100) the approximate values of the adsorption and desorption rate constants in the nonuniform temperature region of the trap were found to be 298 sec^{-1} and 0.435 sec^{-1}, respectively. For these values of the rate constants, the normalized spatial variation of the activity zone during the first 6 minutes of flow in the trap, calculated from expression (2-70), is plotted in Fig. III-10. It illustrates the development of the activity zone profile into a Gaussian distribution.

III-2. Xenon Removal from Charcoal

A major problem encountered in the design of the recycling apparatus for pulmonary function studies was the recovery of xenon gas in a small volume of air. Although it was possible to release xenon from charcoal by heating the trap, total recovery of xenon was not practical because of the high concentration ratio of air/xenon in the trap and the low thermal conductivity of charcoal.

By heating the trap described in Section III-1.2 to 200°C for 30 min, more than 50 percent of the xenon was still trapped in the charcoal column even though the volume of air released during heating of the trap

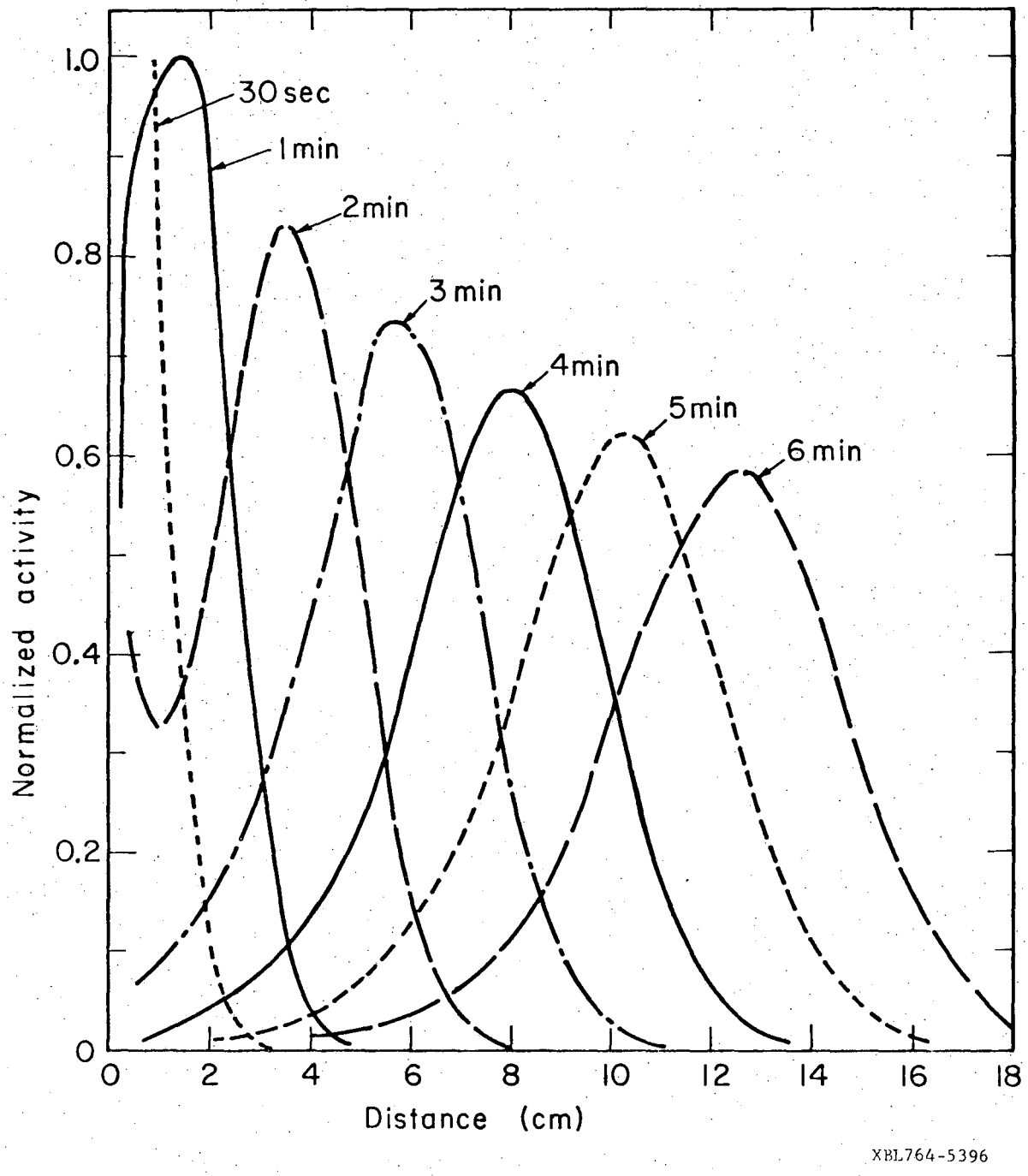

FIGURE III-10. Normalized activity distribution in the trap during the first 6 minutes flow, calculated from expression (2-70).

was more than 8 liters. Further, evacuation of the trap at dry-ice temperature did not improve the collection efficiency since 10 to 20 percent of the xenon was lost while the trap was pumped out.

Previous experiments [115,116] have indicated that water vapor drastically affects the efficiency of charcoal for inert gas adsorption. When the moisture content was increased in a stream of krypton-carrying helium, it was found that the capacity of the charcoal to adsorb krypton was linearly reduced [116]. To determine the feasibility of recovering millicurie amounts of xenon from a charcoal adsorption bed into a small volume of air (less than 5 liters), a series of experiments was made by passing low pressure steam (100°C) through the charcoal column at room temperature.

III-2.1 Adsorption of Water Vapor by Charcoal

Charcoal, being of a porous nature, besides presenting enormous surface and accordingly having high adsorptive capacity, also offers the opportunity of capillary action, especially to the vapor of a liquid that has as high a surface tension as has water. The isotherm of the adsorption of water vapor by activated coconut charcoal at 100°C (Fig. III-11) obtained by Coolidge [117], as well as other studies [118-128], support the view that the mechanism by which water vapor is taken up is some way distinct from that for other vapors and gases. In nearly every other instance, the adsorption isotherm of the gas may be described analytically by an equation of the Langmuir or Freundlich type. In the case of water vapor, however, the form of the curve is that classified by Emmett as a

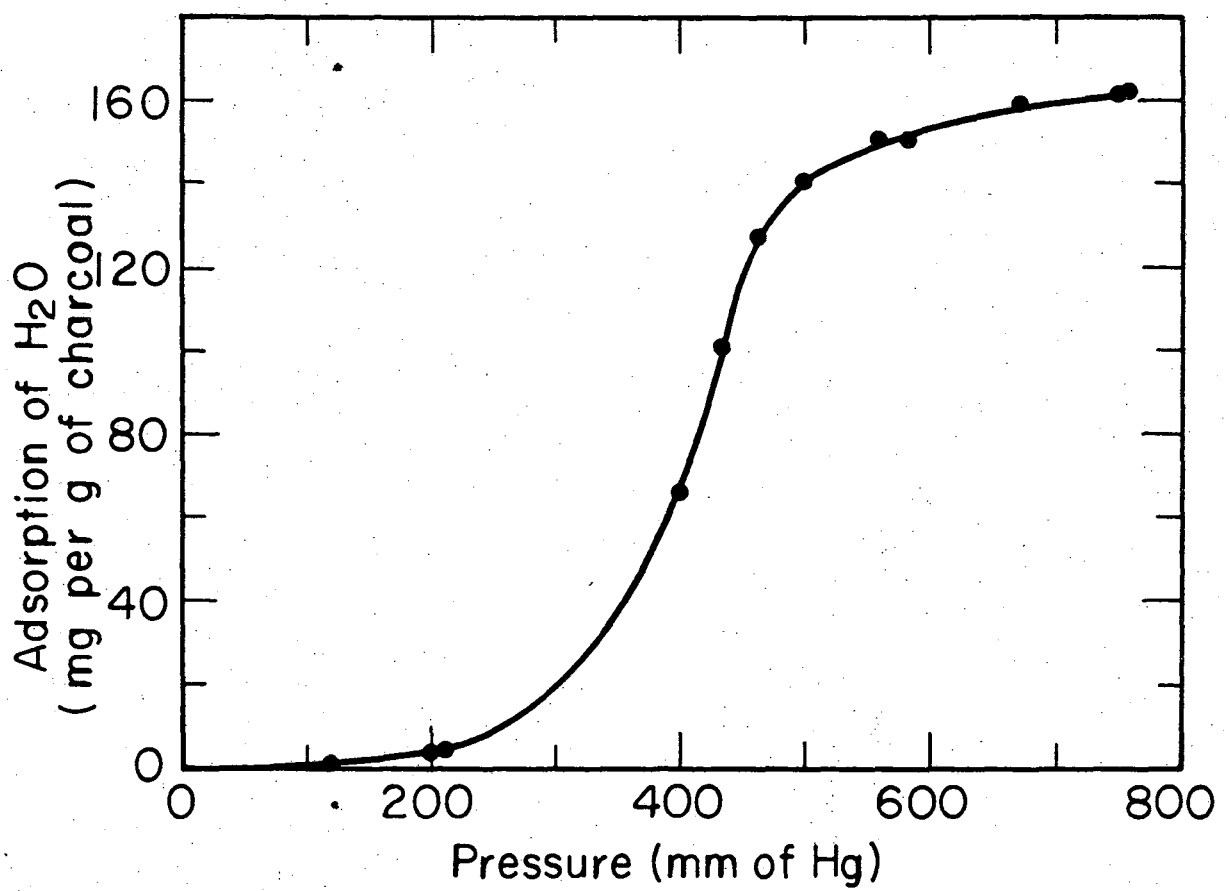

XBL762-5208

FIGURE III-11. Adsorption isotherm of water vapor on coconut charcoal at 100°C [117].

type V isotherm [129]. In contrast with the Langmuir adsorption isotherm, at low values of relative pressure the adsorption curve is convex rather than concave to the pressure axis; very little adsorption is found at low pressure, and the greater part of adsorption occurs over a narrow relative pressure range. Moreover, adsorption is not marked near saturation pressure.

The adsorption behavior of water vapor on activated charcoal shows the characteristic of multilayer formation. From the viewpoint of B.E.T. theory of multilayer adsorption [130], such a curve is explained on the assumption that the energy of adsorption in the first layer is less than the energy of liquification. The region near saturation may be explained on the assumption that all the voids have been filled, and the bulk condensation on the surface does not occur. On the other hand, the form of the curve may also be interpreted from the older conception of capillary condensation [118,121-123,126,128]. The first smooth part of the curve represents the taking up of water by capillary action in some small-size pores. The existence of the sharp rise in the isotherm may be accounted for by the filling of capillaries. This is completed at the pressure below the saturation vapor pressure because the last layer adsorbed in the capillary is attracted from both sides and so condenses more readily.

III-2.2 Experimental Apparatus and Procedure

The schematic drawing of the experimental apparatus is shown in Fig. III-12. It is essentially the same one used in Section III-1.2. The minor modification includes a kettle and hot plate for steam generation. The opening of the kettle is fitted with a cork through which a 1/4-inch

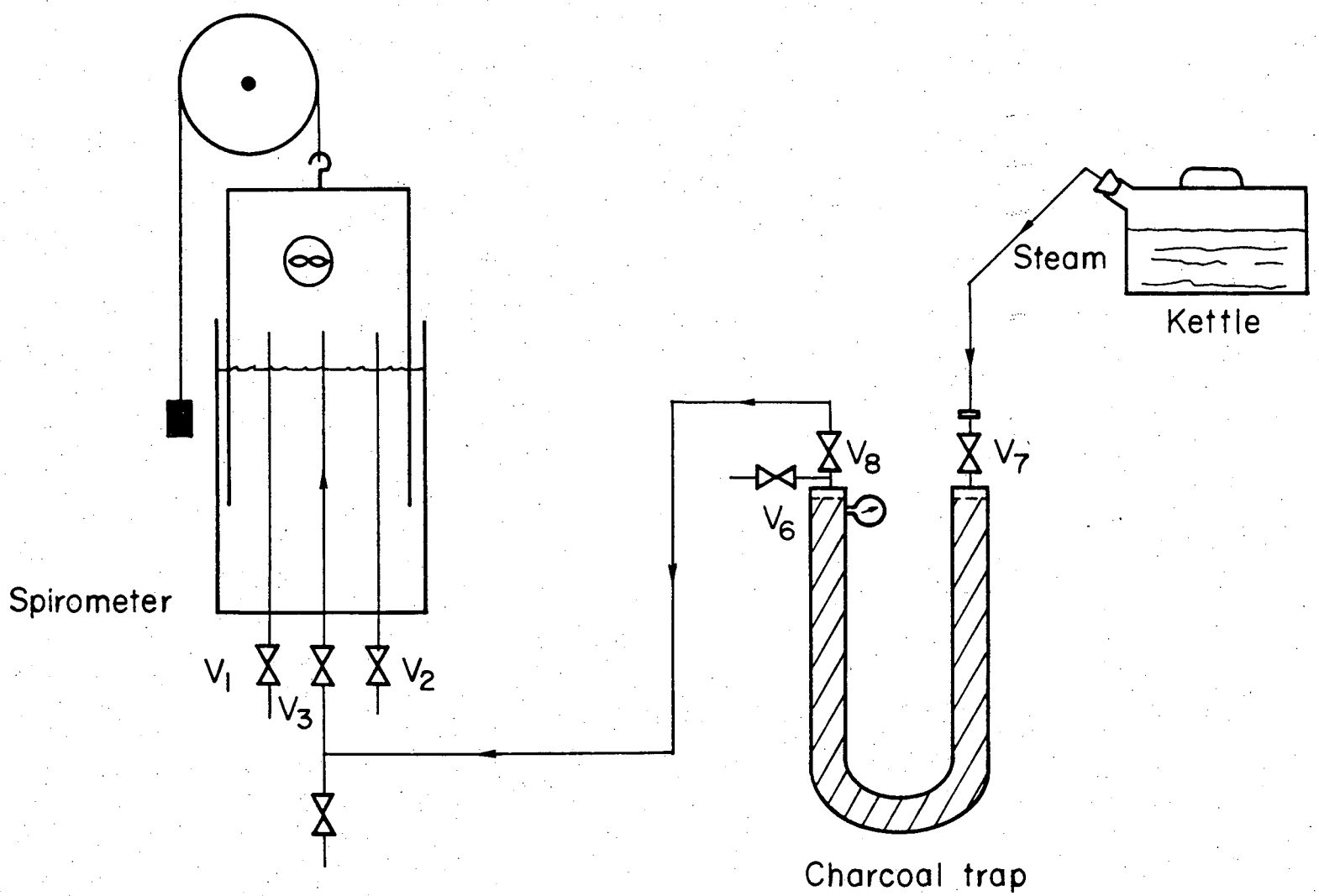

FIGURE III-12. Experimental apparatus used during elution with steam.

insulated copper tubing is passed. The outlet of the tube may be easily connected to valve V_7 of the trap.

When the charcoal trap used in the xenon holdup experiment reached room temperature, all the valves attached to the trap were closed. Valve V_8 of the trap was then connected to valve V_3 of the spirometer with a 1/4-inch diameter, insulated, copper tubing. The flow system was arranged so that the trap was in the camera field again. After discharging the excess air in the spirometer, all valves except V_3, V_7, and V_8 were closed; the steam line out of the kettle was connected to the trap, and the data-collecting system was turned on.

III-2.3 Experimental Results

Normalized activity profiles of xenon are plotted in Fig. III-13 after 30 minutes of flow in the trap at dry-ice temperature (-78°C) and 1.5 hours later, when the trap has reached room temperature (~ 26°C). Comparison of these distributions shows that as the trap warms up to room temperature, peak activity decreases by about 6 percent while the location of the peak remains the same; the width at half maximum of the distribution curve increases from 4.5 to 4.81 cm; and the gas diffuses slightly more in the direction of air flow to the atmosphere.

The distribution of xenon activity in the trap while steam flows through the charcoal column at room temperature is shown in Fig. III-14 as a series of displays in isometric mode. The duration of each frame displayed is 15 sec. A comparison of the displays reveals the effectiveness of steam for removing xenon from the charcoal. By adding the counts in a section of the frame shown in Fig. III-15, activity in this region

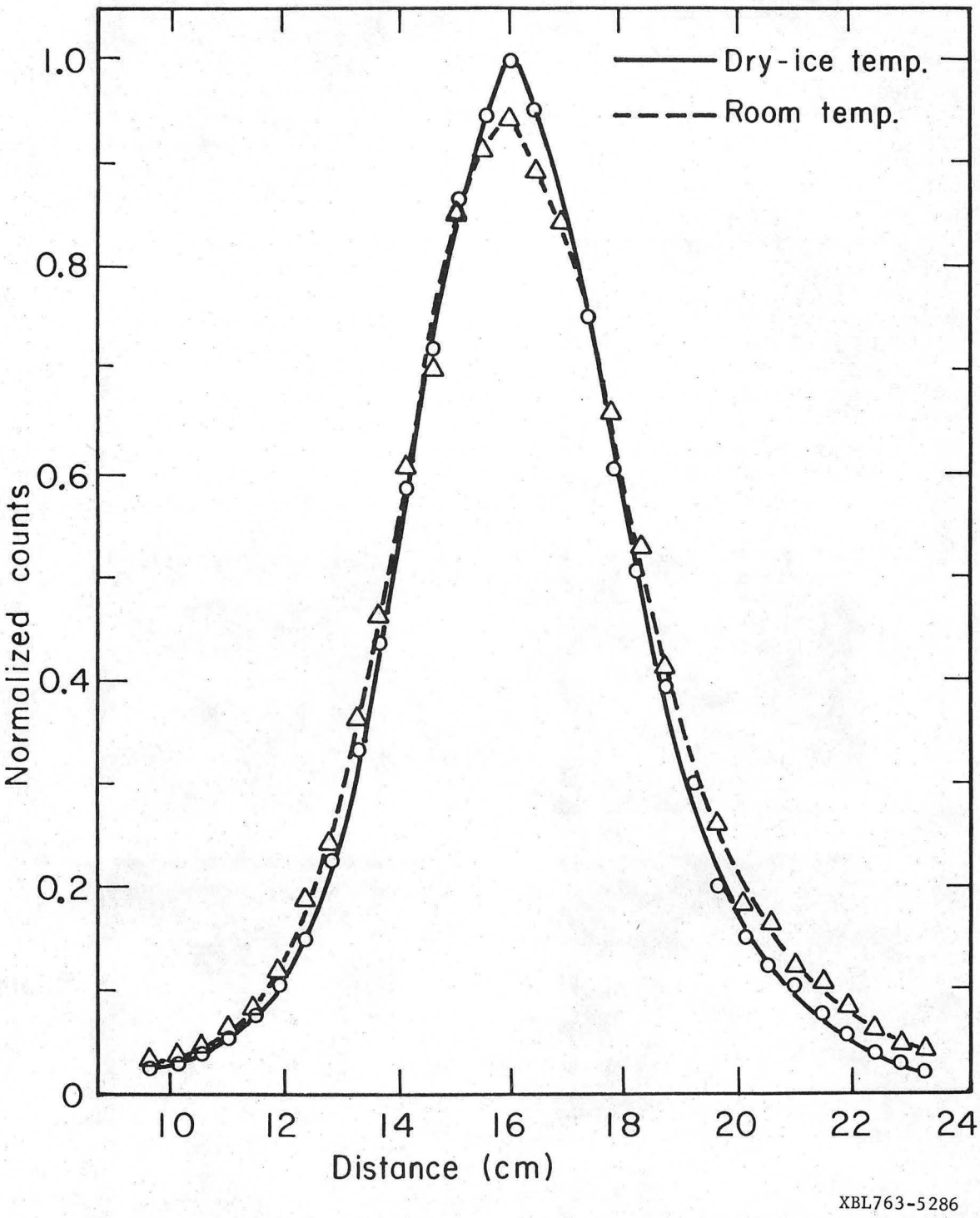

FIGURE III-13. Xenon distribution in the column at dry-ice temperature (-78°C) after 30 minutes flow, and after 1.5-hr warm-up to room temperature (26°C).

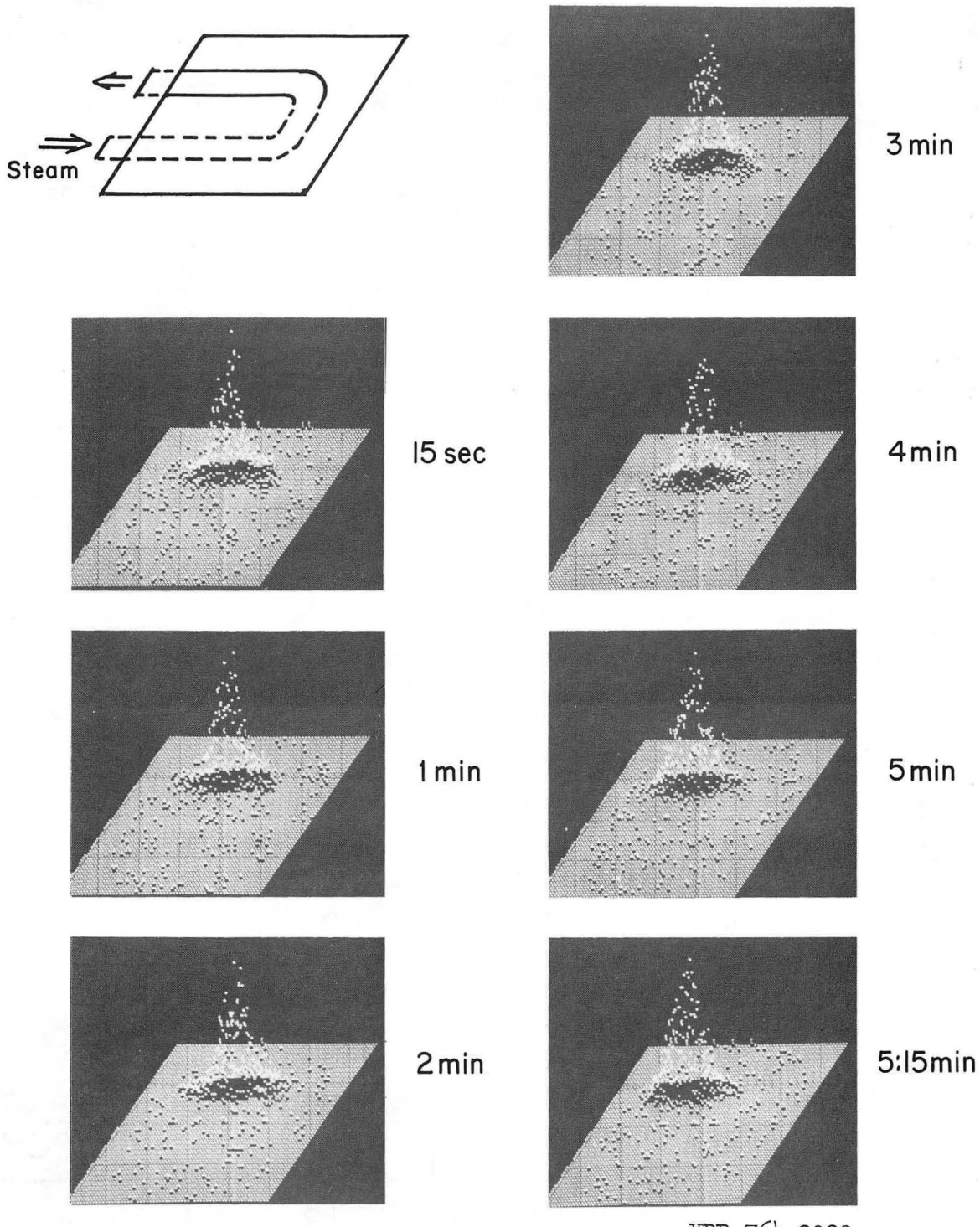

Fig III-14. Distribution of xenon activity in the trap during elution with steam.

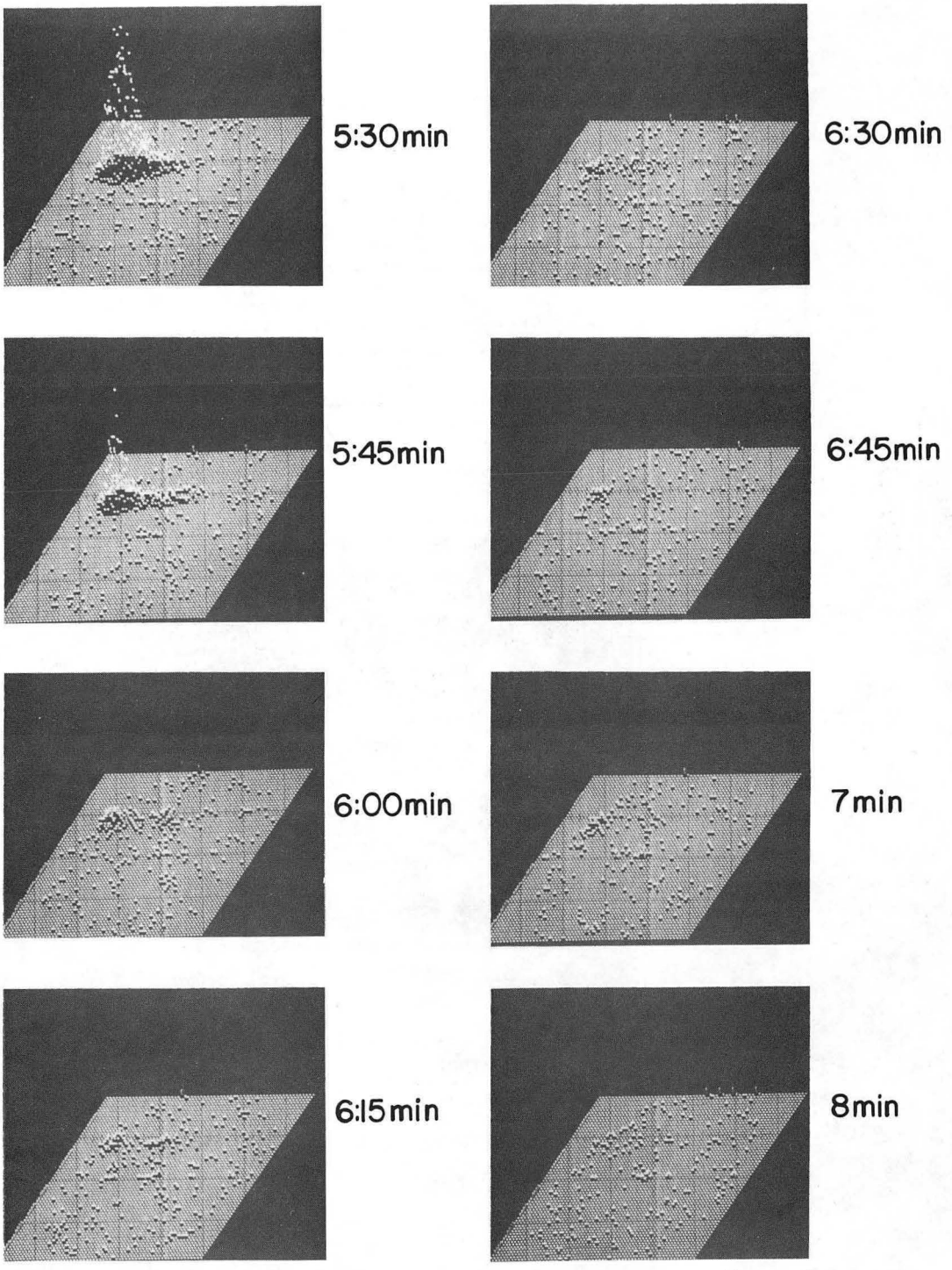

Fig III-14 (Continued.)

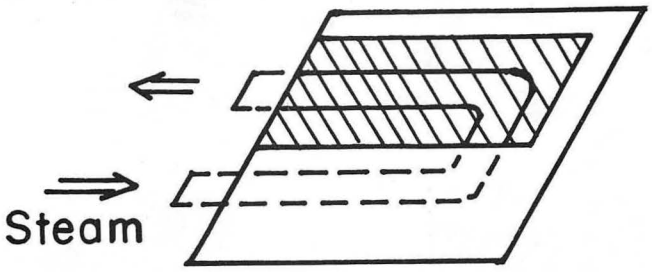

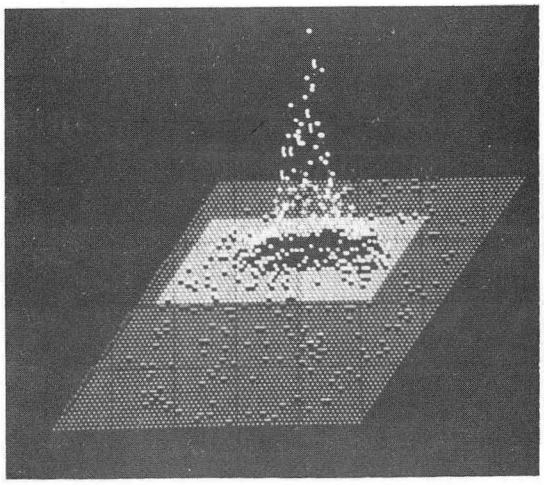

XBB 764-3027

Fig III-15. Selected area of the trap used to obtain time-activity distribution during elution with steam.

of the trap is plotted against time in Fig. III-16, where it can be seen that by passing low pressure steam through the charcoal column, once it has reached room temperature, all the xenon is removed from the trap in about 7 minutes. The slight increase in activity before the sharp decrease is due to flow of xenon from the remainder of the trap.

A close estimate of the traveling rate of the activity zone and the steam linear velocity through the column may be obtained from Figs. III-14 and III-16. It takes about 300 sec for steam to reach the activity zone in the column located 40 cm from the steam inlet port, giving an effective steam velocity of approximately 40/300 = 0.133 cm/sec. In the displayed section, the axis of the activity zone migrates a distance of approximately 4 cm through the column in 30 sec, or a wave velocity of about 0.133 cm/sec. Therefore, the activity zone travels in the column with the same velocity that the steam flows.

The activity of the xenon as it arrived in the spirometer was obtained from the chart recorder tracing as is shown in Fig. III-17. The arrival of steam to the spirometer was delayed due to its passage through connecting lines. Upon reaching the spirometer, the steam is condensed while xenon, being highly insoluble in water, enters the gas mixture in the spirometer. The volume of gas in the spirometer increases during the passage of steam through the charcoal column by an average of about 4.6 liters. Comparison of the counts and volume before pumping xenon out of the spirometer to the counts and volume obtained after steam condensation showed that an average 96% of the xenon is recovered per cycle. The other 4% was presumably lost to the atmosphere during flow through the column and while warming the trap to room temperature.

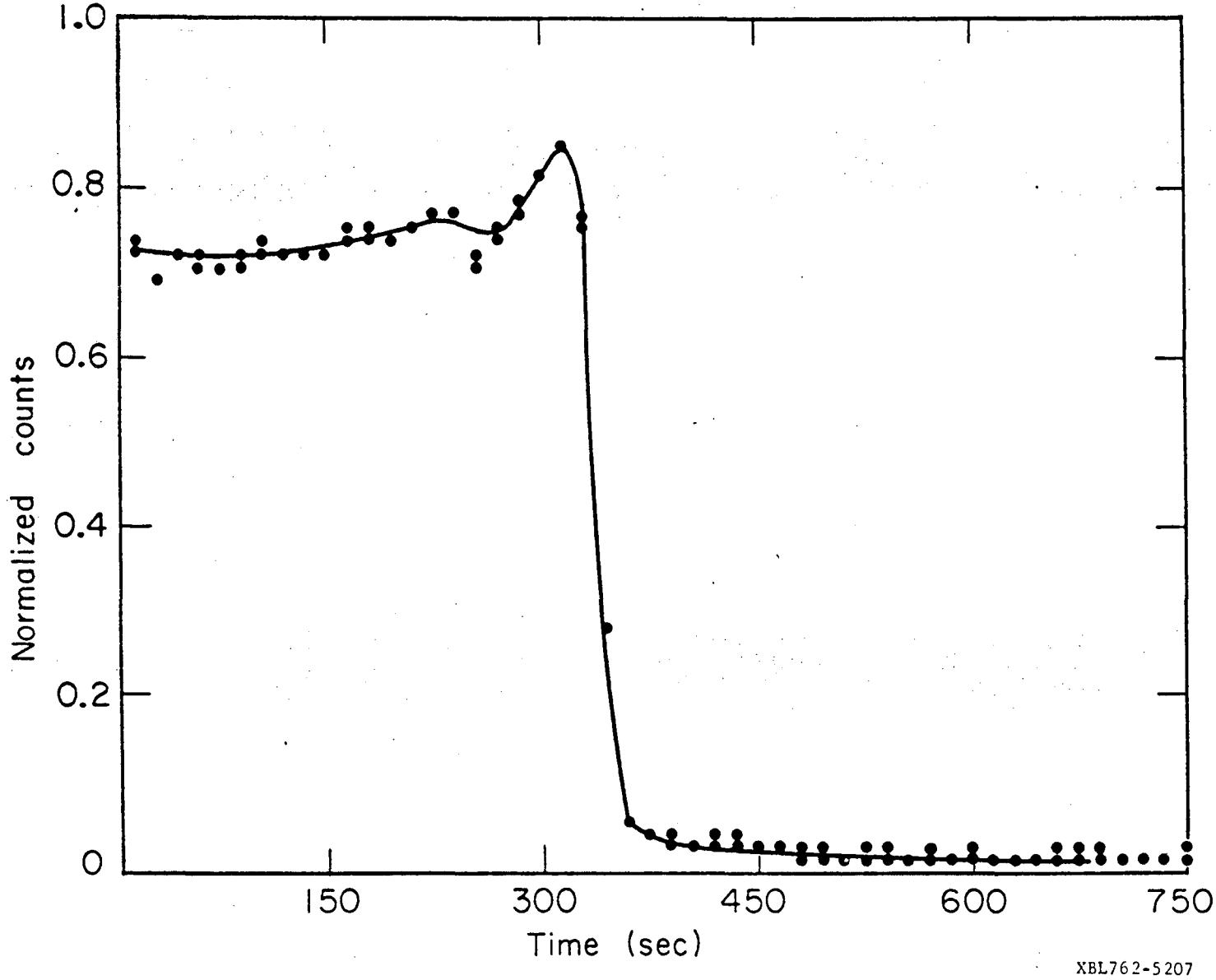

FIGURE III-16. Variation of ^{133}Xe activity in the trap versus time during elution with steam.

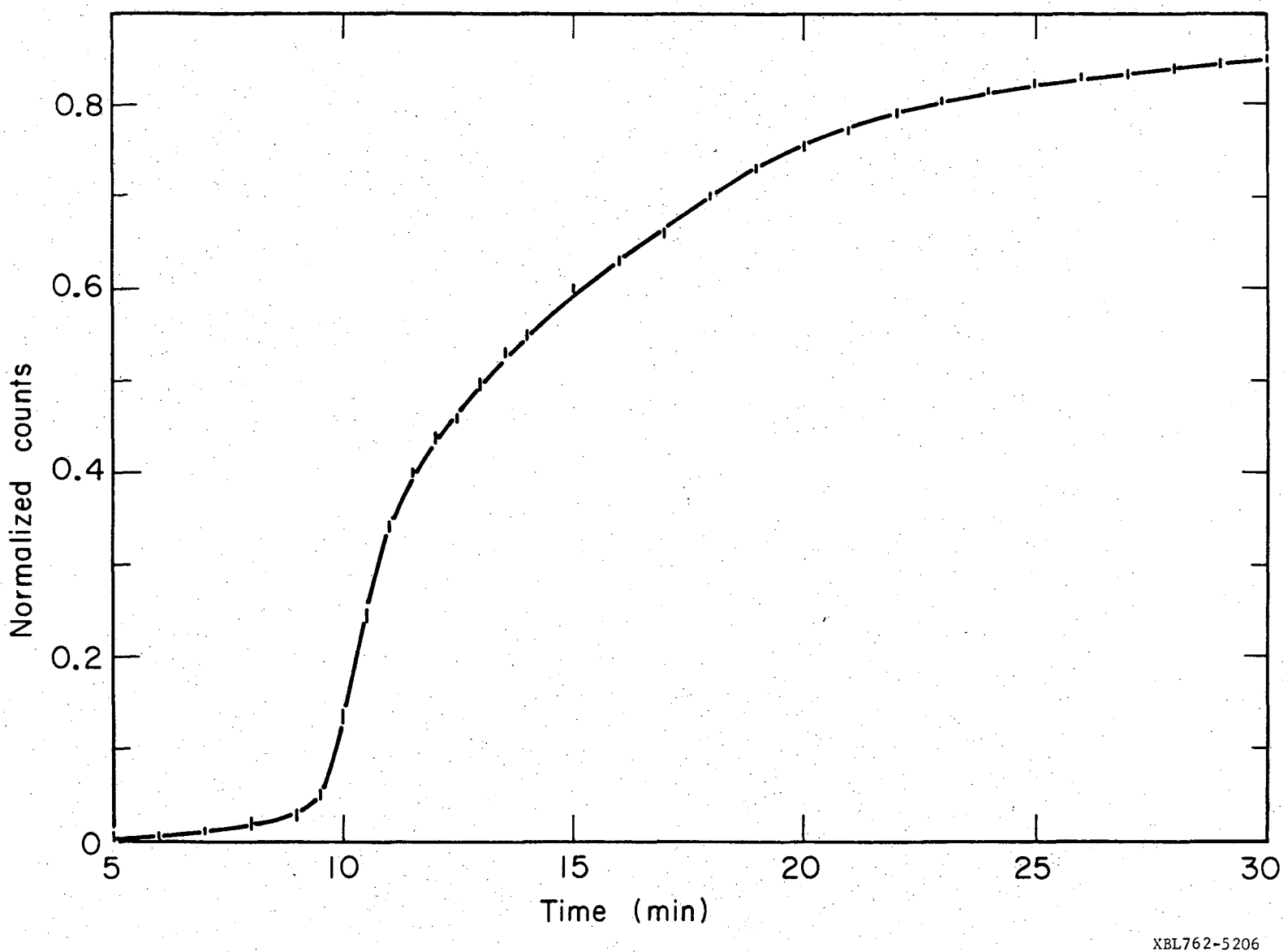

FIGURE III-17. Normalized activity level in the spirometer during arrival of xenon with steam.

III-2.4 Steam-Carbon Reaction

The reaction between carbon and steam is one of the oldest and most useful industrial processes [131], but the actual mechanism of the reaction is still not well understood. At least four reactions may occur, each of which affects the course of the others:

$$C + H_2O \rightarrow CO + H_2 \qquad (A)$$

$$C + 2H_2O \rightarrow CO_2 + 2H_2 \qquad (B)$$

$$CO + H_2O \rightleftarrows CO_2 + H_2 \qquad (C)$$

$$C + CO_2 \rightarrow 2CO \qquad (D)$$

Although a large number of reports on these reactions has appeared in the literature [132-146], most of the work was done at a temperature range of 600 to 1300°C.

There is general agreement [138-142] that at this high temperature range, the primary products of the reaction between steam and carbon are carbon dioxide and hydrogen and that carbon dioxide is formed mainly from the subsequent water-gas reaction (C) which reaches or tends to reach equilibrium. It has been found, however, that for all temperatures throughout the range of 25 to 200°C, the reaction of water with carbon gives hydrogen and a carbon-oxygen complex, which decomposes easily to give carbon dioxide [142,143]. The tendency to form carbon dioxide is not only a function of temperature, but is also critically dependent on the water concentration [144]. Moreover, the steam-carbon reaction depends generally on the forms and resources of carbon used; wide variations were observed even with samples of the same charcoal, which differed only in heat treatment [135].

To determine the gas products obtained after flow of low-temperature steam (~ 100°C) through the charcoal trap, samples of gas mixture in the spirometer were chromatographically analyzed. Table III-6 lists the percentage of each gas found in the spirometer after steam condensation. The presence of 13.4 percent carbon dioxide in the gas mixture is attributed to chemisorption and oxidation of the charcoal by oxygen.

Table III-6. Composition of gas mixture in the spirometer after steam condensation.

Gas Analyzed	Percent in 1 cm^3 at room temperature
N_2	68.300
O_2	18.200
CO_2	13.500
H_2	0.065
CO	0.003

CHAPTER IV.

RECYCLING OF RADIOACTIVE INERT GASES

IV.1 Design Description of Recycling Apparatus for Pulmonary Function Studies

The general system (Fig. IV-1) consists of two separate closed circuits, which can be interchanged by using the four-way walve. With the system in circuit one, the air-xenon mixture circulates between the subject and the spirometer to reach a uniform xenon concentration in the lungs. The oxygen consumed is supplied from the oxygen tank while exhaled carbon dioxide is adsorbed. With the system in circuit two, xenon is washed out of the first circuit and the subject's lungs and into a charcoal-filled trap while air circulates. Again the oxygen consumed is supplied by an oxygen tank while carbon dioxide and water vapor are adsorbed by appropriate adsorbers.

The major components of this system are the spirometer, carbon dioxide adsorber, water adsorber, xenon gas trap, pump, and oxygen supply tank. The arrangement of the component parts of the apparatus is shown schematically in Fig. IV-1.

A. Spirometer

The dimensions of the spirometer are shown in Fig. IV-2. The bottom part of the spirometer is made of nickle-plated brass. The top is made of aluminum and is balanced by a weight suspended from a cord passing over

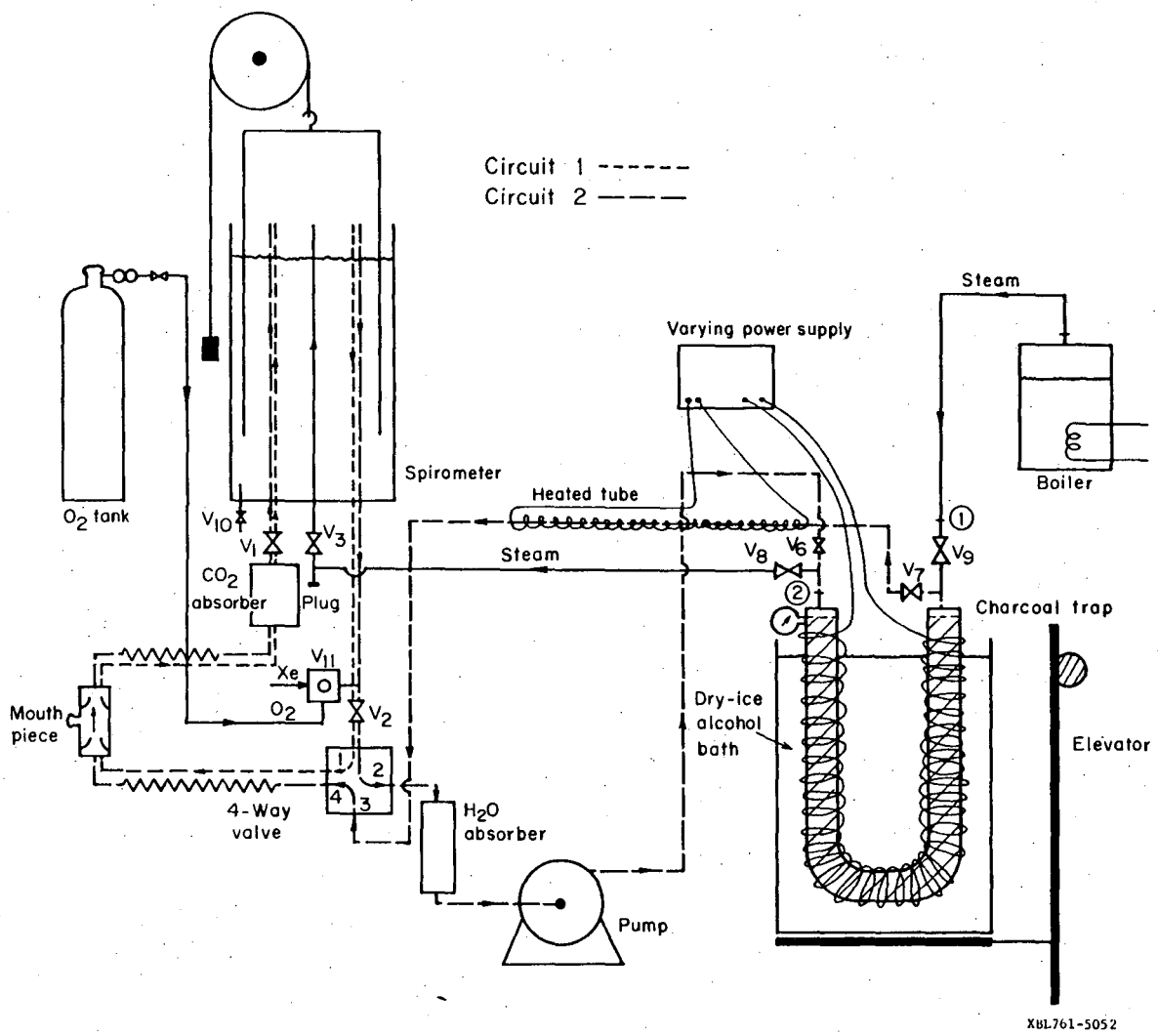

FIGURE IV-1. Schematic diagram of recycling apparatus.

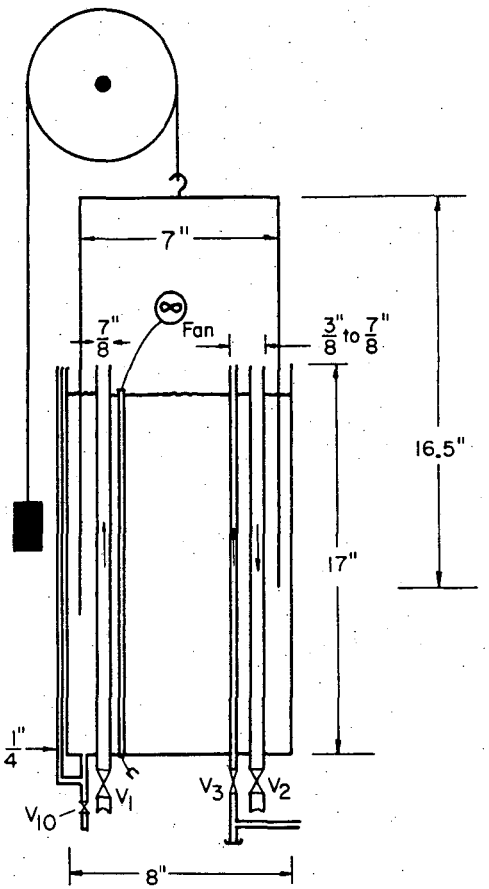

FIGURE IV-2. Spirometer.

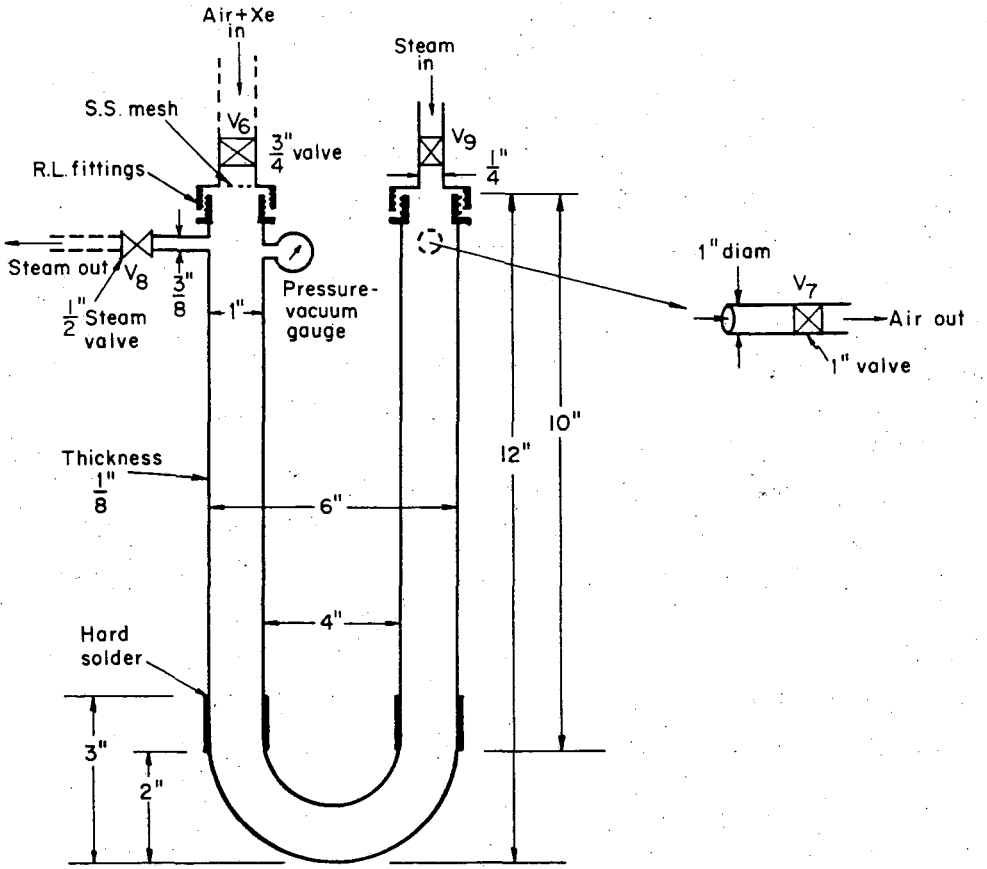

FIGURE IV-3. Xenon trap.

a pulley, which records the respiratory cycle. The maximum air capacity of the spirometer is 10 liters and the volume displacement of the top part is about 9.4 liters. A small fan installed in the inside chamber of the spirometer assures the complete mixing of xenon with air. Three tubes pass through the bottom of spirometer; each tube is connected to appropriate valves, V_1, V_2, and V_3. Air-xenon, movement in and out of the spirometer is through 7/8-inch diameter tubes. The air-xenon inlet tube to the spirometer is connected to the outlet of the CO_2 adsorber through valve V_1. The air-xenon outlet is connected to a four-way valve, V_5, through valve V_2. The other 3/8-inch diameter tube is designed for inlet of the steam-air-xenon mixture. At the end of this tube there is a plug for draining extra water accumulated during steam condensation. The spirometer is also equipped with a valve, V_{10}, at the bottom for water drainage, and with level indicators on the side, to monitor the volume of air and the level of water in the spirometer.

B. Carbon Dioxide Absorber

The container, made of stainless steel,* has a 5-in. diameter and is 3.5 inches high. The inlet of the container is connected to the outlet of the mouthpiece through 7/8-in. i.d. corrugated copper tube. The outlet is connected to the air-xenon inlet tube of the spirometer. The container is fitted with an air-tight removable top to replace soda lime. About a pound of soda lime, loosely packed to allow minimum resistance to air flow, is sandwiched between two stainless-steel mesh screens.

---

*NOTE: Instead of stainless steel, a Lucite container may be used with Carbosorb-type soda lime, which gives a marked color change with the degree of exhaustion.

C. Water Absorber

The container, 2.5-in. diam. by 8-in. high, is made of Lucite and contains about a pound of Drierite with a moisture capacity of 0.2 pound, per pound used. The inlet of the absorber, 1/4-in. diam., is connected to opening #3 of the four-way valve. The outlet, 1/4-in. diam., is connected to the inlet of the pump. The container has a removable top for Drierite replacement. This absorber is capable of keeping the air dry for circulation at a rate of 10 liters/min for two to three hours.

D. Pump

Xenon gas is highly soluble in oil and greases, and is absorbed in significant amounts by rubber as well as by a variety of plastics. This property of xenon complicates the use of a regular pump. The best commercially available pump, chosen for the system, is the rotary, oilless Model No. 0531, air compressor from Gast Manufacturing Company. This model pump delivers pulse-free, oil-free air, and does not need any lubrication.

E. Xenon Trap

The xenon trap is a "U"-shaped nickle-plated copper tube, with 1-in. i.d. and 1/16-in. thickness. It is filled with 6-14 mesh, activated coconut charcoal from Fisher Scientific Company (Fig. IV-3). The overall length of the trap is 22 inches (56 cm). There are four openings to the trap, all fitted with stainless steel mesh. The air inlet is connected to the pump outlet through valve V_6. The air outlet is connected to opening

#3 of the four-way valve through valve V_7 and a 1-in.-diam. copper tube. A heating tape, powered by an adjustable supply, is wrapped around the tube to warm cold air coming from the trap. Though not installed, a thermostat may be used at opening #3 of the four-way valve to regulate the intake gas temperature. The 1/4-in.-diam. steam inlet is connected to the steam generator through valve V_9, and the steam-air-xenon outlet is connected to the spirometer through valve V_8 and 3/8-in.-diam. insulated copper tubing. The trap is equipped with a vacuum pressure gauge to monitor the pressure inside the trap. The trap is firmly attached to the frame and may be easily disconnected to replace the charcoal. A Calrod heating unit with variable power supply is soldered to the trap. The temperature of the tube may be monitored with a stainless-steel clad, copper constantan thermocouple.

The auxiliary components of the system are the intake-outlet assembly, steam generator, mobile dry-ice bath, and four-way valve. The whole system is supported by a frame 16 × 21 × 60 in. high, made of Dexion slotted angle metal bars. Lead shields hinged to the side of the frame surround the apparatus: the shielding being 0.375 in. thick on the side that faces the gamma camera, and 0.187 in. think on each of the other three sides. The frame is mounted on four casters so that it may be moved about easily.

F. Intake-Outlet Assembly

Make of Lucite, the intake-outlet assembly has three openings: one in the middle, which is fitted with a mouthpiece; the inlet port, attached to corrugated, flexible copper tubing, which receives the air-

xenon mixture from the four-way valve and the oxygen from the supply tank; the outlet port, which delivers the expired gas to the carbon dioxide absorber through similar copper tubing. Two flutter valves in the assembly assure the flow of air in the proper direction. The level of the assembly is adjustable with two moving aluminum bars attached to the frame.

G. Steam Generator

The steam generator is used to generate low-pressure steam for removing xenon from the charcoal. It can be filled with 2 liters of water through a 1-in. diam. opening on top. This opening is also used for the steam outlet. An asbestos-insulated 1/4-in.-diam. copper tubing pushed through a rubber stopper that fits snugly over the opening directs steam to the xenon trap. A 6-in. Calrod heating unit is incorporated inside the generator, and is used to boil the water.

H. Dry-Ice Bath

A commercial styrofoam container is filled with about 2 pounds of dry ice and ethanol and is used to cool the xenon trap to -78°C. The dry-ice bath may be raised or lowered with a motor-driven elevator system. Safety switches are installed to control the movement of the dry-ice bath.

I. Four-Way Valve

This home-made four-way valve is used to interchange the two circuits of the system. The body of the valve, made out of nickle-plated brass, has four parts: Opening #1 (7/8-in. diam.) is attached to air outlet

valve, V_2, at the bottom of the spriometer. Opening #2 (1/4-in. diam.) is connected to the inlet of the water absorber through a 1/4-in. copper tube. Opening #3 (1-in. diam.) is attached to the outlet tube of the xenon trap. Opening #4 (7/8-in. diam.) is attached to corrugated copper tubing of the same diameter, which goes to the inlet of the intake-outlet assembly. In circuit one, as shown in Fig. IV-1 and IV-4, port #1 as the inlet is connected to port #4 as the outlet. Though non-operational, ports #2 and #3 are connected at the same time. In cricuit two, port #1 as the inlet is connected to port #2, as the outlet, while port #3 as the inlet is connected to port #4 as the outlet. The seat of the four-way valve, made of aluminum, is equipped with two O-rings to prevent leakage.

IV-2. Operation of Apparatus

The operation procedure of the system consists of four phases: preparation, operation, recovery, and regeneration. Each phase is described in detail below.

A. System Preparation

With the system in circuit one, valves V_1, V_2, V_3 and the three-way valve are closed. All the connections of the system are secured except the one in position (1) between the boiler and xenon trap. After closing valves V_6, V_7, and V_8 and opening valve V_9, the dry-ice container is raised. Dry-ice and ethanol are added slowly to the container until the whole trap is immersed in the bath. Thirty to forty-five minutes is needed for the trap to reach the dry-ice temperature of -78°C. Meanwhile, the oxygen

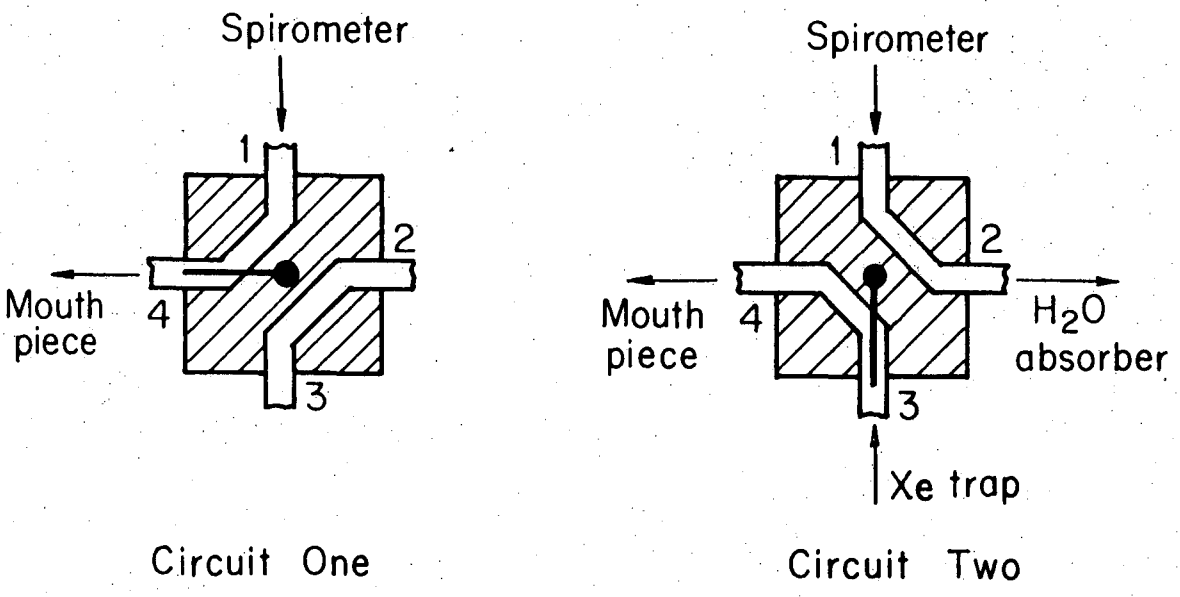

FIGURE IV-4. Positions of the four-way valve during operation of the system.

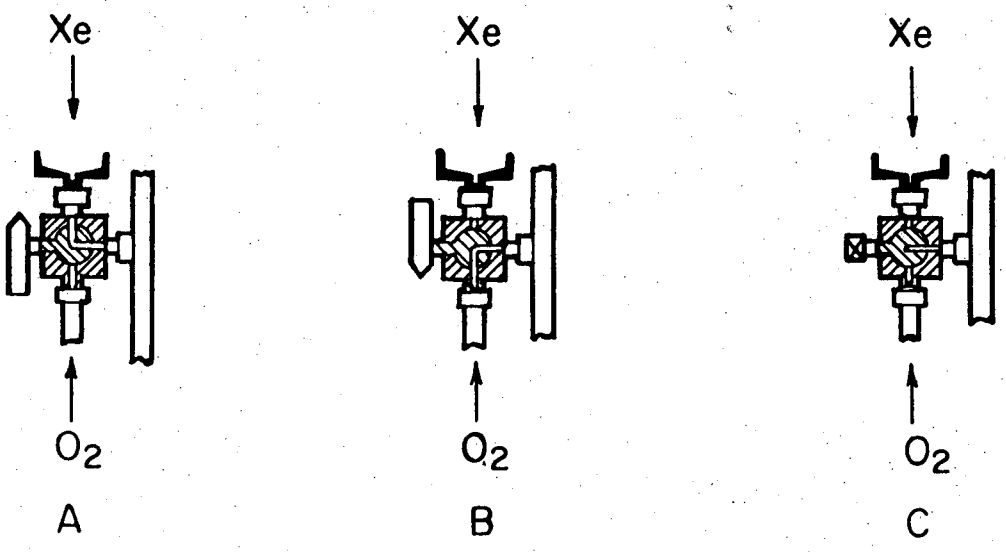

FIGURE IV-5. Positions of the three-way valve during xenon introduction into the system.

gas supply is checked, carbon dioxide and water absorbers are refilled if necessary, and the water level in the spirometer is adjusted to the appropriate level. If radioactive xenon is present in the spirometer, the system is ready to be used when the trap reaches dry-ice temperature. In the absence of any radioactive gas in the spirometer, air in the spirometer is discharged by opening and closing the three-way valve, V_{11}, between position A and B (Fig. IV-5).

By cooling the charcoal to dry-ice temperature, three liters of air inside the xenon trap would be adsorbed on the charcoal. If valve V_9 had been left closed, the gauge on the trap would have indicated a vacuum of 15 mm Hg below atmospheric pressure. Therefore, to replenish the air adsorbed on the charcoal it is necessary that the xenon trap remains open to the atmosphere while being cooled down to dry-ice temperature.

With the system in circuit one, and valves V_1, V_3, and V_6 kept closed, a known dose (10 to 20 mCi) of xenon radioactive gas is introduced to the bottom of spirometer by setting the three-way valve in position A (Fig. IV-5). The three-way valve is then switched to position B and about 0.5 liter of oxygen is introduced to flush xenon gas into the system. By switching back and forth between position A and B, and by introduction of another 1 to 2 liters of oxygen, the system is ready to be used. The three-way valve is set in position C. The patient is seated with his back to the gamma camera and the mouthpiece is adjusted to his mouth.

B. Operation

The apparatus may be used to carry out the following types of studies.

Rebreathing. With the system in circuit one, valves V_1 and V_2 at the bottom of the spirometer are opened to allow gas to circulate. Rebreathing is carried out for 3 to 4 minutes.

Washout. For washout, the first valve V_9 is closed and valves V_6 and V_7 are opened; then the system is switched to circuit two and the pump is turned on. After the washout is complete, the circuit is turned back to circuit one, the pump is turned off, and the mouthpiece is taken out.

Perfusion. After the radioactive xenon gas in saline has been injected intravenously, the expired gas can be rebreathed. The system setting is similar to the rebreathing mode except that priming with radioactive xenon gas is not required. Oxygen may be added to the spirometer if necessary.

C. Xenon Recovery

Steam is used for desorption of xenon gas from charcoal. After opening valve V_9 to release excess air, which will be desorbed from the charcoal surface, the dry-ice bath is lowered and the trap is allowed to come to room temperature; usually, one to two hours is necessary for this transition. This time may be shortened if the Calrod heating unit on the trap is heated slowly. By warming the trap from -78°C to 20°C, about 2 to 5 percent of the xenon and 3 liters of air are discharged to the atmosphere.

While xenon is coming to room temperature, 2 liters of water are added to the boiler, and the inside heater is turned on. After closing valves V_1, V_2, V_6, and V_7 and opening valves V_8 and V_9, the boiler is

connected to the xenon trap at connection (1). Depending on the temperature of the trap, the steam-air-xenon mixture reaches the spirometer 15 to 30 minutes later. In the spirometer steam condenses, leaving 4 to 5 liters of gas inside. At the end, after closing valve V_3 at the bottom of spirometer, the heater is turned off and the steam generator is disconnected from the trap at position (1).

D. Regeneration

It is possible to regenerate steam-contaminated charcoal for reuse without removing it from the trap. After disconnecting the trap from the system at position (2), the remaining water in the trap is boiled away with the Calrod heating unit on the trap. It takes about 2 hours to restore the charcoal to its original adsorptive capacity. The operation may be speeded up considerably by pumping air through the trap.

IV-3. Design Analysis

A. Flow Rate

The volume of air inspired or expired by an average, healthy individual during each respiratory cycle, the tidal volume, is about 400 to 500 ml. The average frequency of breathing is about 14 to 16 times per minute. Therefore an average-size individual moves 6000 to 8000 ml air/min through his lungs. This value also represents the average gas flow rate in the designed system. For a reasonable size scale of apparatus, this range of flow rate implies a high linear velocity of carrier gas in the dynamic adsorption process.

B. Temperature

Since the energy of gas molecules is less at low temperatures, they can not as readily desorb from the charcoal surface into the moving gas stream. To achieve an effective removal of xenon from air streams within this range of flow rates, the temperature of the charcoal granules has to be as low as possible. Dry-ice-ethanol bath (-78°C) was selected as the cooling liquid since it provides the lowest conventiently available temperature above the temperature of liquid nitrogen (-196°C), a cooling agent which would tend to liquify air in the trap.

C. Trap Size

In the design of a charcoal trap for the specific goal of efficient containment of radioactive xenon gas in pulmonary studies, a number of opposing factors must be considered. In Fig. IV-6, the location of peak xenon activity and full width at half maximum of the activity distribution in the trap (after 30-min flow at an air flow rate of 8 liters/min) is plotted against the trap cross-sectional area for values of k_1 = 115 sec^{-1} and k_2 = 0.007 sec^{-1}. It shows that by increasing the trap diameter, for a given flow rate and temperature, the bulk of xenon gas would travel a shorter distance through the trap and dispersion of the activity zone would be less. On the other hand, due to the small heat transfer in the packed beds, and the very low thermal conductivity of the charcoal (2.4×10^{-4} cal/sec cm deg C) at 24°C [147], a narrow-diameter trap would be useful, because xenon adsorption on charcoal is highly sensitive to the temperature. Hence, short tubular adsorber vessels, or containers with a similar con-

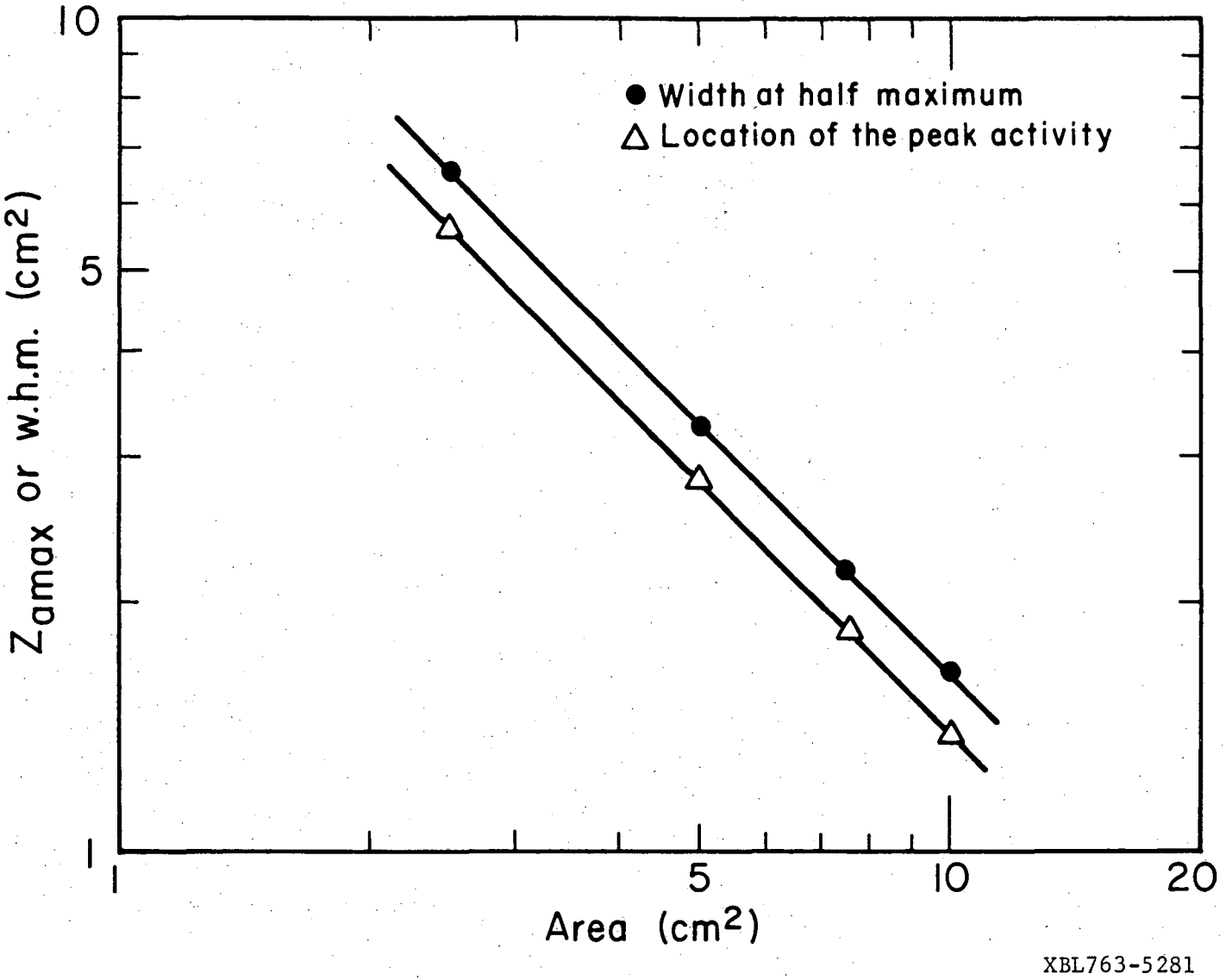

FIGURE IV-6. Variation of location of the peak xenon activity and full width at half maximum of activity distribution with the cross sectional area of the adsorption column.

figuration would minimize the effect of poor heat conduction on retention efficiency of the trap, and simultaneously would take advantage of reduced linear velocity in a wider diameter trap, thus it follows that these are the most suitable traps.

It was shown that by approximating the xenon activity profile in the trap to a Gaussian function, the mean and standard deviation of the resulting distribution, after 30 minutes flow, are 16.25 cm and 2.035 cm, respectively. Therefore, a trap 20 cm long, equal to the sum of the mean and two standard deviations, would theoretically be sufficient to contain 97.72 percent of the xenon activity during this period. Further, considering the low solubility of xenon in the blood, it rarely happens that the washout period in pulmonary function studies extends over half this period. Therefore, the length of the prototype xenon trap selected in the design of the recycling apparatus, is overestimated and may be reduced, as indicated below.

As previously described (Section III-1.4), the prototype xenon trap had to be open to the atmosphere during the temperature rise, allowing possible xenon loss while warming up. Since the excess air volume adsorbed or desorbed from the charcoal during cooling or warming the trap decreases with trap size, reducing the trap size will eliminate the need to discharge excess air to the atmosphere and will shorten the period of steam flow through the trap. If the trap size is reduced to half, then for the same experimental conditions, the volume of excess air would decrease to 1.5 liters (Section III-1.4). Assuming that half the maximum air volume is released during steam flow (i.e., 5.5/2 = 2.75 liters), the total recovered gas volume would be equal to 2.75 + 1.5 = 4.25 liters. Hence, without

reopening the trap to the atmosphere, it would be possible to recover xenon into this smaller 4.25-liter volume of gas.

D. Consideration in Circulation System Dimensions

Circuit one in the system is designed so that the ratio of the total lung capacity to volume of this circuit is as high as practicable, while resistance-free gas circulates between the subject's lungs and the spirometer. By the same token, the tube connecting the outlet of the xenon trap to position #3 of the four-way valve (Fig. IV-4) is sized so that a minute amount of xenon in the air, possibly reaching the subject's lungs during washout procedure, is diluted to a great extent.

E. Materials

The other important factor considered in the design of the recycling apparatus is the solubility of xenon in rubber and plastic materials. To minimize xenon loss to these types of substances, considerable attention has been given in selection of materials used (e.g., oil-free pump, corrugated copper tubing, non-plastic containers, valves with metallic seats, copper connecting lines).

F. Recovery Method

One of the major problems associated with the design of the apparatus is the recovery of xenon gas in a small volume of air. Heating and evacuation methods proposed by others [80,92] were rejected in favor of low-pressure steam, which was found to give virtually complete recovery in a

small air volume. The total lung capacity of a healthy average individual is about 6000 ml and it is usually lower in patients with pulmonary disease. In order to use recycled xenon gas efficiently, it should be recovered in gas volumes comparable to or less than the total lung capacity, so that a greater portion of xenon activity is distributed in the lungs during equilibration. It is not feasible, by heating alone, to recover xenon in the gas volume desired: for example, more than 7 liters of gas would be released out of the trap shown in Fig. IV-3 during 30 minutes of heating at 200°C while more than 50 percent of the xenon would still remain in the trap. Further, combining the evacuation process at dry-ice temperature, with later heating of the trap does not increase the xenon/air ratio in the recovered gas, even though this combination further complicates the simple operation required in such a system. However, as shown before in Fig. IV-3, it is easily possible by passing low-pressure steam through the charcoal trap, to recover xenon effectively from a charcoal surface into a tolerable volume of gas.

One drawback of using steam in xenon recovery is the production of carbon monoxide and carbon dioxide during this process. As was shown in Table III-6, after steam condensation in the spirometer the collected gas contains about 13.4% carbon dioxide and 0.003 % carbon monoxide. The presence of nontoxic CO_2 causes no problem since it constitutes a small fraction of the CO_2 volume exhaled during pulmonary studies, and is easily adsorbed by soda lime. If 4 liters of gas are collected under the spirometer, then the volume of CO_2 produced is 0.54 liters, while an average-sized individual expels some 0.2 liter of CO_2 per minute. Although CO is a toxic gas because it combines with the hemoglobin of the blood, the

concentration present is well below air quality standards adopted by the State of California (120 ppm for one hour average time [148]). Even so, by adding less than 100 grams of "hopcalite," a mixture of oxides of manganese, copper, cobalt, and silver, on top of the soda lime container, all the carbon monoxide would be oxidized to carbon dioxide.

CHAPTER V.

MODELING AND QUANTITATION OF PULMONARY FUNCTION INVESTIGATIONS

Analog scintillation camera images obtained by using radioactive particles and gases constitute an effective qualitative means for assessing regional ventilation and perfusion. Variation in regional image intensity is not restricted to changes in ventilatory gas displacement or perfusion per unit area, but depends on regional lung volume as well. The activity distribution in these images may be distorted by the nonuniform response of the scintillation camera as well as geometric and absorptive differences between areas of the lung. Furthermore, certain important parameters of pulmonary function such as the regional blood flow and the regional ventilation per unit of lung volume, and ventilation-perfusion ratios are difficult to estimate from sequential scintiphotos.

To derive information more directly related to these clinically important physiological variables, a number of methods have been presented, which describe quantitative evaluation of ventilation and perfusion distribution in the human lung using a gamma camera and a data processing system [40-51]. In all these methods, ventilation measurement has been largely confined to the determination of the clearance constant of the ^{133}Xe washout from the entire lung or from a number of sites, assuming that for each site the disappearance constant is proportional to the air flow per unit volume.

In this chapter, taking the respiratory cycle into account, a model is developed that introduces a new relationship between the clearance

rate constant and the fractional air exchange for any area in the lung. Using the result of this approach and the Stewart-Hamilton equation [49-15], FORTRAN programs were written to process pulmonary function data obtained from the scintillation camera. These programs provide the combination of morphological and dynamic exploration of lung ventilation and perfusion with a reliable and exact reference to a great number of regions in the lung. The computer system used has been described in Section III-1.2.

V-1. Functional Description of the Lung

Lung function can be reduced to three basic aspects: ventilation, by which the external surrounding air is exchanged for alveolar air; perfusion, or the amount of blood-exchanging gases per unit of time; and finally, diffusion, the movement of oxygen from the alveolar air to the blood and the movement of carbon dioxide in the reverse direction. The global function of the lung is to clear the blood or carbon dioxide and replenish it with oxygen. With a global or average minimal impairment of any or all of the three elements, the final functional impairment may be larger if the different regions of the lungs have unmatched functional elements. Indeed, a well perfused but unventilated region is totally inactive as far as the global function is concerned, as is a well-ventilated but unperfused region. A region could be lost even though well perfused and ventilated if the diffusion across the alveolar membrane is grossly impaired.

The basic element of the lung is an alveole through which a fraction f_i of the total cardiac output is flowing per unit of time.

This f_i contains a volume V_i of air, and renews a fraction $\dot{V}_i/V_i$ of this volume by every respiration. In the subsequent derivations, unless otherwise stated, it is assumed:

1) the sum of f_i is equal to the total cardiac output;
2) the sum of V_i is the total lung volume; in other words, the bronchial tree volume is ignored;
3) the total expired air in every respiration is the sum of $\dot{V}_i$, so that the bronchial tree volume is ignored in this case as well.

The respiratory movement at the alveolar level can be considered in the following way: During expiration the volume of the alveolus becomes smaller until it reaches $1 - \dot{V}_i/V_i$ of its original volume. These volume changes are accompanied by gas flow from the alveolus, and by minimal pressure changes. During inspiration the alveolar volume returns to its original value, with a corresponding inflow of air and no pressure changes. Good mixing is assumed and the respiratory cycles are of constant length.

V-2. The Alveolar Model with an Inert, Insoluble Gas

An insoluble (in water or blood), inert gas, if mixed with alveloar air, is an exact indicator of ventilation because it does not diffuse into the blood and its kinetics are totally defined by the respiratory volume changes. In view of the basic respiratory movement at the alveolar level, the following can be derived:

If, at the beginning of the expiration the specific tracer activity in the alveolus is SA_o for volume V_i, the total activity present is $SA_o \times V_i$. During expiration the specific activity does not change, so that at the end of expiration the total activity present is

$$SA_o \times V_i \times (1 - \dot{V}_i/V_i) \quad .$$

During inspiration the inspired volume has no radioactivity (we assume that the air was expired into an infinite volume so that the specific activity of the "outside" air remains zero; thus, the inspired air is nonactive). Therefore the total activity remains constant during inspiration, but since there is a volume change, the specific activity changes. At the end of the first inspiration the specific activity is

$$SA_1 = SA_o \times V_i \times \frac{(1 - \dot{V}_i/V_i)}{V_i} \quad .$$

And at the end of the n^{th} inspiration the total activity is

$$SA_o \times V_i \times (1 - \dot{V}_i/V_i)^n \quad .$$

In this way the specific activities and the total activities can be determined at different times in the respiratory cycle, and from one cycle to another.

The function describing the continuous changes depends on the functional form of F_i, the flow of air to the alveolus at each instant of the respiratory cycle. To maintain a steady state in the long run it is necessary that the integral of F_i during inspiration be of an equal but opposite sign to the integral of F_i during expiration. The absolute value of both signs is $\dot{V}_i$.

In general, the functional form of F_i is not known, and the time resolution of the measurements is such that it cannot be determined. If the activity is counted over intervals T, not necessarily corresponding to one respiratory cycle, the relationship between the data points and the functional changes in activity has to be determined. One can show that the equally spaced data points are fitted by an exponential whose slope k_i is related to $\dot{V}_i/V_i$.

We have already shown that the total activity A_{in} at the end of the n^{th} respiratory cycle is given by

$$A_{in} = SA_{io} \times V_i \times (1 - \dot{V}_i/V_i)^n \qquad (5\text{-}1)$$

where SA_{io} is the specific alveolar activity before the first expiration; V_i is the alveolar volume; and $\dot{V}_i$ is the integrated expiratory volume corresponding to the alveolus i. By definition then,

$$SA_{io} \times V_i = A_{io} \quad . \qquad (5\text{-}2)$$

Hence

$$A_{in} = A_{io}(1 - \dot{V}_i/V_i)^n \quad . \qquad (5\text{-}3)$$

The values A_{in} are equidistant in time, situated at the times corresponding to the beginning of each respiratory (expiratory) cycle. If one full cycle is of duration 2T, then A_{in} and $A_{i(n+1)}$ correspond on the time scale to $A_i(t)$ and $A_i(t+2T)$. The relation between A_{io} and A_{in} is also the relation between $A_i(0)$ and $A_i(2nT)$ on a continuous time scale. It is easy to show that if

$$A_i(t+2T) = A_i(t)e^{-k(2T)} \quad , \tag{5-4}$$

then

$$A_i(2nT) = A_i(0)e^{-nk(2T)} \quad ; \tag{5-5}$$

and that therefore

$$e^{-k_i(2T)} = 1 - \frac{\dot{V}_i}{V_i} \quad . \tag{5-6}$$

Thus

$$k_i = -\frac{\ell n(1 - \dot{V}_i/V_i)}{2T} \quad . \tag{5-7}$$

By using these results schematically, it is easy to see in Fig. V-1 that for the same point in the respiratory cycle data points can be fitted to an exponential with slope $k_i = \ell n(1 - \dot{V}_i/V_i)/2T$.

It can also be proven that by taking counts over one or more respiratory cycles, Fig. V-2, the same relationship between k_i and $\dot{V}_i/V_i$ exists. Starting at inspiration $t = 0$, the total count C_1 over the first respiratory cycle, assuming an equal respiratory and expiratory time, is proportional to

$$C_1 \int_0^T A_i(0)dt + \int_T^{2T} \left[\frac{A_i(0) + A_i(1)}{2}\right] dt \quad .$$

Integrating, we obtain

$$C_1 = A_i(0)T + \frac{A_i(0)}{2}T + \frac{A_i(1)}{2}T \quad ,$$

but

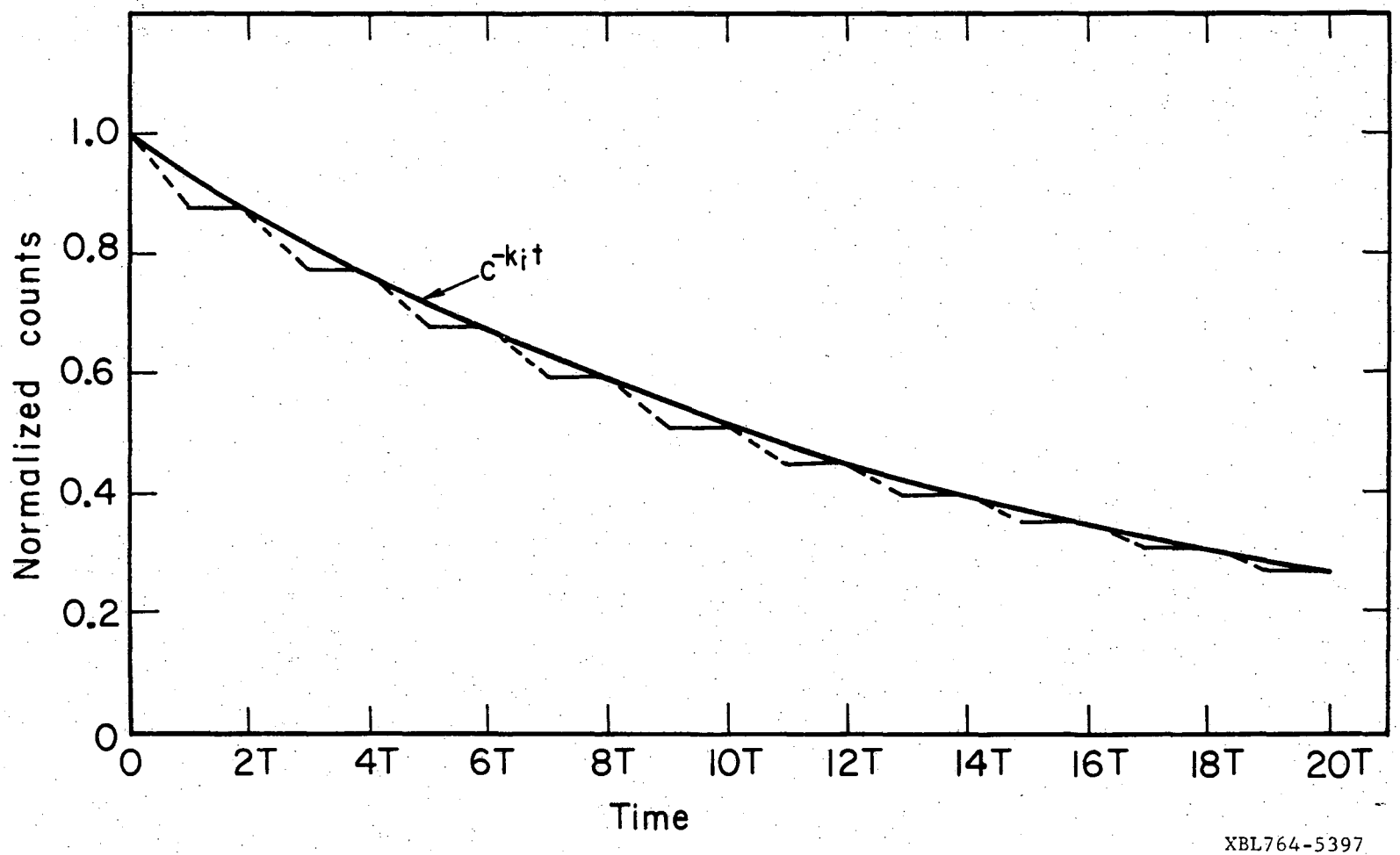

FIGURE V-1. Diagram representing the exponential fit of a hypothetical activity washout curve during respiratory cycles. Respiratory cycle (inspiration and expiration) = 2 T .

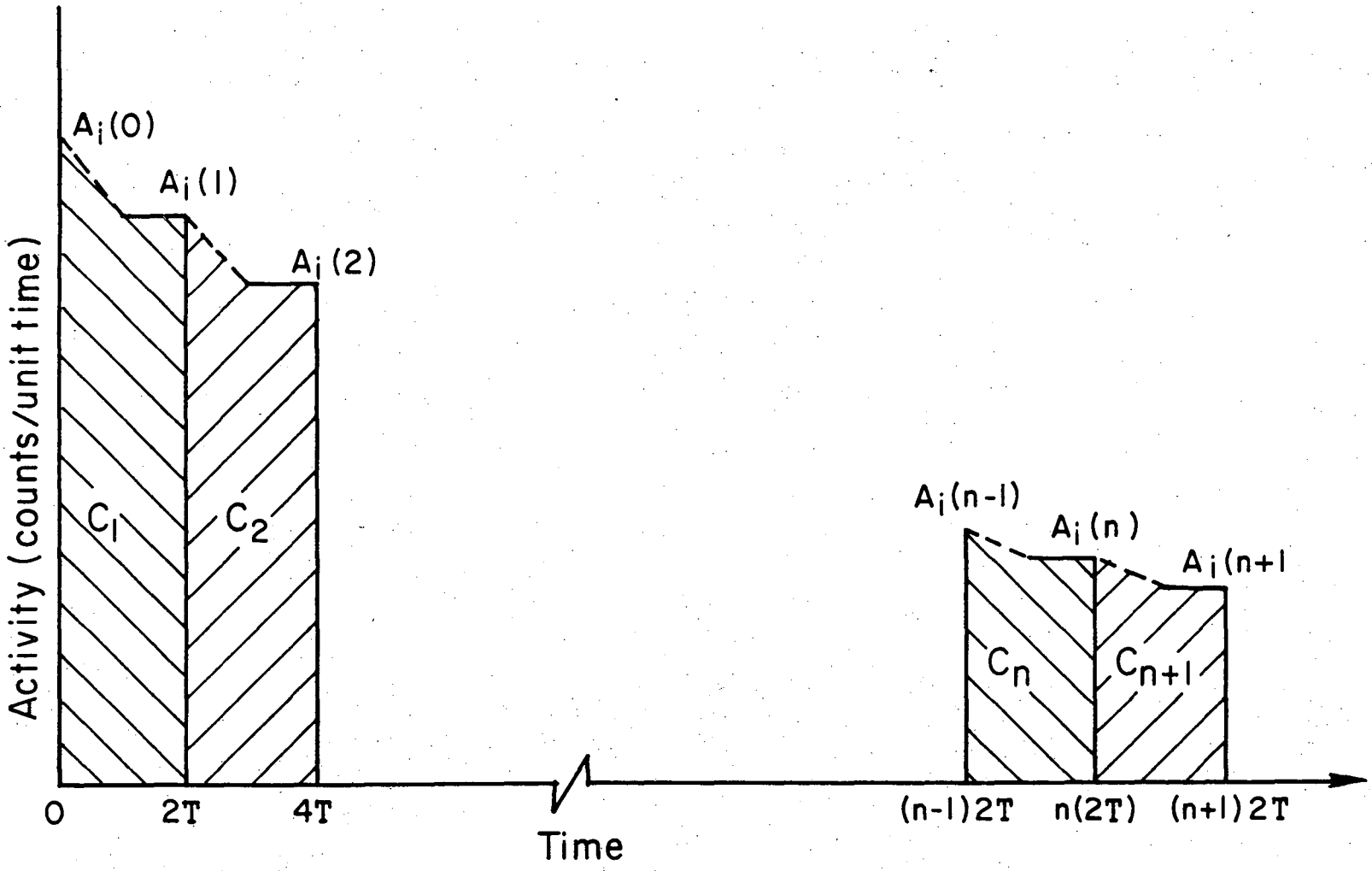

XBL764-5395

FIGURE V-2. Diagram illustrating the variation of total activity present under a hypothetical washout curve in consecutive respiratory cycle. Respiratory cycle (inspiration and expiration) = 2 T .

$$A_i(1) = A_i(0)(1 - \dot{V}_i/V_i) \quad .$$

By substituting, we obtain

$$C_1 = A_i(0)T + \frac{A_i(0)}{2}T + \frac{A_i(0)}{2}T(1 - \dot{V}_i/V_i)$$

$$C_1 = A_i(0)T\left[2 - \frac{\dot{V}_i}{2V_i}\right] \quad .$$

In the same way, the total count over the n^{th} respiratory cycle is

$$C_n = A_i(n-1)T\left[2 - \frac{\dot{V}_i}{2V_i}\right] \quad ,$$

and the total count over the $(n+1)^{th}$ respiratory cycle is

$$C_{n+1} = A_i(n)T\left[2 - \frac{\dot{V}_i}{2V_i}\right]$$

or

$$\frac{C_{n+1}}{C_n} = \frac{A_i(n)T(2 - \dot{V}_i/2V_i)}{A_i(n-1)T(2 - \dot{V}_i/2V_i)} = \frac{A_i(n)}{A_i(n-1)} \quad .$$

From equation (5-4), we obtain

$$\frac{A_i(t+2T)}{A_i(t)} = \frac{A_i(n)}{A_i(n-1)} = 1 - \dot{V}_i/V_i \quad ,$$

or

$$\frac{C_{n+1}}{C_n} = 1 - \dot{V}_i/V_i \quad . \qquad (5\text{-}8)$$

Starting at expiration, or at any other point of the respiratory cycle, this ratio of the total counts taken over consecutive respiratory cycles remains constant. Actually, if the total count is recorded for intervals of time equal to or more than one cycle, the ratio of counts over these intervals is constant in equal to $(1 - \dot{V}_i/V_i)$.

Assuming an exponential fit to the data, the total count C_1' over the first cycle is

$$C_1' = \int_0^{2T} A_i(0)e^{-k_i t}\,dt = \frac{A_i(0)}{k_i}\left[1 - e^{-2k_i T}\right] \quad .$$

In the same way, the total count C_n' over the n^{th} cycle is

$$C_n' = \int_{(n-1)2T}^{n(2T)} A_i(0)e^{-k_i t}\,dt = A_i(0)e^{-(n-1)2k_i T}\left[\frac{1 - e^{-2k_i T}}{k_i}\right] \quad .$$

Over the $(n+1)^{th}$ cycle it is

$$C_{n+1}' = \frac{A_i(0)}{k_i} e^{-n(2kT)}\left[1 - e^{-2k_i T}\right] \quad ,$$

taking the ratio

$$\frac{C_{n+1}'}{C_n'} = e^{-2k_i T} \quad . \qquad (5\text{-}9)$$

Equating the right-hand side of equation (5-8) and (5-9)

$$1 - \frac{\dot{V}_i}{V_i} = e^{-2k_i T} \quad , \qquad (5\text{-}10)$$

or, as before

$$k_i = -\frac{\ln(1 - \dot{V}_i/V_i)}{2T} \quad . \qquad (5\text{-}11)$$

We should also consider the case where data are collected (count integrated) over equal intervals which do not correspond to integer multiples of 2T. In this case the values of C_n' will be scattered around the values defined by the function Ce^{-kt}, but this error will not unduly affect the definition of k and the relation in equation (5-11). The model therefore predicts that for a single alveolus, or a group of alveoli with the same fractional air exchange, the average count rate (over equal time intervals larger than or equal to one respiratory cycle) as a function of time can be fitted by an exponential function where slope is related to the physiological value $\dot{V}_i/V_i$.

V-3. Observation of Multiple Alveoli with Different Ventilation Rates

Since the scintillation camera has no depth resolution and only limited resolution in the projection plane, one cannot obtain a spatial resolution which guarantees that the observed counts come from a single alveolus, or even from a set of alveoli with a common $\dot{V}_i/V_i$ and k_i value. In this case, the sensitivity, counting efficiency, and activities used generally prevent the empirical function from being resolved into a number of alveoli with different k_i values.

There are different alternatives. The preferred one is the determination of the mean residency time for each region, equal to the reciprocal of the disappearance rate constant of the exponential function representing the population of alveoli in the region being examined.

By definition, the mean residency time, T_m, is given as

$$T_m = \int_0^\infty th(t)dt \quad ,$$

where $h(t)$ is the frequency function of the transit time or the fraction of activity at time zero, $q(0)$, leaving this element per unit of time between t and $t+dt$.

The remaining activity in the element at time t is

$$q(t) = q(0)\left[1 - \int_0^t h(s)ds\right] = q(0)\left[1 - H(t)\right] \quad , \qquad (5\text{-}12)$$

where

$$H(t) \equiv \int_0^t h(s)ds \quad .$$

For finite volume, the mean residency time is also given by

$$T_m = \int_0^\infty \left[1 - H(t)\right] dt \quad . \qquad (5\text{-}13)$$

This can be proven by an integration by parts [19]

$$\int_0^t \left[1 - H(s)\right] ds = t\left[1 - H(t)\right] + \int_0^t sh(s)ds \quad ,$$

or

$$\int_0^\infty \left[1 - H(s)\right] ds = \lim_{t \to \infty} t\left[1 - H(t)\right] + \int_0^\infty sh(s)ds \quad .$$

For finite volume, the first term on the right is equal to zero; therefore,

$$\int_0^\infty \left[1 - H(s)\right] ds = \int_0^\infty sh(s)ds \quad ,$$

and using equations (5-12) and (5-13), we get

$$T_m = \frac{\int_0^\infty q(t)dt}{q(0)} \equiv \frac{1}{k_i} \quad . \qquad (5\text{-}14)$$

Although this equation was originally devised to measure cardiac output, Zierler has shown that it applies equally well for measuring blood flow per unit volume where external detectors are used [152]. If the region under examination follows a single exponential process, the height-to-area relationship measures the disappearance rate constant of this process. If more than one exponential process is involved, as is likely in patients with obstructive diseases of the airways, the height-to-area relationship measures the mean rate constant of the various components. Ventilation, as the mean fractional exchange of air in each region of the lung, may be calculated by using this approach and expression (5-11).

V-4. Description of the Computer Program for Processing Pulmonary Function Data

The computer program starts by reading coded information about the patient (name, sex, age, date of exploration) and the data collection procedure (rebreathing time, time per frame during washout, patient's respiratory cycle per minute). This patient information is printed at the beginning of each page in the final print-out.

The camera detects a general field composed of activities from the lungs, chest wall, and background. These data are also stored by the computer system that organizes them into frames of 64×64 element arrays. The stored data may first be processed by a general purpose program, which corrects the data for the nonuniform response of the gamma camera and for the deadtime loss of the system. To improve counting statistics and to simplify calculations, the size of these arrays is reduced to 16×16 elements by adding the counts of four adjacent elements in the array. Next, the maximum counts in the reduced equilibrium ventilation and perfusion frames are determined separately. On this basis all the counts in each frame are normalized to a respective maximum so that they range from one to ten. This method of normalizing the equilibrated ventilation and perfusion data allows determination of the level of tissue background cutoff by direct comparison of the lung margins.

The time activity curve for each of the 256 elements in the array is generated during the washout procedure. The mean rate constant for each element is then calculated according to equation (5-14) by dividing $q(0)$ at the beginning of washout, corrected for the background, by the sum of the counts under each time-function, again with correction for background activity. The background correction method is described in the following section. Next, by using equation (5-11), ventilation or fractional air exchange, $\dot{V}/V$, for each element is determined.

Fractional perfusion, $\dot{P}$, is obtained for each region of the lung by adding all the counts in the perfusion frame and dividing the

counts in each element by this sum. The counts are found for each element in the equilibrium ventilation frame and corrected for tissue background. Then the corrected counts in each element are summed and the normalized volume distribution of xenon activity, $\dot{V}$, in the lungs is determined by dividing the corrected counts in each element by the sum. Next, the ventilated volume, $\dot{V}$, for each region is calculated by multiplying $\dot{V}/V$ by V, and the ventilation-perfusion ratio is determined by dividing $\dot{V}$ by $\dot{P}$. Finally, two new parameters are introduced for further assessment of lung functions

$$\text{Perfusion Ratio} \equiv \frac{\dot{\dot{P}}\dot{V}}{2(\dot{P}^2 + \dot{V}^2)} \quad , \tag{5-15}$$

and

$$\text{Functional Volume Index} \equiv \frac{\dot{\dot{P}}\dot{V}}{2(\dot{P}^2 + \dot{V}^2)} V \quad . \tag{5-16}$$

The value of these new parameters will be compared with the conventional $\dot{\dot{V}}/\dot{P}$ in future studies.

V-4.1 Background Correction

Since xenon is only slightly soluble in blood and more soluble in fat, during the period of equilibration a small amount of xenon gas is taken up by the blood and carried to the body tissues, including the chest wall. As a result, the counts recorded are from the underlying chest wall as well as from the lungs. The amount of xenon in the chest wall increases rather slowly and if the rebreathing time is limited to a few minutes, the chest wall activity will be rather small. In well

ventilated areas, xenon clears the lung very rapidly: essentially complete washout in these areas is usually achieved in about one minute.

To correct for the contribution of chest wall radiation to the total external count rate, the following method has been incorporated in the calculation: First, by comparing the normalized equilibrium ventilation and perfusion frames, the percent level of background cut of in ventilation frame is specified such that the outline of the lung is similar in both frames. A background count "level" is then obtained by multiplying the chosen background fraction by the maximum count in the equilibrium ventilation frame. A frame is then selected with a washout time beyond that at which the normal lung is clear. In this frame all the elements which have counts greater than the background "level" (i.e., areas of abnormal lung) are set equal to zero, the rest are set equal to one. In this way a frame is obtained where locations with background counts are marked with unit value: we call it a "mask" frame. All the washout frames existing after the selected frame are then multiplied by this mask frame, and the sum of the counts in each frame is obtained. An average background count is then calculated for the elements labeled one. By using the least-square method, the logarithms of these counts are then fitted to a straight line, and the slope is found. Now a frame, called a background frame, is formed in which all elements in the selected frame with counts greater than the background counts, are given the average background count, and for those elements in the selected frame with counts below average background, the slope of the time-function for that element between selected frame time and

the end of the study is checked; for a positive slope, the corresponding element in the background frame is set equal to the average count over the time interval between the selected and the last frame of the washout procedure; and for elements with a negative slope, the actual value is used in the background frame. Finally, the counts in the background frame are extrapolated back to values at the beginning of the washout by using the slope of the logarithm of the sum of the counts obtained from the designated background elements.

V-4.2 Computer Print-Out

A patient, F.J., with mild obstructive airway disease was studied. The following scintiphotos (Fig. V-3) and print-outs were obtained. They show minor variability in ventilation and perfusion with reduced ventilation on both apices.

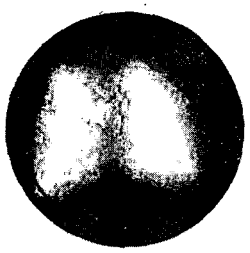

Single Breath

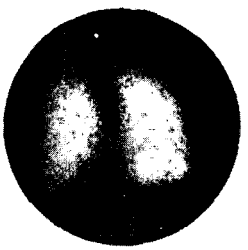

Equilibrium

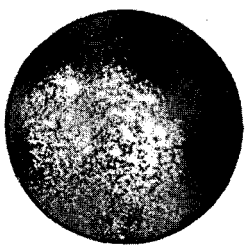

Washout
(2.5 min)

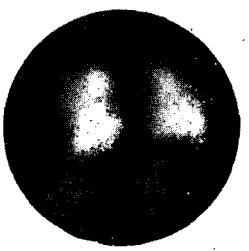

Perfusion

XBB 764-3501

Fig V-3. Selected scintiphotograms obtained during a pulmonary function study.

FRACTIONAL PERFUSION

0	0	0	0	0	0	0	0	0	0	0	0	0	0	0	0
0	0	0	0	0	0	0	0	0	0	0	0	0	0	0	0
0	0	0	0	0	1	2	2	3	2	1	0	0	0	0	0
0	0	0	1	8	17	9	11	23	14	5	3	0	0	0	0
0	0	0	12	71	111	45	37	99	77	23	6	2	0	0	0
0	0	4	44	152	231	132	64	195	197	78	16	4	1	0	0
0	1	13	81	226	333	189	60	183	319	204	57	6	2	0	0
0	1	14	100	287	360	202	71	169	369	367	144	14	3	1	0
0	1	12	88	317	393	262	71	184	315	368	203	21	2	1	0
0	0	8	93	277	317	211	48	98	126	181	147	16	1	0	0
0	0	6	72	133	122	81	17	21	21	39	46	5	0	0	0
0	0	2	18	22	16	9	4	5	5	6	7	1	0	0	0
0	0	0	1	4	5	4	2	2	3	4	2	0	0	0	0
0	0	0	0	0	1	1	0	0	1	0	0	0	0	0	0
0	0	0	0	0	0	0	0	0	0	0	0	0	0	0	0
0	0	0	0	0	0	0	0	0	0	0	0	0	0	0	0

This display expresses perfusion data per element as a fraction of the total activity in the perfusion frame.

VENT.FRACT/VENTILATION

.00	.00	.00	.00	.00	.00	.00	.00	.00	.00	.00	.00	.00	.00	.00	.00
.00	.00	.00	.00	.00	.00	.00	.00	.00	.00	.00	.00	.00	.00	.00	.00
.00	.00	.00	.00	.00	.00	.00	.00	.00	.00	.00	.00	.00	.00	.00	.00
.00	.00	.00	.00	.00	.00	.00	.00	.00	.00	.00	.00	.00	.00	.00	.00
.00	.00	.00	.00	.13	.11	.00	.10	.15	.00	.00	.00	.00	.00	.00	.00
.00	.00	.00	.11	.18	.15	.13	.13	.17	.16	.14	.00	.00	.00	.00	.00
.00	.00	.00	.15	.18	.17	.14	.14	.18	.18	.16	.00	.00	.00	.00	.00
.00	.00	.00	.17	.20	.18	.15	.17	.18	.18	.16	.15	.00	.00	.00	.00
.00	.00	.00	.20	.21	.20	.16	.17	.18	.19	.19	.17	.00	.00	.00	.00
.00	.00	.00	.27	.25	.20	.22	.16	.19	.20	.20	.22	.00	.00	.00	.00
.00	.00	.21	.33	.25	.28	.25	.00	.16	.15	.18	.25	.44	.00	.00	.00
.00	.00	.00	.29	.36	.31	.00	.00	.00	.09	.00	.00	.00	.00	.00	.00
.00	.00	.00	.18	.00	.00	.00	.00	.00	.00	.00	.00	.00	.00	.00	.00
.00	.00	.00	.00	.00	.00	.00	.00	.00	.00	.00	.00	.00	.00	.00	.00
.00	.00	.00	.00	.00	.00	.00	.00	.00	.00	.00	.00	.00	.00	.00	.00
.00	.00	.00	.00	.00	.00	.00	.00	.00	.00	.00	.00	.00	.00	.00	.00

This display presents the fraction of air exchange per breath in each element, i.e., $\dot{V}/V$.

VOLUME DISTRIBUTION

0	0	0	0	0	0	0	0	0	0	0	0	0	0	0	0
0	0	0	0	0	0	0	0	0	0	0	0	0	0	0	0
0	0	0	0	0	0	0	0	0	0	0	0	0	0	0	0
0	0	0	0	0	0	0	0	0	0	0	0	0	0	0	0
0	0	0	0	53	72	0	63	96	32	6	0	0	0	0	0
0	0	0	58	161	173	80	124	239	204	61	0	0	0	0	0
0	0	13	116	204	252	124	107	299	348	196	19	0	0	0	0
0	0	13	126	239	248	152	94	290	336	283	68	4	0	0	0
0	0	15	108	248	277	137	84	243	381	320	96	3	0	0	0
0	0	10	87	233	200	120	67	205	321	313	130	12	0	0	0
0	0	12	103	159	105	47	33	135	181	178	78	18	0	0	0
0	0	3	60	77	46	9	0	9	34	24	15	0	0	0	0
0	0	0	8	6	5	0	0	0	0	0	0	0	0	0	0
0	0	0	0	0	0	0	0	0	0	0	0	0	0	0	0
0	0	0	0	0	0	0	0	0	0	0	0	0	0	0	0
0	0	0	0	0	0	0	0	0	0	0	0	0	0	0	0

This displays V per element, which is a measure of relative volume distribution.

VENTILATED VOLUMES

0	0	0	0	0	0	0	0	0	0	0	0	0	0	0	0
0	0	0	0	0	0	0	0	0	0	0	0	0	0	0	0
0	0	0	0	0	0	0	0	0	0	0	0	0	0	0	0
0	0	0	0	0	0	0	0	0	0	0	0	0	0	0	0
0	0	0	0	70	79	0	60	144	0	0	0	0	0	0	0
0	0	0	64	289	266	103	161	400	324	84	0	0	0	0	0
0	0	0	173	364	428	178	149	528	617	320	0	0	0	0	0
0	0	0	220	475	435	233	156	525	693	443	102	0	0	0	0
0	0	0	213	518	543	212	142	444	734	615	166	0	0	0	0
0	0	0	238	583	393	259	104	397	642	636	283	0	0	0	0
0	0	24	338	401	292	115	0	212	279	327	193	78	0	0	0
0	0	0	172	280	141	0	0	0	30	0	0	0	0	0	0
0	0	0	14	0	0	0	0	0	0	0	0	0	0	0	0
0	0	0	0	0	0	0	0	0	0	0	0	0	0	0	0
0	0	0	0	0	0	0	0	0	0	0	0	0	0	0	0
0	0	0	0	0	0	0	0	0	0	0	0	0	0	0	0

This display expresses the ventilated volumes (V) per element, which are the product of volume distribution (V) and ventilation fraction/ventilation (V/V).

PERFUSION RATIOS

0	0	0	0	0	0	0	0	0	0	0	0	0	0	0	0
0	0	0	0	0	0	0	0	0	0	0	0	0	0	0	0
0	0	0	0	0	0	0	0	0	0	0	0	0	0	0	0
0	0	0	0	0	0	0	0	0	0	0	0	0	0	0	0
0	0	0	0	84	68	0	98	96	0	0	0	0	0	0	0
0	0	0	96	98	90	72	94	98	98	86	0	0	0	0	0
0	0	0	98	98	94	80	94	90	98	98	0	0	0	0	0
0	0	0	98	98	92	90	98	86	98	92	66	0	0	0	0
0	0	0	94	98	96	74	98	96	96	98	74	0	0	0	0
0	0	0	94	98	92	92	98	74	62	80	98	0	0	0	0
0	0	74	66	88	96	96	0	34	26	40	72	22	0	0	0
0	0	0	36	26	38	0	0	0	54	0	0	0	0	0	0
0	0	0	24	0	0	0	0	0	0	0	0	0	0	0	0
0	0	0	0	0	0	0	0	0	0	0	0	0	0	0	0
0	0	0	0	0	0	0	0	0	0	0	0	0	0	0	0
0	0	0	0	0	0	0	0	0	0	0	0	0	0	0	0

This display represents a measure of ventilation-perfusion ratio per element.

FUNCTIONAL VOLUME INDEX 162

0	0	0	0	0	0	0	0	0	0	0	0	0	0	0	0
0	0	0	0	0	0	0	0	0	0	0	0	0	0	0	0
0	0	0	0	0	0	0	0	0	0	0	0	0	0	0	0
0	0	0	0	0	0	0	0	0	0	0	0	0	0	0	0
0	0	0	0	44	48	0	61	92	0	0	0	0	0	0	0
0	0	0	55	157	155	57	116	234	199	52	0	0	0	0	0
0	0	0	113	199	236	99	100	269	341	192	0	0	0	0	0
0	0	0	123	234	228	136	92	249	378	260	44	0	0	0	0
0	0	0	101	243	265	101	82	233	365	313	71	0	0	0	0
0	0	0	81	228	184	110	65	151	199	250	127	0	0	0	0
0	0	8	67	139	100	45	0	45	47	71	56	3	0	0	0
0	0	0	21	20	17	0	0	0	18	0	0	0	0	0	0
0	0	0	1	0	0	0	0	0	0	0	0	0	0	0	0
0	0	0	0	0	0	0	0	0	0	0	0	0	0	0	0
0	0	0	0	0	0	0	0	0	0	0	0	0	0	0	0
0	0	0	0	0	0	0	0	0	0	0	0	0	0	0	0

This display expresses the functional volume index per element, which is the product of the perfusion ratio [$\ddot{P}V/2(\dot{P}^2 + \dot{V}^2)$] and volume distribution (V).

APPENDIX A

The following program, in FORTRAN, language, was used to evaluate and plot the xenon activity distribution in the adsorption column, expression (2-70).

```
      PROGRAM ADSORPT(INPUT,OUTPUT,TAPE3=OUTPUT)
      REAL K1,K2,K,KK
      DIMENSION FI(2),C(500),Z(500),CNORM(500)
      COMMON K1,K2,KK,X,Y,CO,SLAND,C
      EXTERNAL F1,F2,G1,G2,H1,H2
      PRINT 1001
 1001 FORMAT(1H1)
      PRINT 1000
 1000 FORMAT(25X,57HXENON CONCENTRATION ON CHARCOAL VS. LENGTH ALONG THE TUBE)
     1 TUBE,19X,4HC(X))
      READ 300,MAXI,E
  300 FORMAT(I4,F6.3)
      READ 200,K1,K2
  200 FORMAT(2F13.6)
      READ 201,Z1,Z2,DELZ
  201 FORMAT(3F13.3)
      READ 410,T
  410 FORMAT(F10.0)
      READ 202,CO,U
  202 FORMAT(F10.0,F10.3)
      A=5.
      VOID=.72
      VSP=6650.0
      FLOW=U*A*VOID*60.0
      SLAND=FLOW/(VSP*60.0*VOID)
      K=K1/K2
      KK=K1*K2
      PRINT 420, MAXI,E
  420 FORMAT(/,5HMAXI=,I4,/,2HE=,F6.3,/)
      PRINT 1,K1,K2
    1 FORMAT(/,3HK1=,F10.6,/,3HK2=,F10.6)
      PRINT 205,Z1,Z2,DELZ
  205 FORMAT(/,/,9HORIGINAL=,F10.3,/,     6HFINAL=,F13.3,/,     10HINCREME
     1NT,F11.4,/,/)
      PRINT 203,T
  203 FORMAT(/,5HTIME=,F6.0,/)
      PRINT 3,A,VOID,FLOW,SLAND
    3 FORMAT(/,/,/,5HAREA=,F10.3,/,14HVOID FRACTION=,F5.3,/,10HFLOW RATE=,F10.3
     2,F10.3,/,6HLANDA=,F10.6,5X,6H1/SEC.)
      L=(K2*CO)/SLAND
      PRINT 990,C
  990 FORMAT(/,2HC=,E12.4)
      PRINT 204,CO,U
  204 FORMAT(/,12HINPUT COUNT=,F11.0,/,16HLINEAR VELOCITY=,F10.3)
      NUM=INT((Z2-Z1)/DELZ+1.0)
      DO 30 I=1,NUM
      Z(I)=0.
      C(I)=0.
      CNORM(I)=0.
   30 CONTINUE
      I=1
      IPOINT=1
      PRINT 400
  400 FORMAT(/,/,/,10X,6HLENGTH,19X,13HCONCENTRATION,27X,10HNORMALIZED)
      DO 50 J=1,NUM
```

```
      I=I+1
      IPOINT=IPOINT+1
      Z(I)=FLOAT(I-1)*DELZ+Z1
      X=Z(I)/U
      Y=VOID*(T-X)
      IF(T.LE.X) GO TO 50
      P=2*SQRT(KK*X*Y)
      PRINT 500,P
  500 FORMAT(2HP=,E18.4)
      C1=EXP(-(K1*X+K2*Y))
      IF(P.EQ.0.) GO TO 31
      GO TO 34
   31 FI(1)=1.0
      FI(2)=0.0
      GO TO 33
   34 CALL BESNIS(P,2,FI)
   33 C1=-K1*FI(1)
      C2=SQRT((KK*Y)/X)*FI(2)
      CALL SIMPS(0.,X,E,MAXI,F1,XIP,INDEX)
      C3=-K1*XIP
      CALL SIMPS(0.,Y,E,MAXI,F2,XIP,INDEX)
      C4=(K2-D)*XIP
      CALL SIMPS(0.,Y,E,MAXI,G1,XIP,INDEX)
      C5=-K1*(D-CO)*XIP
      CALL SIMPS(0.,Y,E,MAXI,G2,XIP,INDEX)
      C6=-K1*(K2-D)*XIP
      C7=+K1*EXP(K1*X)
      CALL SIMPS(0.,P,E,MAXI,H1,XIP,INDEX)
      C8=K1*XIP
      CALL SIMPS(0.,Y,E,MAXI,H2,XIP,INDEX)
      C9=(D-CO)*XIP
      C(I)=C4*(C1+C2+C3+C4+C5+C6+C7+C8+C9)
      CNORM(I)=C(I)/CO
      PRINT 66,Z(I),C(I),CNORM(I)
   66 FORMAT( 9X,F10.3,10X,E20.4,2UX,E20.4)
   50 CONTINUE
      ZMAX=0.
      CMAX=0.
      SUM=0.
      DO 70 I=1,IPOINT
      IF(C(I).LT.0.) GO TO 71
      IF(C(I).LT.CMAX) GO TO 75
      CMAX=C(I)
      ZMAX=Z(I)
      GO TO 75
   71 C(I)=0.
   75 SUM=SUM+C(I) *A*DELZ
   70 CONTINUE
      PRINT 72,CMAX,ZMAX,SUM
   72 FORMAT(3(/),14HMAXIMUM COUNT=,E15.4,10X,8HLENGTH=,F10.3,9X,14HSUM
     1 OF COUNTS=,E18.4)
      F=CO*VSP*(1.-EXP(-(FLOW*T)/(VSP*60.)))
      PRINT 500,F
  500 FORMAT( /,29HXENON ATOMS PUMPED INTO TUBE=,E20.4)
      CALL PLOT(Z,C,Z1,Z2,0.,CMAX,NUM)
      STOP
      END
      FUNCTION F1(SY)
      COMMON K1,K2,KK,X,Y,CO,SLANG,D
      DIMENSION FI(2)
      REAL K1,K2,K,KK
      P=2*SQRT(KK*Y*(X-SY))
```

```
      IF(P.NE.0.) GO TO 10
      FI(1)=1.0
      FI(2)=0.
      GO TO 11
   10 CALL BESNIS(P,2,FI)
   11 F1=K1*EXP(K1*SY)*FI(1)
      RETURN
      END
      FUNCTION F2(SY)
      COMMON K1,K2,KK,X,Y,CC,SLANC,C
      DIMENSION FI(2)
      REAL K1,K2,K,KK
      P=2*SQRT(KK*X*(Y-SY))
      IF(P.NE.0.) GO TO 10
      FI(2)=0.
      GO TO 11
   10 CALL BESNIS(P,2,FI)
   11 F2=    (EXP(K2*SY))*(SQRT((KK*(Y-SY))/X))*FI(2)
      RETURN
      END
      FUNCTION G1(ZU)
      REAL K1,K2,K,KK
      DIMENSION FI(2)
      COMMON K1,K2,KK,X,Y,CC,SLANC,C
      P=2*SQRT(KK*X*(Y-ZU))
      IF(P.NE.0.) GO TO 10
      FI(1)=1.0
      GO TO 11
   10 CALL BESNIS(P,2,FI)
   11 G1=        (EXP((K2-SLANC)*ZU))*FI(1)
      RETURN
      END
      FUNCTION G2(ZU)
      REAL K1,K2,K,KK
      DIMENSION FI(2)
      COMMON K1,K2,KK,X,Y,CC,SLANC,C
      P=2*SQRT(KK*X*(Y-ZU))
      IF(P.NE.0.) GO TO 10
      FI(1)=1.0
      GO TO 11
   10 CALL BESNIS(P,2,FI)
   11 G2=        (EXP(K2*ZU))*FI(1)
      RETURN
      END
      FUNCTIONF1(ZE)
      REAL K1,K2,K,KK
      DIMENSION FI(2)
      COMMON K1,K2,KK,X,Y,CC,SLANC,C
      DUM=X-((ZE*ZE)/(4.0*KK*Y))
      IF(ZE.NE.0.) GO TO 10
      FI(2)=0.0
      GO TO 11
   10 CALL BESNIS(ZE,2,FI)
   11 F1= EXP(K1*DUM)*FI(2)
      RETURN
      END
      FUNCTION H2(SY)
      COMMON K1,K2,KK,X,Y,CC,SLANC,C
      DIMENSION FI(2)
      REAL K1,K2,K,KK
      P=2*SQRT(KK*X*(Y-SY))
      IF(P.NE.0.) GO TO 10
```

```
      FI(2)=0.
      GO TO 11
   10 CALL BESNIS(P,2,FI)
   11 H2=(EXP((K2-SLANC)*SY)*SQRT((KK*(Y-SY))/X))*FI(2)
      RETURN
      END
      SUBROUTINE SIMPS (A,B,E,MAXI,XINTG,XIP,INDEX)
      FAFB=XINTG(A)+XINTG(B)
      XH=B-A
      XIR=XH*.5
      XJ=XIR*FAFB
      XNEW=A+XIR
      XHA=XIR/3.
      INDEX=0
 1006 FNEWX=XINTG(XNEW)
 1001 IF (INDEX .GT. 0) GO TO 1003
 1002 INDEX=1
      XI=XHA*(FAFB+FNEWX*4.)
 1004 XJ=(XJ+XI*3.)*.25
      INDEX=INDEX+1
      IF (INDEX .GT. MAXI) GO TO 1009
 1010 XH=XH*.5
      XNEW=A+XH*.5
      S=0.
 1005 IF (XNEW .LT. B) GO TO 1006
 1007 XIP=(XJ+XH*2.*S)/3.
      IF (ABS (XIP-XI) .LE. ABS (E*XIP)) GO TO 1009
 1008 XI=XIP
      GO TO 1004
 1003 S=S+FNEWX
      XNEW=XNEW+XH
      GO TO 1005
 1009 RETURN
      END
      SUBROUTINE BESNIS(X,NMAX,FI)
      DIMENSION FI(NMAX), PI(473)
      DATA MAXX/400/,MAXN/51/,RINDEF/17770000000000000008/
C     MAXX= MAX VALUE OF X ALLOWED  .LE.100
C     MAXN-1= MAX ORDER THAT WILL BE RETURNED  .LE.50
C     FI MUST BE DIMENSIONED TO MAXX+ NUMAX+3
C     NOTE THAT (-100.LE.X.LE.100)
      XX= ABS(X)
      IF(NMAX.GT.MAXN) GOTO 1000
      IF(XX.GT. .0001) GO TO 100
C     COMMENT SERIES EXPANSION USED FOR SMALL X
C       SHOULD BE GOOD TO 13 SIG FIGURES FOR X.LE. .0001
C     N-1 IS THE ORDER OF I(X)
      DO 56 N=1,NMAX,1
      N1= N-1
      TZ= X*.5
      SUM= 1.0+TZ*TZ/N
      F=1.0
      FF= 1.0
      DO 52 I=1,N1,1
        F=F*TZ
        FF=FF*I
   52 CONTINUE
      IF(N1.EQ.0) F=1.0
      FI(N)= F/FF*SUM
   56 CONTINUE
      RETURN
C     COMMENT DOWNWARD RECURSION
```

```
  100 CONTINUE
      SUM=0.
      I= IFIX(XX)
      IF(I.GT.MAXX) GOTO 10000
      NADD= 16-NMAX
      IF(NADD.LT.3) NADD=3
      JMAX= 1+NMAX+NADD
      TZ=2./XX
      JM2 = JMAX + 2
      PI(JM2)= 0.0
      PI(JMAX+1)=1.E-5
      DO 1 J=1,JMAX
       K= JM2-J
       DK=K-1
       PI(K-1)=DK*TZ*PI(K)+PI(K+1)
       SUM= SUM+PI(K)
    1 CONTINUE
      SUM=SUM+SUM
      A=EXP(XX)/(PI(1)+SUM)
      DO 2 N=1,NMAX
        FI(N)= A*PI(N)
    2 CONTINUE
      IF(X.GE.0.0) RETURN
      DO 4 N= 2,NMAX,2
        FI(N)= -FI(N)
    4 CONTINUE
      RETURN
10000 CONTINUE
C     COMMENT ERROR EXIT ,ARGUEMENT OUT OF RANGE
      XX=RINDEF*RINDEF
      RETURN
      END
      SUBROUTINE PPLT (X, Y, XMIN, XMAX, YMIN, YMAX, NUM)
C
C
C     THIS SUBROUTINE, GIVEN A SET OF N X-Y COORDINATES, WILL PLOT THEM
C     BY THIS ROUTINE AND OUT OF RANGE POINTS ARE IGNORED
C     ON A 51 BY 101 XY GRID----------THE X ANY Y ARRAYS ARE UNAFFECTED
C
C
      DIMENSION X(1), Y(1), XGRID(11), YGRID(11), GRID(101)
      DIMENSION BLA(37)
      DATA (BLA(I),I=1,37)/1H ,1H*,1H2,1H3,1H4,1H5,1H6,1H7,1H8,1H9,
     *  1HA,1HB,1HC,1HD,1HE,1HF,1HG,1HH,1HI,1HJ,1HK,1HL,1HM,1HN,1HO,1HP,
     *  1HQ,1HR,1HS,1HT,1HU,1HV,1HW,1HX,1HY,1HZ,1H$/
      INTEGER BLA,GRID
   20 T1 = (XMAX - XMIN) / 10.
      T2 = (YMAX - YMIN) / 10.
      XGRID(1) = XMIN
      YGRID(1) = YMAX
      DO 25 I = 2, 11
      XGRID(I) = XGRID(I - 1) + T1
   25 YGRID(I) = YGRID(I - 1) - T2
      WRITE (3, 35)
   35 FORMAT (1H1)
      DO 45 I = 1, 3
   40 WRITE (3, 45)
   45 FORMAT (20X, 1H*, 10(9X, 1H*))
      L = 1
      M = 1
      DO 65 K = 1, 10
```

```
50 GRID(I)=1
   A=M
   G = (YMAX * (51. - A) + YMIN * (A - 1.))/ 50.
   DO 53 IL = 1, NUM
   IF (ABS(G - Y(IL)) - (YMAX - YMIN) / 100.) 41, 53, 53
41 IXP = 100. * (X(IL) - XMIN) / (XMAX - XMIN) + 1.5
51 IF(IXP.GE.1 .AND. IXP.LE.101) GRID(IXP)=GRID(IXP)+1
53 CONTINUE
52 DO 54 J1=1,101
   J2=MIN0(GRID(J1),37)
54 GRID(J1)=BLA(J2)
   WRITE (3,75) YGRID(L),(GRID(I), I = 1, 101)
   N = M + 1
   M = N + 3
   DO 60 J = N, M
   DO 55 I = 1, 101
55 GRID(I)=1
   A=J
   G = (YMAX * (51. - A) + YMIN * (A - 1.))/ 50.
   DO 57 IL = 1, NUM
   IF (ABS(G - Y(IL)) - (YMAX - YMIN) / 100.) 46, 57, 57
46 IXP = 100. * (X(IL) - XMIN) / (XMAX - XMIN) + 1.5
56 IF(IXP.GE.1 .AND. IXP.LE.101) GRID(IXP)=GRID(IXP)+1
57 CONTINUE
   DO 59 J1=1,101
   J2=MIN0(GRID(J1),37)
59 GRID(J1)=BLA(J2)
60 WRITE (3,76) GRID
   M = M + 1
65 L = L + 1
   DO 66 I = 1, 101
66 GRID(I)=1
   DO 72 IL = 1, NUM
   IF (ABS(YMIN - Y(IL)) - (YMAX - YMIN) / 100.) 69, 72, 72
69 IXP = 100. * (X(IL) - XMIN) / (XMAX - XMIN) + 1.5
70 IF(IXP.GE.1 .AND. IXP.LE.101) GRID(IXP)=GRID(IXP)+1
72 CONTINUE
71 DO 73 J1=1,101
   J2=MIN0(GRID(J1),37)
73 GRID(J1)=BLA(J2)
   WRITE (3,75) YGRID(11),(GRID(I), I = 1, 101)
75 FORMAT (10X, 1PE9.2, 1X, 101A1)
76 FORMAT (20X, 101A1)
   DO 80 I = 1, 3
80 WRITE (3, 45)
   WRITE (3,85) (XGRID(I), I = 1, 11)
85 FORMAT (16X, 11(1PE9.2, 1X))
   RETURN
   END
```

APPENDIX B

Listing of the FORTRAN program written for the Hewlett-Packard 5407-A Scintillation Data Analyzer to process pulmonary function data obtained from an Anger scintillation camera.

```
FTN,B
      PROGRAM PNEU
      DIMENSION A(5),IN(4),IA(4140),X(256),IB(256),IX(256),IC(256)
     1,Y(16)
      COMMON A,IN,IA,IB,IX
      EQUIVALENCE (IB(1), X(1))
      EQUIVALENCE (IA(1), IC(1))
      WRITE(2,100)
      WRITE(2,101)
      READ(1,102) (A(I),I=1,5),(IN(I),I=1,4),T1,T2,V
      ILINE=64
      IPAGE=0
      CALL PAGE (IPAGE,ILINE)
      L=1
      M=1
      CALL READ (L,M,IA(1),K)
      DO 4 J=1,4096
      X(1)=FLOAT(IA(J))*T2/T1
    4 IA(J)=IFIX(X(1))
      CALL WRITE(L,M,IA(1),K)
      DO 8 L=33,34
      DO 8 M=1,16
      MM=(L-33)*16+M
      IK=1
      CALL READ (IK,MM,IA(1),K)
      DO 13 I=1,64,4
      DO 13 J=1,64,4
      IK=((I+3)/4-1)*16+(J+3)/4
      IB(IK)=0
      DO 13 IL=1,4
      DO 13 IM=1,4
      MM=(I+IL-2)*64+(J+IM-1)
   13 IB(IK)=IB(IK)+IA(MM)
      IK=1
      CALL READ (IK,L,IA(1),K)
      DO 17 J=1,256
      MM=(M-1)*256+J
   17 IA(MM)=IB(J)
      CALL WRITE(IK,L,IA(1),K)
    8 CONTINUE
      DO 29 L=33,34
      CALL READ (IK,L,IA(1),K)
      X(L)=0.
      DO 25 I=1,256
      J=(L-33)*3840+I
```

```
   IF(IFIX(X(L))-IA(J))26,25,25
26 X(L)=FLOAT(IA(J))
25 CONTINUE
   DO 27 I=1,256
   J=(L-33)*3840+I
27 IX(I)=IFIX(FLOAT(IA(J))*10./X(L))
   J=(L-33)*31+1
   IF(ILINE-40)22,22,28
28 CALL PAGE (IPAGE,ILINE)
22 ILINE=ILINE+19
   WRITE(2,103) J,X(L)
29 WRITE(2,104) IX
   WRITE(2,105)
   READ(1,*) MM
   ILINE=ILINE+2
   BG=FLOAT(MM)*X(33)/100.
   L=34
   CALL READ (IK,L,IA(1),K)
   DUM=0.
   DO 35 J=1,256
   L=3840+J
   IF(IA(J)-IFIX(BG))36,36,37
36 IB(J)=1
   GO TO 35
37 IB(J)=0
35 DUM=DUM+FLOAT(IA(L))
   DO 5 L=3841,4096
   J=L-3840
 5 IX(J)=IFIX(FLOAT(IA(L))*10000./DUM)
   CALL WRITE(3,4,IX(1),K)
   CALL PAGE(IPAGE,ILINE)
   WRITE(2,113)
   WRITE(2,110) IX
   ILINE=ILINE+35
   DO 38 J=129,143
   X(J)=0.
   DO 39 I=1,256
   MM=(J-129)*256+I
39 X(J)=X(J)+FLOAT(IA(MM)*IB(I))
38 X(J)=ALOG(X(J)+0.01)
   DO 30 I=144,147
30 X(I)=0.
   DO 40 J=129,143
   X(144)=X(144)+FLOAT(J-128+16)
   X(145)=X(145)+FLOAT(J-128+16)**2.
   X(146)=X(146)+FLOAT(J-128+16)*X(J)
40 X(147)=X(147)+X(J)
   SLOPE=(X(146)*15.-X(144)*X(147))/(X(145)*15.-X(144)*X(144))
   DO 41 J=1,256
   DUM=0.
   DO 42 I=1,15
   MM=(I-1)*256+J
42 DUM=DUM+FLOAT(IA(MM)*IB(J))
   IF(IB(J))43,43,44
43 IX(J)=IFIX(BG*10.)
```

```
      GO TO 41
   44 IF(SLOPE)46,45,45
   45 IX(J)=IFIX(DUM*10./15.)
      GO TO 41
   46 DUM=DUM*10.*(1.-EXP(SLOPE))/(EXP(SLOPE*16.)-EXP(SLOPE*31.))
      IX(J)=IFIX(DUM)
   41 CONTINUE
      L=33
      CALL READ(IK,L,IA(1),K)
      DO 31 J=1,256
      IF(FLOAT(IA(J))*10.-FLOAT(IX(J)))32,31,31
   32 IX(J)=IA(J)*10
   31 CONTINUE
      IK=3
      L=1
      CALL WRITE(IK,L,IX(1),K)
      DO 50 J=1,256
   50 IX(J)=IFIX(FLOAT(IX(J))/BG)
      IK=1
      DO 51 J=1,256
   51 X(J)=0.
      DO 53 L=33,34
      MM=16-L+33
      CALL READ (IK,L,IA(1),K)
      DO 53 J=1,MM
      DO 53 I=1,256
      M=(J-1)*256+I
   53 X(I)=X(I)+FLOAT(IA(M))
      L=33
      CALL READ (IK,L,IA(1),K)
      DO 56 I=1,256
      J=256+I
      L=512+I
      IA(L)=IA(J)
   56 IA(J)=IA(I)
      IK=3
      L=1
      DUM=0.
      CALL READ (IK,L,IC(1),K)
      DO 54 I=1,256
      J=256+I
      L=512+I
      BG=(FLOAT(IA(J))*30.-FLOAT(IA(L))*10.)/2.-FLOAT(IC(I))
      IF(BG)80,80,81
   80 BG=.01
   81 DUM=DUM+BG
      IF(SLOPE)57,58,58
   57 X(I)=X(I)-FLOAT(IC(I))*(1.-EXP(SLOPE*31.))/(10.*(1.-EXP(SLOPE)))
      IF(X(I))60,60,59
   58 X(I)=X(I)-FLOAT(IC(I))*31./10.
   59 IF(BG-0.8*FLOAT(IC(I)))60,60,61
   60 X(I)=1000.
      GO TO 54
   61 X(I)=X(I)*10./BG
```

```
 54 X(I)=X(I)*T2/6000.
    L=2
    CALL WRITE(IK,L,IB(1),K)
    L=3
    CALL WRITE(IK,L,IX(1),K)
    DO 62 I=1,256
    X(I)=1./(V*X(I))
    J=256+I
    L=512+I
    K=768+I
    BG=(FLOAT(IA(J))*30.-FLOAT(IA(L))*10.)/2.-FLOAT(IC(I))
    IF(BG)82,82,83
 82 BG=.01
 83 IC(I)=IFIX(BG*10000./DUM)
    IA(K)=IC(I)
 62 IA(J)=IFIX(X(I)*FLOAT(IC(I))*10.)
    CALL PAGE(IPAGE,ILINE)
    WRITE(2,107)
    DO 200 I=1,16
    DO 300 J=1,16
300 JJ=(I-1)*16+J
    WRITE(2,108) Y
200 CONTINUE
    ILINE=ILINE+35
    CALL PAGE(IPAGE,ILINE)
    WRITE(2,109)
    WRITE(2,110) IC
    ILINE=ILINE+35
    CALL PAGE(IPAGE,ILINE)
    WRITE(2,111)
    WRITE(2,110) (IA(I),I=257,512)
    ILINE=ILINE+35
    CALL PAGE(IPAGE,ILINE)
    CALL READ(3,4,IA(1025),K)
    X(256)=0.
    BG=0.
    DO 70 J=257,512
 70 BG=BG+FLOAT(IA(J))
    DO 71 I=1,256
    J=256+I
    K=768+I
    L=1024+I
    DUM=FLOAT(IA(J))*10000./BG
    DEN=DUM*DUM+FLOAT(IA(L))*FLOAT(IA(L))
    IF(DEN)72,72,73
 72 DEN=1000000.
 73 IC(I)=IFIX(DUM*FLOAT(IA(L))*100./DEN)*2
    IB(I)=IFIX(FLOAT(IC(I))*FLOAT(IA(K))/100.)
 71 X(256)=X(256)+FLOAT(IB(I))
    WRITE(2,112)
    WRITE(2,110) IC
    ILINE=ILINE+35
    CALL PAGE(IPAGE,ILINE)
    WRITE(2,106)
```

```
      WRITE(2,110) IB
      WRITE(2,114) X(256)
      ILINE=ILINE+38
      CALL PAGE(IPAGE,ILINE)
  100 FORMAT("NAME,NUMBER,DATE,T OF F1-F2-F31,VENT.RATE/MIN")
  101 FORMAT("AAAAAAAAAAJJJJJMMDDYYYYXXXXXYYYYYYVVV")
  102 FORMAT(5A2,I5,2I2,I4,2F6.0,F3.1)
  103 FORMAT(/,/,10X,"FRAME  ",I6,"  MAX ",F7.0)
  104 FORMAT(10X,16I2)
  105 FORMAT("PERCENT BCKGR CUTOFF LEVEL")
  106 FORMAT(/,/,10X,"FUNCTIONAL VOLUME INDEX")
  113 FORMAT(/,/,10X,"FRACTIONAL PIRFUSION")
  114 FORMAT(/,/,10X,"CUMULATIVE ",F7.3)
  107 FORMAT(/,/,10X,"VENT.FRACT/VENTILATION")
  108 FORMAT(/,5X,16(X,F3.2),X)
  109 FORMAT(/,/,10X,"VOLUME DISTRIBUTION")
  110 FORMAT(/,5X,16I4)
  111 FORMAT(/,/,10X,"VENTILATED VOLUMES")
  112 FORMAT(/,/,"           PERFUSION RATIOS")
      STOP
      END
      SUBROUTINE PAGE(IPAGE,ILINE)
      DIMENSION A(5),IN(4)
      COMMON A ,IN
      IPAGE=IPAGE+1
      IF(ILINE-65)1,2,2
    1 ITEST=65-ILINE
      DO 3 I=1,ITEST
    3 WRITE(2,100)
  100 FORMAT(" ")
    2 WRITE(2,101) (A(I),I=1,5),(IN(I),I=1,4),IPAGE
  101 FORMAT(10X,"...",10X,"...",/,/,5A2,2X,I6,3I5,10X,"PAGE",I4)
      ILINE=3
      RETURN
      END
      ENDS
```

REFERENCES

1. Knipping, H.W., Ludes, H., Valentine, H., and Venrath, H., Beitrag zur Differenzierung der Inssuffizienz des linken, des rechten Herzens und der nebst Remerkungen zur Herzsondierung und zum Defizitproblem. Med. Klin. 6:161 (1953).

2. Knipping, H.W., Bolt, W., Valentine, H., Venrath, H., and Endler, P., Regionale Funktionsanalyse in der Kreislauf-und Lungen-Klinik mit Hilfe der isotopenthorakographie und der selektiven Angiographie der Lungengefaesse. Muench. Med. Wochenschr. 99:1 (1957).

3. Knipping, H.W., Bolt, W., Venrath, H., Valentine, H. Ludes, H., and Endler, P., Eine neue Methode zur Pruefung der Herz-und Lungen-function. Deut. Med. Wochenschr. 80:1146 (1957).

4. Dyson, N.A., Hugh-Jones, P., Newbery, G.R., Sinclair, J.D., and West, J.B., Studies of Regional Lung Function Using Radioactive Oxygene. Brit. Med. J. 2:231 (1960).

5. West, J.B., and Dollery, C.T., Distribution of Blood Flow and Ventilation-Perfusion Ratio in the Lung, Measured with Radioactive CO_2. J. Appl. Physiol. 15:405 (1960).

6. West, J.B., Holand, R.A.B., Dollery, C.T., and Matthews, C.M.E., Interpretation of Radioactive Gas Clearance Rates in the Lung. J. Appl. Physiol. 17:14 (1962).

7. Ball, W.C., Stewart, P.B., Newsham, L.G.S., and Bates, D.V., Regional Pulmonary Function Studied with Xenon-133. J. Clin. Invest. 41:519 (1962).

8. Bontivoglio, L.G., Beerel, F., Bryan, A.C., Stewart, P.B., Rose, B., Bates, D.V., Regional Pulmonary Function Studied with Xenon-133 in Patients with Bronchial Asthma. J. Clin. Invest. 42:1193 (1963).

9. Bryan, A.C., Bontivoglio, L.G., Beerel, F., MacLeish, H., Zidulka, A., and Bates, D.V., Factors Affecting Regional Distribution of Ventilation and Perfusion in the Lung. J. Appl. Physiol. 19:395 (1964).

10. Halpern, B.N., Biozzi, G., Benaceraf, B., Stiffel, C., and Hillemand, B., Cinétique de la Phagocytose d'une Serumalbumine Humaine Specialement Traiteé et Radiomarqué et son Application a 1'Etude Circulation Hepatic Chez 1'Homme. Compt. Rend. Soc. Biol. 150:1307 (1956).

11. Taplin, G.V., Johnson, D.E., Dore, E.K., and Kaplan, H.S., Lung Photoscans with Macroaggregates of Human Serum Radioalbumin, Experimental Basis and Initial Clinical Trials. Health Phys. 10:1219 (1964).

12. Wagner, H.N., Sabiston, D.C., Jr., Iio, M., McAfee, J.G., Meyer, J.K., and Langan, J.K., Regional Pulmonary Blood Flow in Man by Radioisotope Scanning. J. A. M. A. 187:601 (1964).

13. Johnson, A.E., and Gollan, F., Lung and Liver Scans with Chromium-51 Labeled Dextran. J. Nucl. Med. 8:306 (1967).

14. Stern, H.S., Goodwin, D.A., and Wagner, H.N., Jr., ^{113m}In -- A Short-Lived Isotope for Lung Scanning. Nucleonics 24(10):57 (1966).

15. Benjamen, P.P., A Rapid and Efficient Method of Preparing ^{99m}Tc Human Serum Albumin: Its Clinical Applications. Int. J. Appl. Radiat. 20:187 (1969).

16. Depaoli, T., Hager, A., Nicolini, J.D., and Radicella, R., Albumin Macroaggregates Labeled with ^{99m}Tc. Int. J. Appl. Radiat. 17:551 (1966).

17. Gwyther, M.M., and Field, E.O., Aggregated ^{99m}Tc-Labeled Albumin for Lung Scintiscanning. Int. J. Appl. Radiat. 17:485 (1966).

18. Stern, H.S., Zolle, I., and McAfee, J.G., Preparation of ^{99m}Tc Labeled Serum Albumin (Human). Int. J. Appl. Radiat. 16:283 (1965).

19. Yano, Y., McRae, J., Honbo, D.S., Anger, H.D., ^{99m}Tc-Ferric Hydroxide Maccroaggregates for Pulmonary Scintiphotography. J. Nucl. Med. 10:683 (1969).

20. Craggin, M.D., Webber, M.M., Victery, W.K., and Pintauro, D., Techniques for the Rapid Preparation of Lung Scan Particles Using ^{99m}Tc-Sulfur and Human Serum Albumin. J. Nucl. Med. 10:261 (1969).

21. Ficken, V., Halpern, S., Smith, C., Miller, L., and Bogerdus, C., Evaluation of $^{99m}Tc_2$-S_7 Macroaggregates for Lung Scanning. J. Nucl. Med. 10:402 (1969).

22. Burdine, J.A., Somemaker, R.E., Ryder, L.A., and Spjurt, H.J., Perfusion Studies with ^{99m}Tc Human Serum Albumin Microspheres (HAM). Radiology 95:101 (1970).

23. Subramanian, G., Bell, E.G., and McAfee, J.G., Preparation and Labeling of Gelatin, Amylose, and Human Serum Albumin Microspheres in vivo Use in Nuclear Medicine. J. Nucl. Med. 10:373 (1969).

24. Anger, H.O., Radioisotope Cameras. Lawrence Berkeley Laboratory report UCRL-11978 (1975).

25. Loken, M.K. and Westgate, H.D., Using Xenon-133 and a Scintillation Camera To Evaluate Pulmonary Function. J. Nucl. Med. 9:45 (1968).

26. Newhouse, M.T., Wright, F.J., Ingham, G.K., Archer, N.P., Hughes, L.B., and Hopkins, O.L., Use of Scintillation Cameras and Xenon-135 for Study of Topographic Pulmonary Function. Respir. Physiol. 4:141 (1968).

27. Werner, R.G., and Govan, I.O., Gamma Mapping of the Liver with the Digital Computer. Lawrence Berkeley Laboratory report UCRL-14866 (1966).

28. Myers, M.J., Kenny, P.J., Langhlin, J.S., Quantitative Analysis of Data from Scintillation Cameras. Nucleonics 24:58 (1966).

29. Brown, D.W., Digital Computer Analysis and Display of the Radionuclide Scan. J. Nucl. Med. 7:740 (1966).

30. Tauxe, W.N., Digital Computer Processing of Radioisotope Scintiscan Matrices. J. A. M. A. 205:85 (1966).

31. Powell, M.R., Gamma Photography. Calif. Med. 108:412 (1968).

32. Kingaby, G.P., Glazier, J.B., Hughes, J.M.B., Maloney, J.E., and West, J.B., Automation of Data Collection and Analysis in Lung Scanning with Radioactive Gases. Med. Biol. Eng. 6:403 (1968).

33. Gilson, A.J., Marks, A., Smith, E.M., and Smook, W.M., Regional Ventilation-Perfusion Determined by Rapid Scanning. J. Nucl. Med. 9:309 (1968).

34. Loken, M.K., Medina, J.R., Lillehei, J.P., L'Heureux, Ph., Kush, G.S., and Ebert, R.V., Regional Pulmonary Function Evaluation Using Xenon-133, a Scintillation Camera, and Computer. Radiology 93:1261 (1969).

35. Natarajan, T.K., Wagner, H.N., Jr., A New Image Display and Analysis System (IDA) for Radionuclide Imaging. Radiology 93:823 (1969).

36. Brownell, G.L., Burham, C.A., Numedics, Computer System for Processing Radioisotope Data from Multiple Sources. USAEC Conf.-710425. Oak Ridge, Tenn. (1971).

37. Budinger, T.F., Clinical and Research Quantitative Nuclear Medicine System. Medical Radioisotope Scintigraphy. Vienna, IAEA (1973).

38. Brill, A.B., Erikson, J.J., Lindhal, C.E., Digital Systems for Acquisition and Storage; in Kenney, P.J., Smith, E.M. (Eds), Quantitative Organ Visualization in Nuclear Medicine. Coral Gables, Fla., University of Miami Press (1971).

39. Alpert, N.M., Burnham, C.A., Devean, L.A., Correll, J.E., Chesler, D.A., Pizer, S.M., and Brownell, G.L., Numedics: A System for On-Line Data Processing in Nuclear Medicine. J. Nucl. Med. 16:386 (1975).

40. Marks, A., Chervony, I., Lankford, R., Smith, E.M., Gilson, A.J., and Smook, W., Ventilation-Perfusion Relationship in Humans Measured by Scintillation Scanning. J. Nucl. Med. 9:450 (1968).

41. DeRoo, M.J.K., Goris, M., Cosemans, J., Gyselen, A., Billiet, L., and Van Der Schueren, Computerized Dynamic Scintigraphy of the Lungs. Respiration 26:408 (1969).

42. MacIntyre, W.J., Inkley, S.R., Roth, E., Drescher, W.P., and Ishii, Y., Spatial Recordings of Disappearance Constants of Xenon-133 Washout from the Lung. J. Lab. Clin. Med. 76:701 (1970).

43. Loken, M.K., Ponto, R.A., Kush, G.S., Quantification of Image Studies Obtained with a Scintillation (Anger) Camera. Radiology 95:505 (1970).

44. Strauss, H.W., T.K. Natarajan, Sziklas, J.J., Poulose, K.P., Fukushima, T., and Wagner, H.N., Computer Assistance in the Interpretation and Quantification of Lung Scans. Radiology 97:277 (1970).

45. Jones, R.H., Coulam, C.M., Goodrich, J.K., et al., Radionuclide Quantitation of Lung Function in Patients with Pulmonary Disorders. Surgery 70:891 (1971).

46. Loken, M.K., Camera Studies of Lung Ventilation and Perfusion. Semin. Nucl. Med. 1:229 (1971).

47. Natarajan, T.K., Wagner, H.N., "Functional Imaging" of Regional Ventilation and Perfusion of the Lungs. J. Nucl. Med. 13:456 (1972).

48. Selker-Walker, R.H., Hill, R.I., Markham, J., and Potchen, E.J., Clinical Applications of Regional Ventilation Measured with a Scintillation Camera and a Small Digital Computer. J. Nucl. Med. 13:466 (1972).

49. Burdine, J.A., Murphy, P.H., Alagarsamy, V., Ryder, L.A., and Carr, W.A., Functional Pulmonary Imaging. J. Nucl. Med. 13:933 (1972).

50. Selker-Walker, R.H., Hill, R.I., Markham, J., Baker, J., Wilhelm, J., Alderson, Ph. O., Potchen, E.J., The Measurement of Regional Ventilation in Man: A New Method of Quantitation. J. Nucl. Med. 14:752 (1973).

51. Inkley, S.R., MacIntyre, W.J., Measurement of Regional Area Gas Exchange by Perfusion and Clearance of ^{133}Xe from the Lung. J. Nucl. Med. 14:490 (1973).

52. Richards, P., Lebowitz, E., and Stang, L.G., Jr., The Brookhaven Linac Isotope Producer (BLIP). IAEA Symposium on Radiopharmaceuticals and Labeled Compounds, Volume I., Copenhagen, 26-30 March 1973.

In the final stage of preparation of this presentation the author has learned, through a private communication with Dr. Powell Richards of Brookhaven National Laboratory, that ^{133}Xe has become commercially available at a reasonable cost.

53. Lederer, C.M., Hollander, J.M., and Perlman, I., Table of Isotopes, sixth edition. John Wiley and Sons, New York (1968).

54. Knipping, H.W., Bolt, W., Valentine, H., Venrath, H., and Endlery, P., Functionsanalyse in der Kreislanf-und Lungen-Klinik mit Hilfe der Isotopenthorakographic und der selektiven Angiographie der Lungengefässe. Muench. Med. Wochenshr. 99:46 (1957).

55. Dollory, C.T., Hughes-Jones, P., and Matthews, C.M.E., Use of Radioactive Xenon for Studies of Regional Lung Function: A Comparison with Oxygen-15. Brit. Med. J. 2:1006 (1962).

56. Hoffer, P.B., Harper, P.V., Beck, R.N., Stark, V., Krizek, H., Heck, L., and Lembares, N., Improved Xenon Images with ^{127}Xe. J. Nucl. Med. 14:172 (1973).

57. Jones, T., Clark, J.C., Hughes, J.M., and Rosenzweig, D.Y., ^{81m}Kr Generator and Its Uses in Cardiopulmonary Studies with the Scintillation Camera. J. Nucl. Med. 11:118 (1970).

58. Yano, Y., McRae, J., and Anger, H.O., Lung Function Studies Using Short-Lived ^{81m}Kr and the Scintillation Camera. J. Nucl. Med. 11:674 (1970).

59. _____, Research Materials, Separated Isotopes, Radioisotopes, Special Preparations, Oak Ridge National Laboratories, sixth edition (April 1973).

60. Veall, N., The Handling and Dispensing of Xenon-133; Gas Shipments for Clinical Use. Int. J. Appl. Radiat. Isot. 16:385 (1965).

61. Marks, A., and Chervoney, I.A., Simplified Technique for the Transfer of ^{133}Xe. Radiology 90:800 (1968).

62. Tilbury, R.S., Dramer, H.H., Wahl, W.H., Preparing and Dispensing Xenon-133 in Isotonic Saline. J. Nucl. Med. 8:401 (1967).

63. Ponto, R.A., Kush, G.S., Loken, M.K., Considerations of Problems in Handling and Radiation Dosimetry of ^{133}Xe. J. Nucl. Med. 11:352 (1970).

64. Steiman, K., and Aspin, N., A Device for Dispensing Radioactive Xenon Gas. Radiology 92:396 (1969).

65. Rummerfield, P., Jones, G., and Asburn, W., Health Physics Aspects of Xenon-133 Lung Studies. Health Phys. 21:547 (1971).

66. Loken, M., Kush, G.S., Handling, Use and Radiation Dosimetry of Xenon-133. USAEC Symposium Series 20, Medical Radionuclides: Radiation Dose and Effects (1970).

67. Snyder, R.E., and Overton, T.R., System for Handling and Dispensing ^{133}Xe. J. Nucl. Med. 14:56 (1972).

68. Gutkowski, R.F., Horwitz, N.H., and Dworkin, H.J., A Calibrated Dose Dispenser for Gaseous ^{133}Xe. J. Nucl. Med. 16:1197 (1975).

69. Case, F.N., Facillo, D.A., Jr., and Ewing, S.B., ORNL Radioisotopes Procedure Manual. ORNL-3633 (1964).

70. Arnot, R.N., Clark, J.C., and Glass, H.I., Investigation of ^{127}Xe as a Tracer for the Measurement of Regional Cerebral Blood Flow. Proceedings of the Sixth International Symposium on the Regulation of Cerebral Blood Flow (Cords), Russ Russel, R.W., Ed., London, Pitman (1970).

71. Conn, H.L., Jr., Equilibrium Distribution of Radioxenon in Tissue: Xenon-Hemoglobin Association Curve. J. Appl. Physiol. 16:1065 (1961).

72. Lassen, N.A., Assessment of Tissue Radiation Dose in Clinical Use of Radioactive Inert Gases, with Examples of Absorbed Doses from $^{3}H_2$, ^{85}Kr, and ^{133}Xe. Minerva Nucl. 8:211 (1964).

73. Brownell, G.L., Ellett, W.H., and Reddy, A.R., Absorbed Fractions for Photon Dosimetry, MIRD Pamphlet No. 3. J. Nucl. Med. 9, Supplement No. 1:29 (1968).

74. Snyder, W.S., Ford, M.R., Warner, G.G., and Fisher, H.L., Jr., Estimates of Absorbed Fractions for Monoenergetic Photon Sources Uniformly Distributed in Various Organs of a Heterogeneous Phantom, MIRD Pamphlet No. 5. J. Nucl. Med. 10, Supplement No. 3:7 (1969).

75. Loevinger, R., and Berma, M., A Scheme for Absorbed-Dose Calculations for Biologically-Distributed Radionuclides, MIRD Pamphlet No. 1. J. Nucl. Med. 9, Supplement No. 1:9 (1968).

76. Goddard, B.A., and Ackey, D.M., Xenon-133, ^{127}Xe, and ^{125}Xe for Lung Function Investigations: A Dosimetry Comparison. J. Nucl. Med. 16:780 (1975).

77. United States Nuclear Regulatory Commission, Rules and Regulations. Code of Federal Regulation, Title 10 - Part 20, May 1975.

78. Mantell, J., Cook, K.J., and Corrigan, K.E., Radioactive Krypton and Xenon Trapping by Cryogenic Technics. Radiology 90:590 (1968).

79. Corrigan, K.E., Mantell, J., and Corrigan, H.H., Trapping Systems for Radioactive Gas. Radiology 96:571 (1970).

80. Liuzzi, A., Keany, J., and Freedman, G., Use of Activated Charcoal for the Collection and Containment of ^{133}Xe Exhaled during Pulmonary Studies. J. Nucl. Med. 13:673 (1972).

81. Boer, J.H., The Dynamic Character of Adsorption. Oxford University Press, London (1953).

82. Frenkel, J., Z. Physik 26:117 (1924), as cited in reference 83.

83. Brunauer, S., Adsorption of Gases and Vapors, Vol. 1. Princeton University Press, Princeton (1945).

84. de Saussure, T., Gilbert's Ann. der Phys. 47:113 (1814); Ann. Phil. 6:241 (1815), as cited in reference 83.

85. Peters, K., and Weil, K., Adsorption Isotherms with Noble Gases. Z. Phys. Chem., A148:1 (1930).

86. Freundlich, H., Colloid and Capillary Chemistry. Methwen, London (1926).

87. Langmuir, I., Adsorption of Gases by Solids. J. Am Chem. Soc. 38:2267 (1916); 40:1361 (1918).

88. Glueckauf, E., The Theoretical Plate Concept in Column Separations. Trans. Faraday Soc. 51:34 (1955).

89. Browning, W.E., and Bolta, C.C., Measurement and Analysis of the Holdup of Gas Mixtures by Charcoal Adsorption Traps. Oak Ridge National Laboratory report ORNL-2116 (1956).

90. Thomas, H.C., Heterogeneous Ion Exchange in a Flowing System. J. Am. Chem. Soc. 66:1064 (1944).

91. Thomas, H.C., The Kinetics of Fixed-Bed Ion Exchange. Ann. N.Y. Acad. Sci. 49:161 (1948).

92. Kenney, W., and Eshaya, A.M., Adsorption of Xenon on Activated Charcoal. Brookhaven National Laboratory report BNL-689 (1960).

93. Eshaya, A.M., and Kalinowski, W., Adsorption of Krypton and of Mixed Xenon and Krypton on Activated Charcoal. Brookhaven National Laboratory report BNL-774 (1961).

94. Wirsing, E., Jr., Hatch, L.P., and Dodge, B.F., Low Temperature Adsorption of Krypton on Solid Adsorbents. Brookhaven National Laboratory report BNL-50254 (1970).

95. Amphlett, C.B., and Greenfield, B.F., Krypton and Xenon Adsorption Isotherms on Charcoal Irradiated with 1 MeV Electrons. United Kingdom Atomic Energy Authority, Atomic Energy Research Establishment report AERE-C/R-2632 (1958).

96. Burdick, J.N., Adsorption of Krypton and Xenon. Tonawanda Linde Research Laboratory report ORO-118 (1951).

97. Underhill, D.W., Dynamic Adsorption of Fission-Product Noble Gases on Activated Charcoal. Harvard School of Public Health report NYO-841-8 (1967).

98. Kovach, J.L., Review of Krypton-Xenon Adsorber Design. Part 1. North American Carbon Inc., report NACAR-10005 (1970).

99. Burnette, R.D., Graham III, W.W., and Morse, D.C., The Removal of Radioactive Krypton and Xenon from a Flowing Helium Stream by Fixed-Bed Absorption. Nuclear Reactor Chemistry Second Conference, Gatlinburg, Tenn. October 10-12, 1961, USAEC Report TID-7622, pp. 218-235 (1962).

100. Keilholtz, G.W., Krypton-Xenon Removal Systems. Nucl. Saf. 12:591 (1971).

101. Cantelow, H.P., Adsorption of Xenon in an Activated Charcoal Column. Lawrence Berkeley Laboratory report UCRL-8755 (1959).

102. Forster, K., Delaying Radioactive Fission Product Inert Gases in Cover Gas and Offgas Streams of Reactors by Means of Activated Charcoal Delay Lines. Kerntechnik 13;214 (1971).

103. First, M.W., Underhill, D.W., Hall, R.R., et al., Semiannual Progress Report (9-8-70 to 2-28-71), NYO-841-24; (3-1-71 to 8-31-71), NYO-841-25. Harvard Air Cleaning Laboratory, Boston.

104. Madey, R., Barker, J.J., Beebe, M.R., and Stephenson, T.E., Adsorption of Radioactive Gases on Activated Carbon. AEC Research and Development report NYO-9068 (1961).

105. Ackley, R.D., Adams, R.E., Browning, W.E., Sixth AEC Air Cleaning Conference, July 7-9, 1959. USAEC report TID-7593 (1960).

106. Holmes, J.M., Design of the Dissolver Off-Gas System for the Idaho Chemical Processing Plant. Oak Ridge National Laboratory report ORNL-CF-52-11-39 (1952).

107. Adams, R.E., Browning, W.E., Fission Gas Holdup Tests on HRT Charcoal Beds. Oak Ridge National Laboratory report ORNL-CF-58-4-14 (1958).

108. Kovach, J.L., Adsorbent; Review and Projection, in 10th AEC Air Cleaning Conference, New York, pp. 149-166 (1968).

109. Lloydand, M.H., McNees, R.A., Adsorption of Krypton and Xenon by Various Materials. Oak Ridge National Laboratory report ORNL-3228 (1961).

110. Briggs, R.B., et al., Homogeneous Reactor Project Quarterly Report; for period ending January 1, 1958. Oak Ridge National Laboratory report ORNL-2493 (1958).

111. Briggs, R.B., et al., Homogeneous Reactor Project Quarterly Progress Report for period ending April 30 and July 31, 1958. Oak Ridge National Laboratory report ORNL-2561 (1959).

112. Kovach, L.J., Krypton Xenon Adsorption on Nacon Carbons. North American Carbon Inc., report NACAR-10004 (1967).

113. Kitani, S., Takada, J., Adsorption of Krypton and Xenon on Various Adsorbents. J. Nucl. Sci. Technol. 2:51 (1965).

114. Budinger, T.F., Clinical and Research Quantitative Nuclear Medicine System. Lawrence Berkeley Laboratory report LBL-1328 (1972).

115. Adams, R.E., Browning, W.E., Jr., Containment of Radioactive Fission Gases by Dynamic Adsorption. Ind. Eng. Chem. 51:1467 (1959).

116. Roemberg, E., The Effect of Moisture on the Adsorption of Krypton on Charcoal. United Kingdom Atomic Energy Authority. DP-Report-276 (1964).

117. Coolidge, A.S., The Adsorption of Water Vapor by Charcoal. J. Am. Chem. Soc. 49:708 (1927).

118. Allmand, A.J., Hand, P.G., and Shiels, D.O., Sorption of Water Vapour by Activated Charcoals. J. Phys. Chem. 33:1682 (1929).

119. McBain, J.W., Porter, J.L., and Sessions, R.F., The Nature of the Sorption of Water by Charcoal. J. Am. Chem. Soc. 55:2294 (1933).

120. King, A., and Lawson, C.G., The Influence of Activation on the Sorption of Water Vapour. Trans. Farraday Soc. 30:1094 (1934).

121. Lizins, J.L. and Allmand, A.J., The Simultaneous Sorption of Carbon Bisulphide and Water Vapours by Activated Charcoals. Proc. Roy. Soc. London, Series A, 169:25 (1938).

122. Culbertson, J.L., and Winter, L.L., Compressed Films of Solid-Liquid Interfaces. J. Am. Chem. Soc. 63;95 (1941).

123. Broad, D.N., and Fosler, A.G., Comparative Isothermals of Water and Deuterium Oxide on Porous Solids. J. Chem. Soc. pp. 372 (1945).

124. Morrisson, J.A., and McIntosh, R., The Apparent Density of Water Absorbed on Activated Charcoal. Can. J. Research B24:137 (1946).

125. Fineman, M.N., Guest, R.M., and McIntosh, R., The Adsorption of Water Vapour and Its Dependence on Pore Size. Can. J. Research B24:109 (1946).

126. Emmett, P.H., Adsorption and Pore Size Measurements on Charcoal and Whetlerites. Chem. Rev. 43:69 (1948).

127. Pierce, C., Smith, R.N., Wiley, J.W., and Cords, H., Adsorption of Water by Carbon. J. Am. Chem. Soc. 73:4551 (1951).

128. McBernot, J.L., and Arnel, F.P., Charcoal Sorption Studies. Can. J. Chem. 30:177 (1952).

129. Emmett, P.H., Advances in Colloid Science, Ed. by E.O. Kraemer, F.E. Bantell, S.S. Kistler. Interscience Publishers, Inc., New York (1942).

130. Brunaner, S., Emmett, P.H., and Teller, E., Adsorption of Gases in Multimolecular Layers. J. Am. Chem. Soc. 60:309 (1938).

131. Kohl, A.L., and Riesenfeld, F.C., Gas Purification. McGraw-Hill Co., New York (1960).

132. Gadsby, J., Hinshel, C.N., and Sykes, K.W., The Kinetics of the Reactions of the Steam-Carbon System. Proc. Roy. Soc. London, Series A 187:129 (1946).

133. Strickland-Constable, R.F., Interaction of Steam and Charcoal at Low Pressures. Proc. Roy. Soc. London, Series A 189:1 (1947).

134. Long, F.J., and Sykes, K.W., The Mechanism of Steam-Carbon Reaction. Proc. Roy. Soc. London, Series A 193:377 (1948).

135. Muller, S., and Cobb, J.W., The Steam-Carbon Complex. J. Chem. Soc., pp. 177 (1940).

136. Mayers, M.A., The Rate of Reduction of Carbon Dioxide by Graphite. J. Am. Chem. Soc. 56:70 (1934).

137. Pitcher, J.M., Walker, P.L., Jr., and Wright, C.C., Influence of Temperature, Partical Pressure of Water Vapor, and Nature of Carbon on Gasification Rates. Ind. Eng. Chem. 47:1742 (1955).

138. Goring, G.E., Curran, P.G., Tarbox, R.P., and Goring, E., Effect of Pressure and Carbon Burnoff on Rate of Interaction of Low Temperature Char with Steam-Hydrogen Mixtures at 1600°F. Ind. Eng. Chem. 44:1057 (1952).

139. Tuddenham, W.M., and Hill, G.R., Catalytic Effects of Cobalt, Iron, Nickel, and Vanadium Oxides on Steam Carbon Reaction. Ind. Eng. Chem. 47:212a (1955).

140. Binford, J.S., and Eyring, H.J., Kinetics of Steam Carbon Reaction. J. Phys. Chem. 60:486 (1956).

141. Warner, B.R., Mechanism of the Steam-Carbon Reaction. J. Am. Chem. Soc. 65:1447 (1943).

142. Walker, P.L., Jr., Rusinko, F., Jr., and Austin, L.G., Gas Reactions of Carbon, in Advances in Catalysis, Vol. 11, Ed. D.D. Eley, P.W. Selwood, and P.B. Weisz. Academic Press Inc., New York (1959).

143. Smith, R.N., Pierce, C., and Joel, C.D., The Low Temperature Reaction of Water with Carbon. J. Phys. Chem. 58:298 (1954).

144. Barret, P.B., Joyner, L.G., and Hallenda, P.P., Determination of Port Volume and Area Distribution in Porous Substances. J. Am. Chem. Soc. 73:377 (1951).

145. Johnston, H.F., Chen, C.Y., and Scott, D.S., Kinetics of the Steam-Carbon Reaction in Porous Graphite Tubes. Ind. Eng. Chem. 44:1564 (1952).

146. Blyholder, G., and Eyring, H., Kinetics of the Steam-Carbon Reaction. J. Phys. Chem. 63:693 (1959).

147. _____, Heat Transfer in Activated Carbon Beds, NCS-1102. Nuclear Containment Systems, Inc. (1972).

148. Lund, H.F., Industrial Pollution Control Handbook, McGraw-Hill Co., New York (1971).

149. Steward, G.N., Researches on the Circulation Time and on the Influences Which Effect It. J. Physiol. 22:159 (1897).

150. Stewart, G.N., The Pulmonary Circulation Time, the Quantity of Blood in the Lungs and the Output of the Heart. Am. J. Physiol. 58:20 (1921).

151. Hamilton, W.F., Moore, J., Kinsman, J.M., and Spurling, R.G., Studies on the Circulation. Am. J. Physiol. 99:534 (1932).

152. Meier, P., and Zierler, K.L., On the Theory of the Indicator-Dilution Method for Measurement of Blood Flow and Volume. J. Appl. Physiol. 6:731 (1954).

TECHNICAL INFORMATION DIVISION
LAWRENCE BERKELEY LABORATORY
UNIVERSITY OF CALIFORNIA
BERKELEY, CALIFORNIA 94720